

ABSTRACT

Title of Document: FEM IMPLEMENTATIONS OF
MAGNETOSTRICTIVE-BASED
APPLICATIONS

Jonathan G. Benatar, Master of Science, 2005

Directed By: Associate Professor, Alison B. Flatau,
Department of Aerospace Engineering

Magnetostrictive transducers are used in a broad variety of applications that include linear pump drive mechanisms, active noise and vibration control systems and sonar systems. Optimization of their performance relies on accurate modeling of the static and dynamic behavior of magnetostrictive materials. The nonlinearity of some properties of magnetostrictive materials along with eddy current power losses occurring in both the magnetostrictive material and the magnetic circuit of the system makes this task particularly difficult.

This thesis presents continuum level, three dimensional, finite element analysis of magnetostrictive-based applications for different operating conditions. The Finite element models (FEMs) are based on boundary value problems which are first introduced in the “differential” form (Chapter 2) and then derived to a “weak” form (Chapter 3) suitable for the implementation on the commercial finite element software, FEMLAB 3.1©. Structural mechanics and electromagnetics BVPs are used to predict the behavior of, respectively, structurally-involved parts and the electromagnetic circuit of a magnetostrictive-based application. In order to capture

the magnetostrictive material's behavior, static and dynamic three-dimensional multi-physics BVPs include magneto-mechanical coupling to model magnetostriction and the effect of the magnetic stress tensor, also known as Maxwell stress tensor, and electromagnetic coupling to model eddy current power losses (time-harmonic and dynamic case only). The dynamic formulation is inspired by the finite element formulation in the Galerkin form introduced by Perez-Aparicio and Sosa [1], but focuses on a weak form formulation of the problem suitable for implementation in the commercial finite element software FEMLAB 3.1©. Implementation methods of the introduced models are described in Chapter 4. Finally, examples of these models are presented and, for the coupled magneto-mechanical FEM, compared to experimental results.

FEM IMPLEMENTATIONS OF MAGNETOSTRICTIVE-BASED
APPLICATIONS

By

Jonathan G. Benatar

Thesis submitted to the Faculty of the Graduate School of the
University of Maryland, College Park, in partial fulfillment
of the requirements for the degree of
Master of Science
2005

Advisory Committee:
Professor, Alison B. Flatau, Chair
Professor, Sung Lee
Assistant Professor, Benjamin Shapiro

© Copyright by
Jonathan G. Benatar
2005

Acknowledgements

I wish to address my first words of gratitude to my thesis committee: Dr A. Flatau, Dr. B. Shapiro, and Dr. S. Lee. I was fortunate to find such understanding and flexible professors, which I could never thank enough for accepting on such short notice to be part of my committee. Among them, I would like to give a special thanks to Dr Flatau for guiding me through those two years of graduate school. Without your support and patience, I would never have been able to achieve a work of this quality. I would also like to thank all my class teachers and especially Dr Lee, Dr Dasgupta and Dr Hubbard who provided me with the tools necessary to achieve this research. Thank you also to Dr Shapiro and his team of graduate students who help me made my first models on FEMLAB.

To the graduate students working with me, Dr. Yoo, Dr. Na, Supratik Datta, Jayasimha Atulasimha, Patrick Downey and Luke Twarek, I would like to express my sincere gratitude for all the time they help me out in the lab and in class. The many discussions on magnetostriction-related topics were essential to completion of many of my FEMs. Thank you especially to Supratik Datta and Jayasimha Atulasimha for providing me with key experimental data used to implement and validate some of the FEMs implemented.

I would like to acknowledge DARPA for their financial support in the form of a Research Assistantship (contract number: F336150C3320) and for the sufficient financial resource to provide me with a computer and other equipment used in this work. To the people at ETREMA products, Inc., I would like to express my gratitude

for the many free polycrystal samples provided for the testing of the electrical resistivity.

To my parents, Brigitte and Daniel, my brother, Marc, and my little sister, Sarah, thank you for the continuous moral support. They gave me the opportunity and the strength to achieve this work. Thanking them would be meaningless; nevertheless, I would like to acknowledge their understanding and express the hope that my efforts and work are worthy of their kindness. And to my girlfriend, Aurore, I will never be able to thank her enough for her support and her patience during those long four years of long-distance relationship. Don't worry, it's over, I'm coming home.

Table of Contents

Acknowledgements.....	ii
Table of Contents.....	iv
List of Tables.....	vi
List of Figures.....	vii
Chapter 1: Introduction.....	1
1.1. Scope of the Objective.....	4
1.2. Smart Structure.....	7
1.3. Magnetostrictive Material.....	11
1.3.1. Magnetostrictive material behavior.....	12
1.3.2. Terfenol-D, Galfenol and other magnetostrictive materials.....	25
1.3.3. Applications.....	28
1.4. Modeling Magnetostrictive Materials.....	31
1.5. Outline of Approach and thesis.....	33
Chapter 2: Differential Formulation of the Governing Equations.....	35
2.1. The Mechanical Governing Equation.....	36
2.1.1. The non-coupled, purely mechanical, Boundary Value Problem.....	36
2.1.2. Modified Hooke’s Law for Elastic Materials under Pre-stress.....	41
2.2. The Electromagnetic Governing Equations.....	43
2.2.1. The dynamic electromagnetic boundary value problem.....	44
2.2.2. Additional electromagnetic variables.....	47
2.2.3. Simplification for the magnetostatic and time-harmonic applications.....	51
2.3. The Mechanical and Electromagnetic Governing Equations for Magnetostrictive Materials.....	54
2.3.1. Electromagnetic Stress Tensor and Modified Equilibrium Equation for Magnetizable Material.....	54
2.3.2. Simplified Maxwell’s Equations.....	55
2.3.3. The Linearized Coupled Constitutive Equations.....	56
Chapter 3: Weighted-Residual Formulations.....	60
3.1. The “Weak” Form Formulation of the Structural Mechanics BVPs.....	62
3.2.1. The Static fully coupled electro-mechanical “weak” form formulation for piezoelectric material.....	67
3.2.2. The static fully coupled magneto-mechanical “weak” form formulation for magnetostrictive material.....	72
3.3. The “weak” formulation of dynamic fully coupled electro-magneto- mechanical BVP.....	74
Chapter 4: FEM Implementations on FEMLAB 3.1©.....	77
4.1. Brief Overview of FEMLAB 3.1 ©.....	77
4.2. Implementation of the static BVPs.....	80
4.2.1. Structural mechanics FEM of a purely elastic material.....	80
4.2.2. Magnetostatic FEM.....	95
4.2.3. Fully coupled magneto-mechanical FEM of a magnetostrictive material.....	98

4.3.	Implementation of the dynamic BVPs	105
4.3.1.	Electromagnetic, time-harmonic FEM.....	105
4.3.2.	Fully coupled electro-magneto-mechanical FEM of a magnetostrictive material	109
Chapter 5:	Validation of the FEM implementations on FEMLAB 3.1©.....	115
5.1.	Examples of Uncoupled Finite Elements Models based on existing Application Modes.....	116
5.1.1.	Example using the magnetostatic application mode.....	116
5.1.2.	Example using the time-harmonic, electromagnetic application mode	130
5.2.	Example of Coupled Finite Element Model of a Magnetostrictive-based Application.....	138
5.2.1.	Magnetostrictive material properties selection	139
5.2.2.	Results and comparison to experimental data.....	144
Chapter 6:	Conclusion.....	151
6.1.	Summary	151
6.2.	Suggestions for future work.....	152
Appendix 1:	Electrical Resistivity Measurements	154
References	157

List of Tables

1.1. Most common Smart Materials and their functionality	10
1.2. Smart material comparison chart when used as an actuator (top) and sensor (bottom)	10
1.3. Comparison chart between Terfenol-D and Galfenol.....	14
1.4. Unit system and conversion factors for magnetic quantities.....	22
4.1. Summary of the important variables displayed in the “Variable” tab of a magnetostrictive subdomain.....	104
4.2. Suggested implementation of the Variables for a magnetostrictive subdomain in an electro-magneto-mechanical model.....	110-111
4.3. Suggested implementation of the time derivative “Variables” for a magnetostrictive subdomain in an electro-magneto-mechanical model.....	112
4.4. Suggested implementation of the time independent parts of the governing equations in the “weak” tab.....	114
4.5. Suggested implementation of the time dependent parts of the governing equations in the “dweak” tab.....	114
5.1. Calibration of the permanent magnets chart.....	118

List of Figures

1.1. Schematics of the magnetostrictive effect	13
1.2. Independence of strain on polarity of applied field	13
1.3. Sample magneto-mechanical actuator characterization curves of a 19% Gallium Galfenol sample under various compressive stresses at 22°C.....	17
1.4. Effect of compressive pre-stress on magnetostriction	17
1.5. Range of application when using a bias magnetic field to operate in a linear region	17
1.6. Sample magneto-mechanical sensor characterization curves of a 19% Gallium Galfenol sample	18
1.7. Illustration of the Delta-E effect in magnetostrictive Galfenol	18
1.8. Sample magnetic characterization curves for a 19% Gallium Galfenol sample under various compressive stresses at 22°C	19
1.9. Sample λ -T° curves at various temperature for a Terfenol-D sample.....	24
1.10. Coupling diagram.....	24
1.11. Magnetostriction versus Gallium content in single crystal Galfenol	28
2.1. Illustration of the effect of reducing the cross sectional area of a magnetizable material to limit eddy current power losses (top left: circular cross section, top right: laminated cross section, bottom left: hollow cylinder cross-section, bottom right: hollow cylinder cross section with a slit).....	50
2.2. Summary of the differential form of the electro-magneto-mechanical BVP for magnetostrictive material under dynamic application.....	58

2.3. Summary of the differential form of the magneto-mechanical BVP for magnetostrictive material under static application.....	59
3.1. Summary of Structural mechanics BVPs for purely elastic material.....	62
3.2. Summary of the differential form of the electro-magneto-mechanical BVP for magnetostrictive material under dynamic application.....	76
4.1. Model Navigator window.....	81
4.2. Option menu in the FEMLAB geometry window.....	82
4.3. Axis and Grid setting window.....	83
4.4. 2-D work plane with beam cross-section and “extrude” window.....	84
4.5. Setting “weak” form display of the equation system.....	85
4.6. “weak” tab in the equation setting/Subdomain window.....	85
4.7. “Variable” tab in the “Equation setting / Subdomain” window.....	87
4.8. “Material” tab in the “subdomain setting” window.....	88
4.9. “Material library” window.....	88
4.10. “Constraint” tab of the BC setting window.....	89
4.11. “Load” tab of the BC setting window.....	90
4.12. “Mesh parameters” window and meshed structure.....	92
4.13. “Plot parameter” window and final solution.....	94
4.14. “Cross-section plot parameter” window and line plot of the “z” component of the strain along the neutral axis.....	94
4.15. Geometry of the magnetic circuit.....	97
4.16. Geometry of the example implemented for the static coupled magneto-mechanical model.....	99

4.17. “Constants” window.....	101
4.18. “D” matrix window and the “subdomain setting” window for an anisotropic material.....	102
4.19. “weak” tab of the “subdomain setting/ equations system” window.....	102
4.20. Pump model geometry.....	105
4.21. “Electric parameter” tab of the “subdomain setting” window.....	107
4.22. “Application scalar variables” window.....	108
4.23. “application mode properties” window.....	108
4.24. “constant” window.....	108
5.1.3-D plot of the normalized magnetic induction (in Tesla) (slice plot) and the magnetic field’s path (streamlines) inside, respectively, (a) the 12mm and (b) the 43.2 mm air gap models with no Galfenol sample between the permanent magnets.....	119
5.2. Line plot of the magnetic field (in A/m) along the x-axis between the two magnets (no sample) for respectively (a) a 12mm and (b&c) a 43.2 mm gap size, and using value of, respectively, (a&b) 6000 and (c) 8000 for the magnetic steel permeability.....	122
5.3.B-H curves of 19% Galfenol polycrystal (a) production grade sample and (b) research grade sample.....	124
5.4. Line plots of the magnetic induction (in Tesla) along the x-axis of (a) a single crystal sample in the 12 mm gap model, (b) a single crystal sample in the “43.2 mm gap” model, (c) a production grade polycrystal sample in the 12 mm gap	

model, and, (d) a production grade polycrystal sample in the 43.2 mm gap model.....	125
5.5. 2-D slice plots of the magnetic induction (in Tesla) inside the sample for (a) a single crystal sample in the 12 mm gap model, (b) a single crystal sample in the 43.2 mm gap model, (c) a production grade polycrystal sample in the 12 mm gap model, and, (d) a production grade polycrystal sample in the 43.2 mm gap model.....	126-127
5.6. (Figure 5.4b modified) Line plots of the magnetic induction (in Tesla) in a single crystal sample accounting for the saturation effects for in the “43.2 mm gap” model.....	129
5.7. Geometry of the magnetostrictive pump with the four slit subdomains shaded.....	131
5.8. Magnetic field distribution and flux path for a coil modeled in air.....	133
5.9. Sample 2-D slice plot of the normalized magnetic induction for an operating frequency of 2KHz with (a) no slit in the housing, (b) a half slit housing and (c) a full slit housing	133-134
5.10. Magnetic Induction along the 2 inch magnetostrictive rod under various actuation frequency.....	135
5.11. Magnetic Induction along the ¼ inch diameter of the magnetostrictive rod....	136
5.12. Experimental set up	138
5.13. Magnetostriction vs Magnetic field curves of 18.4% production grade polycrystal Galfenol for various stress level	140

5.14. (a) a 3-D plot of the “x” component of the magnetic flux density and (b) the line plot of the magnetic field “x” component on the top surface of the upper sensor plate.....	142
5.15. (a) 2-D plot of the “x” component of the stress tensor and (b) the line plot of the same quantity along the z-axis on the plane 37 mm from the attached end.....	143
5.16. (a) 3-D plots of the magnetic induction and field for the calibration of the permanent magnets in air obtained by a purely magnetostatic model (top), and (b) for a 0.552N loading on the beam using the coupled magneto-mechanical model (bottom).....	146
5.17. Magnetic Flux density (Tesla) on the top of the Galfenol plate.....	147
5.18. Strain x-component on the top of the beam (lower surface plot) and on the top of the Galfenol sensor plate (higher surface plot).....	147
5.19. Line plot of the magnetic induction along the white line plotted in Figure 5.17 for a) no loading and b) 0.552N loading.....	148
5.20. Experimental results provided by S. Datta [13] and modeled results computed from the FEM model. Change in magnetic induction, strain on the sensor surface and strain on the beam surface next to the sensor for (a) 0.0833N (top left), (b) 0.255N (top right), (c) 0.338N (bottom left) and (d) 0.552N (bottom right).....	150
A.1. Resistivity measurements for various stoichiometries and various crystallographic orientation.....	154
A.2. Resistivity vs Temperature plots with quadratic and linear analytical model.....	156

Chapter 1: Introduction

Over the last two decades, magnetostrictive materials have received significant interest from the smart materials and structures community. A better understanding of the electro-magneto-mechanical coupling behavior of these smart materials has led to novel, more efficient, active and adaptive applications. Part of the research effort on the design of magnetostrictive-based devices includes the development of various computational tools with predictive and detailed analysis capabilities for use in optimizing the performance in the design phase. Most of these computational tools are based upon simplifying assumptions specific to the structural or functional configuration of the application under consideration. Only recently was a dynamic, fully coupled, non-linear, three-dimensional Finite Elements Method (FEM) for magnetostrictive materials introduced [1].

For most magnetostrictive-based applications, there are three types of FEM implementations necessary to capture the coupled mechanical and electromagnetic behavior of all the components that makes a transducer: (1) a fully coupled Electro-Magneto-Mechanical Finite Element Method (EMMFEM) implementation capable of capturing the behavior of the magnetostrictive material; (2) an electromagnetic FEM capable of predicting the behavior of the part involved in the electromagnetic circuit; and (3) an uncoupled continuum mechanics FEM capable of predicting the mechanical behavior of the structurally involved parts. Note that some parts may be structurally involved and magnetically involved like the magnetic steel housing of a magnetostrictive

transducer that serves both to conduct a magnetic field in the magnetic circuit and to insure the structural integrity of the transducer.

When modeling magnetostrictive materials, various coupling behaviors must be taken into account. First, the magneto-elastic interactions, also known as magnetostriction, must be included in the EMMFEM implementation. Although this coupling behavior is non-linear, under the assumption of small increments of the mechanical and magnetic independent variables, two linear coupled constitutive equations can be used to take into account this bidirectional magneto-mechanical coupling behavior. Second, the EMMFEM implementation and the mechanical FEM must take into account the effects of body-force and body-moment of magnetic origin. This form of coupling is unidirectional and is implemented by adding non-linear terms to the mechanical constitutive equations (i.e. the constitutive equations that link stress to strain and magnetic field). Note that this type of magneto-mechanical coupling does not apply to non-magnetizable materials like Aluminum. Third, an electromagnetic coupling occurs in non-static purely electromagnetic problems. An example of this coupling can be illustrated by the creation of a magnetic field around a wire with an electric current passing through it. A consequence of this type of coupling is often observed in the form of eddy current power losses occurring in magnetizable materials under time-harmonic or dynamic conditions. This type of coupling is accounted for by using the general form of the Maxwell equations as governing equations. Additional information on the behavior of a magnetostrictive material is given in more detail in section 1.3.

All three types of FEM implementations must be 'compatible', meaning they must have common independent variables in order to be able to solve all implementations

simultaneously. When writing your own FEM code of a multi-physic problem, ‘compatibility’ of the models is usually insured by using a single multi-physic FEM scheme in the Galerkin form where some of the coefficients of the tangent matrix are zeroed depending on the type of material modeled (i.e. the magneto-mechanical coupling coefficients are zeroed for non-magnetostrictive parts) [2,3]. However writing your own FEM can be tedious especially when modeling 3-D structures with complicated geometries. An alternative is to implement this multi-physics problem on commercially available software, in which case, compatibility may become an issue, especially when modifying pre-written uncoupled FEM schemes [4].

The objective of this work is to capture the behavior of all parts involved in a magnetostrictive-based application by using various three dimensional FEM schemes implemented on a commercially available software, FEMLAB 3.1©, by modifying pre-existing FEM schemes. The interest of using FEMLAB 3.1© is that the user can integrate application specific equations that describe the physics of the problem by modifying the FEM code using a MATLAB© language interface to add the desired formulation [4]. Some FEM schemes investigated in this work are based on formulations used by FEMLAB 3.1©. These include:

- A static mechanical FEM implementation,
- A dynamic mechanical FEM implementation,
- A magnetostatic FEM implementation , and,
- A time-harmonic electromagnetic FEM implementation.

In addition to those four implementations, a three-dimensional, static, fully coupled MMFEM implementation and a three-dimensional, dynamic, fully coupled, EMMFEM

implementation are introduced. The static MMFEM implementation is a coupled version of the static mechanical FEM implementation and the magnetostatic FEM implementation. The dynamic EMMFEM is coupled version of the dynamic mechanical FEM implementation and a non-coupled dynamic electromagnetic FEM implementation yet to be developed on FEMLAB 3.1©. Both coupled FEM schemes are inspired by existing schemes discussed in section 1.4.

On FEMLAB 3.1©, an FEM implementation is input either in the ‘differential’ form or in the ‘weak’ form of the Boundary Value Problem (BVP). For coupled multi-physic FEM, the ‘weak’ form of the BVP is often the easiest to implement on FEMLAB 3.1© [4]. Each FEM implementation discussed in this work is based on a BVP in the ‘differential’ form given in Chapter 2 and in the ‘weak’ form given in Chapter 3 when required. Chapter 4 describes the implementation methods on FEMLAB 3.1© and Chapter 5 validates the FEM implementations by comparison of simple models to standard computational analysis or experimental results.

1.1. Scope of the Objective

The work presented in this thesis, in accordance with the above-mentioned objectives, pertains to either static or dynamic behavior. Although a time-harmonic, electromagnetic FEM implementation is used to study the magnetic circuit of the magnetostrictive-based applications, attempts to create a fully-coupled, time-harmonic, EMMFEM implementation were unsuccessful. Some necessary assumptions used in the derivation of the time-harmonic electromagnetic FEM implementation, when used in a coupled

multi-physic model, resulted into a form of the BVP which could not be reduced to a weak form needed for implementation on FEMLAB 3.1© [1].

In this section, general assumptions and modeling considerations for various FEM implementations are given. These include: (1) the description of the physics behavior at the macroscopic continuum level, (2) the linearization of the coupled constitutive equations of a magnetostrictive material in the coupled MMFEM & EMMFEM implementations, (3) the use of small deformation theory in mechanical FEM implementations, and (4) the effect of various hysteresis loss mechanisms.

In the implementations presented in this work, the modeling is at a macroscopic continuum level, implying that magnetic quantities, such as magnetization and magnetic induction, are volume average quantities. As a result, the implementations are not intended to model microscale magnetic and magnetostrictive details such as magnetic and elastic domains configuration. Instead, the magnetostriction is modeled using an empirical linear model extrapolated from experimentally obtained characterization curves. The magneto-mechanical coupling behavior of a magnetostrictive material is non-linear over a large range of magnetic field or mechanical stress. When modeling devices in which the maximum peak-to-peak value of these quantities are significantly small with respect to the non-linearity observed, linearized coupled constitutive equations are used in the BVP. The term ‘non-linear’ when referring to a dynamic coupled MMFEM or EMMFEM refers only to the nonlinear coupling terms added to the linearized coupled mechanical constitutive equation to account for the magnetic body forces and moments occurring in the magnetostrictive material. In terms of continuum mechanics, the small deformation theory for deformable solids is used in all mechanical and magnetostrictive

implementations by neglecting the second order spatial-differential terms in the strain-displacement relationship. A typical value for the largest achievable magnetostriction in a magnetostrictive material is of the order of 2000 μ strain (peak magnetostriction of Terfenol-D under static conditions) and strain observed in the other structurally involved parts of a magnetostrictive-based device are generally of the same order of magnitude. Therefore, using the theory of small deformation in deformable solids is a valid assumption [5].

There are three major types of hysteresis losses occurring in a magnetostrictive-based application: eddy current power losses occurring in magnetic materials under dynamic conditions, internal structural damping in structurally involved parts, and internal magnetic wall friction creating hysteresis that can be observable in the bidirectional coupled magneto-mechanical interaction of a magnetostrictive material. Eddy current power losses are automatically taken into account when using the general form of the Maxwell's equations as the governing equations of the electromagnetic BVP. This type of power loss only occurs for applications run under dynamic conditions [6].

Internal magnetic wall frictions are microscale magnetic details that create hysteresis power losses when switching the orientation of the magnetic domain configuration. At the present time, this type of hysteresis loss is not completely understood and simple computational models capable of quantifying this phenomenon properly do not exist yet [6]. Some mathematical models using the Preisach operator were developed to predict hysteresis losses by recording the history of the magnetic and mechanical state of the material and using it when computing the new state. The modeling of hysteresis using the Preisach operator is largely developed for ferromagnetism, magnetostriction, shape-

memory alloys and piezoelectric in [7, 8, 9, and 10]. However, the new magnetostrictive material Galfenol used in the devices modeled in this thesis exhibit negligible hysteresis of this type. Consequently, additional matter on the subject and possible addition of a Preisach operator in the implementation introduced are not further discussed.

Hysteresis losses due to internal structural damping are included in the dynamic mechanical FEM implementation under the form of Rayleigh damping coefficients. However, some of the assumptions made to obtain such a formulation make it very difficult to account for such an effect in a fully coupled, dynamic, electro-magneto-mechanical implementation of a magnetostrictive material. Therefore, the fully coupled EMMFEM presented in this thesis does not account for hysteresis losses induced by internal structural damping or, for that matter, by internal wall friction. The extent to which this type of hysteresis loss affects the performance of a magnetostrictive material remains to be studied.

The next three sections will successively present brief accounts from the literature on smart material, magnetostrictive materials, and the existing modeling tools developed to capture their behavior. The approaches adopted in this work to achieve the stated objective are presented in section 1.5.

1.2. Smart Structure

The general definition of a smart structure is a material or combination of materials with the ability to sense external stimuli specific to their functionality and by providing an intended response to these sensed stimuli. In other words, these materials transform one type of energy into another. A large community of researchers is working on the

development of viable forms of such structures for a variety of applications. The sensing of the stimulus, the identification of the proper nature and magnitude of the response, and, the actual manifestation of the response are the three major functions that a smart structure must necessarily perform in addition to providing reliable passive functionality.

In order to use these structures in modern applications, the sensed stimulus must be quantitatively correlated to the desired response to allow proper prediction of the behavior of the structure studied. The concept of a ‘truly’ smart structure or device would include fully integrated sensing, actuation and control functions in a functional material. Such a smart structures have not been fully realized yet, but intermediate technologies such as active and adaptive structures using smart materials, also called ‘coupled’ materials, exist [11].

Nowadays, the smart structure research community focuses extensively on smart materials for their transduction properties which are particularly convenient for characterizing the stimulus-response relationship. The ‘textbook’ smart material is piezoelectric. It is a bidirectional smart material that transforms electrical energy into mechanical energy and vice-versa. In other words, an electrical stimulus induces a mechanical response and a mechanical stimulus generates an electrical response. The transformation of mechanical energy into electrical energy is called the ‘*direct effect*’ and the inverse transformation is called the ‘*converse effect*’. The strict definition of the direct effect is ‘*electric polarization produced by mechanical strain, being directly proportional to the applied strain*’. Similarly, the definition of the converse effect is the appearance of mechanical strain induced by an applied electrical current. Neglecting hysteresis and

temperature effects within the useful strain-voltage transduction region, these two effects are linear and can be modeled using the following coupled constitutive equations

$$S_{ij} = s_{ijkl}^E T_{kl} + d_{kij} E_k \quad (1.1)$$

$$D_i = d_{ikl} T_{kl} + \epsilon_{ik}^T E_k \quad (1.2)$$

where S is the mechanical strain, T is the mechanical stress, E is the electrical field, D is the electric displacement, s is the stiffness matrix, ϵ is permittivity matrix and d is the coupling matrix. The two categories of applications of a smart material are ‘actuators’ and ‘sensors’. Equation (1.1) is the ‘sensor’ equation used to model the ‘*direct effect*’ and equation (1.2) is the ‘actuator’ equation used to model the ‘*converse effect*’ [12]. Both these effects include power losses of various origins, also called hysteresis, which are not taken into account in the constitutive equations presented above. All smart materials exhibit more or less hysteresis in their coupling behavior, making the energy transformation an irreversible process. For piezoelectric materials, the efficiency of energy conversion can be quantified by the ratio of strain energy to electrical energy – about 0.55 for PZT-5H, the most common type of piezoelectric.

Other than piezoelectric materials, the most common types of smart materials used in aerospace, mechanical and naval engineering application include SMA, magnetostrictive and electrostrictive and ER and MR fluids. Each type of coupled material has a unique set of advantages and disadvantages relative to the others depending on their transduction capabilities in specific applications. The diverse nature of potential smart structure applications allows a functional area of application to be identified for each of these materials. In Table 1.1, the most common smart materials are identified and briefly described, their touching on functionality, linearity or non-linearity of their coupling

behavior and existing materials displaying the type of behavior described [13]. Tables 1.2a and 1.2b provide a comparison of smart materials used as actuator (Table 1.2a) and on sensor (Table 1.2b) [13]. In table 1.2b, the ‘linearity’ refers to the linearity of the coupling occurring in the concerned type of smart structure. The ‘embedability’ refers to the ability of the concerned type of smart structure to be used embedded in a structure. The information referring to linearity and embedability is a comparison provided by J. Hubbard during a class oral presentation on smart materials in application operated under dynamic condition [13]

Type of Smart Structure	Energy Transformation	Smart Materials
Piezoelectric	Electrical <~> Mechanical	Cadnium Sulphide
Shape-Memory alloy	Thermic ~> Mechanical	Nickel Titanium
Magnetostrictive	Magnetic <~> Mechanical	Terfenol-D, Galfenol
Electrostrictive	Electrical <~> Mechanical	PMN
Pyroelectric effect	Thermic ~> Electrical & Mechanical	Quartz, Tourmaline
Photoelectric	EM radiation such as light ~> Electrical	Copper Oxide
Photoconductive	Light affect Conductivity	Germanium
Viscoplastic	Magnetic or electric field affect Viscosity	E-R/M-R Fluid

Table 1.1: Most common Smart Materials and their functionality (Data provided mostly from [13], but also from [12] and [14]).

Actuators	Maximum Strain	Linearity	Response(Hz)	Embedability	Cost
Electrostrictive	300	Fair	1-20000	Good	Moderate
Magnetostrictive	2000	Fair	0-20000	Good	Moderate
Piezoelectric Ceramic	200	Good	1-20000	Excellent	Moderate
Shape-Memory alloy	5000	Good	0-5	Excellent	Low
Sensors	Maximum Strain	sensitivity	Linearity	Response(Hz)	Max T°
Strain Gauge	10000	2	Good	0-500000	Good
Magnetostrictive	2000	0.001-0.1	Fair	0-20000	T°>300°C*
Piezoelectric Ceramic	550	0.001-0.01	Good	1-20000	200°C
Shape-Memory alloy	5000	0.1-1	Good	0-10000	300°C

Table 1.2: Smart material comparison chart when used as: (a) an actuator (top); and (b) sensor (bottom) [13] (* 300°C for Terfenol-D, 670°C for Galfenol).

The type of applications in which smart materials are used mostly depends on the transduction properties –actuation or sensing capabilities, magnitude and nature of response, bandwidth, sensitivity– and other material properties unrelated to transduction which may influence the design of any application –stiffness, coefficient of thermal expansion, resistivity, permittivity, permeability. Using the ‘*converse effect*’, smart materials are used as actuators in various types of applications including linear pump mechanism, hybrid motors, servovalves, micropositioner... Using the ‘*direct effect*’, smart materials can either be used as simple sensors –i.e. pressure sensor, strain sensor – or as more innovative applications such as energy harvester, vibration-control systems, health-monitoring systems, sonar systems. Extensive discussion on the various applications of smart materials can be found in introductory books by Banks [15] and Srinivasan [16].

1.3. Magnetostrictive Material

It has been known for more than a century that some ferromagnetic materials exhibit dimensional changes occurring with change in magnetization (Joules effect), and inversely, change in magnetization when subjected to mechanical stresses (Villari effect). This phenomenon is called magnetostriction [6]. For the first half of the twentieth century, the low magnitude of the magnetostriction observed in the available ferromagnetic materials focused the interest of the smart materials and structures community to sensor applications as Nickel-based sonar systems. In the early seventies, the introduction of Terfenol-D, a new material with magnetostriction up to 200 times the one of Nickel, opened the doors to new actuator applications. In the last two decades, the

increased interest for magnetostrictive induced significant progress on the understanding of the origin of the phenomenon, the characterization of the materials properties, and the modeling of the coupled behavior exhibited by these materials. This last decade, the magnetostrictive research community has shown a growing interest in a new promising magnetostrictive material, Galfenol, with peak magnetostriction of $420\mu\text{strain}$ and robust mechanical properties. In this section, the various phenomena observed in magnetostrictive materials such as magnetostriction, characterization curves or hysteresis, are introduced and explained. In addition, a comparison between the main magnetostrictive materials and a short summary of the various applications are given.

1.3.1. Magnetostrictive material behavior

Magnetostriction

The phenomenon of magnetostriction, previously described, can be regarded as an energy transduction (or transformation) from mechanical to magnetic and vice-versa. It can be described as a bidirectional magneto-mechanical coupling between the mechanical and magnetic fields in the magnetostrictive material. The origin of this phenomenon can be traced to the alignment of the magnetic domains inside the material. Figure 1.1 is a schematic of the effect simplified to one dimension [12]. When no magnetic field is applied to the system, the series of domains have randomly oriented magnetic moments. Whereas when a magnetic field is applied, the series of domains rotate to partially align themselves to the magnetic field direction resulting in a change in length Δl . Applying a sufficiently high magnetic field will result in perfectly aligned domains, in which case the material achieves the maximum magnetically induced strain (i.e. peak magnetostriction).

Magnetostriction requires the magnetic domains to be longer in one dimension than the other two to obtain a change in length when the domain rotates, as illustrated in Figure 1.1. This, in general, results in anisotropy of the crystal structure of the material, whether it is body center cubic (i.e. Galfenol) or hexagonal (i.e. Terfenol-D). Because magnetostriction originates from the motion of magnetic domains occurring at a molecular level, range of operation frequencies for a magnetostrictive material goes from static to several kilohertz. Additional information on the role of “anisotropy” in magnetostriction can be found in [14] for Terfenol-D and [17, 18] for Galfenol.

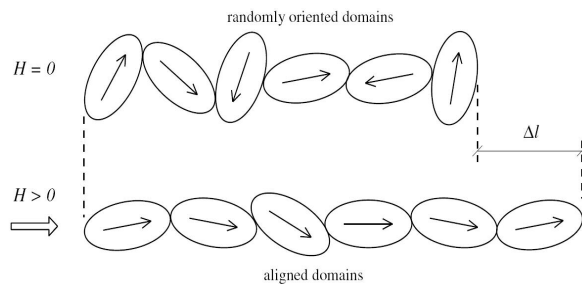


Figure 1.1: Schematics of the magnetostrictive effect [12].

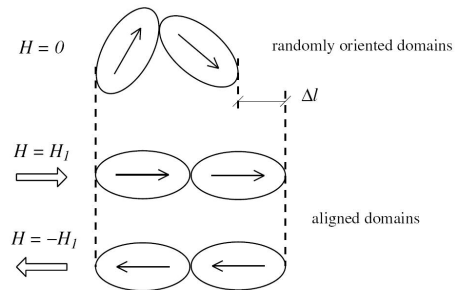


Figure 1.2: Independence of strain on polarity of applied field [12].

Magnetostrictive materials and comparison of magnetostrictive materials properties

James Joules first observed magnetostriction on Nickel in 1842. Later, Cobalt and Iron, along with their alloys, were shown to exhibit the same behavior. The ferromagnetic materials exhibited peak magnetostriction up to 50 μ strain. Alfenol 13 is an example of Iron-Gallium-Aluminum alloy exhibiting such level of magnetostriction. The low saturation strain limited the range of applications to sensor systems. In the first half of the twentieth century, Nickel-based telephone receiver, a sonar transducer and a torque-meter

were among the first devices made using the magnetostrictive effect. Table 1.3 shows properties for Galfenol, Terfenol-D, pure Iron and pure Nickel.

	Terfenol-D ^a	Galfenol ^b	Iron ^{a,d}	Nickel ^{a,d}
Magneto-Mechanical Properties				
3/2 λ_s (μ strain)	1600~2400	150~420	-24	-66
coupling factor	0.7-0.8	0.69-0.76		
Hysteresis in λ -H and B-H curves	moderate	very low	low	low
preferred plane for magnetostriction	<111>	<100>	<100>	<111>
Mechanical Properties				
Modulus of Elasticity (Gpa)	25-35	65	200	207
Ultimate tensile strength (MPa)	28	580	400	500
yield tensile strength (MPa)	28	500	250	140
Magnetic Properties				
Saturation Magnetization (Tesla)	1	1.8	2.2	0.6
relative permeability	2~8	60~360	150~5000	110~600
Magnetic field needed to get 90% of peak magnetostriction (kA/m)	120	8		
Thermal properties				
Temperature dependence of magnetostriction	high	moderate		
Curie Temperature ($^{\circ}$ C)	357	675	1044	627
coefficient of thermal expansion @ room T $^{\circ}$	11	10~12 ^c	12.2	13.1
Other				
raw material cost (\$/g)	0.5	0.08	0.014	
crystallographic structure	hexagonal	bcc	bcc	fcc
electrical resistivity ($\mu\Omega$.cm)	60	120	8.9	6.4

Table 1.3: Property comparison chart between Terfenol-D, Galfenol, Iron and Nickel.

Data from: **a**=> [14], **b**=> [19], **c**=> [20] and **d**=> [21].

Single crystal and polycrystalline structures

Generally, single crystal magnetostrictive alloys serve great purpose in research to characterize the material properties and observe the material behavior in the design stage of the material. However, most applications using magnetostrictive materials use polycrystalline alloy, especially when dealing with macroscale applications due to the lower production cost and a faster production rate with respect to single crystal alloy. In

terms of performance, a strong dependence exists between the orientation of the crystal structure and the magnetostriction phenomenon resulting in smaller peak magnetostriction in polycrystalline alloys where the control over the orientation of the domains is more difficult. Information on the crystallographic structure of magnetostrictive materials are discussed in more detail by R. Kellogg for application to bcc structures (Galfenol) [19] and D. MacMasters for rare-earth magnetostrictive alloys [14].

λ -H curves and Linearized Constitutive Equation for a Magnetostrictive Material

Conversely to piezoelectric, magnetostrictive materials induce strain irrespective of the polarity of applied field. Figure 1.2 explains why the direction of the magnetic field does not affect the strain induced [12]. This effect results in a quadratic-like relationship between magnetostriction and magnetic field and is similar to what occurs in electrostrictive material. Magnetostriction versus magnetic field curves, or λ -H curves, are typical characterization curves often displayed for various levels of applied mechanical stress. Figure 1.3 is a set of λ -H curves measured for Galfenol, an Iron Gallium magnetostrictive alloy discussed in more detail in the next section. These curves are provided by Kellogg [19]. The peak magnetostriction or saturation magnetostriction, highest value of the induced strain, can be read on λ -H curves.

Applying a moderate compressive pre-stress to the sample is a common practice for magnetostrictive materials. It allows orienting the domains normal to the direction of the applied stress and increases the recoverable strain relative to the case with zero pre-stress (see explanatory sketches Figure 1.4 [12]). Too high a pre-stress can only be overcome by a very high magnetic field. A moderate pre-stress is desirable to achieve optimal

transduction performance. Note that the effect of pre-stress on a λ -H curve can be seen in Figure 1.3 [19]. The slope of a λ -H curve is the magneto-mechanical coupling coefficient. Generally, the coupling coefficient is assumed constant over a certain range of applied magnetic fields. For AC applications a biasing field is generally applied to the magnetostrictive sample (see Figure 1.5 [12]). The linearized, uniaxial, one-dimensional, constitutive law for magnetostrictive material is very similar to the one for piezoelectric materials but with magnetic variables. They are given by

$$\mathbf{S} = \mathbf{c}^{\mathbf{H}} \mathbf{T}_{\text{mech}} + (\mathbf{d}^{\mathbf{T}})^{\dagger} \mathbf{H} \quad (1.3)$$

$$\mathbf{B} = \mathbf{d}^{\mathbf{H}} \mathbf{T}_{\text{mech}} + \boldsymbol{\mu}^{\mathbf{T}} \mathbf{H} \quad (1.4)$$

where \mathbf{S} is the mechanical strain tensor, \mathbf{T} is the mechanical stress tensor, \mathbf{c} is the stiffness matrix, \mathbf{H} is the magnetic field tensor, \mathbf{B} is the magnetic induction tensor, $\boldsymbol{\mu}$ is the permeability matrix, and, finally, \mathbf{d} is the magneto-mechanical coupling coefficient. The superscripts (\mathbf{H} and \mathbf{T}) indicate that the coefficients of the matrices concerned are measured under respectively constant magnetic field or constant mechanical stress. For example, $\mathbf{d}^{\mathbf{T}}$, is the magneto-mechanical coupling coefficient measured from λ -H curve with pre-stress of magnitude \mathbf{T} (see Figure 1.3 [19]).

Using a magnetostrictive material as a sensor requires slightly different curves. In this case a plot of the induced magnetic induction (or magnetization) with respect to the applied stress for various magnetic fields is necessary for measuring the sensing coupling factor, $\mathbf{d}^{\mathbf{H}}$. A typical characterization B - T curves for Galfenol is shown in Figure 1.6 [22]. However, the most common way to get this coupling factor is to derive it from the actuator coupling factor, $\mathbf{d}^{\mathbf{T}}$. Another manifestation of magneto-mechanical coupling is the ΔE -effect, a change in elastic moduli accompanying a change in magnetization. An

example of this phenomenon can be seen in Figure 1.7, a plot of the modulus of elasticity with respect to the applied stress for various magnetic field levels [22].

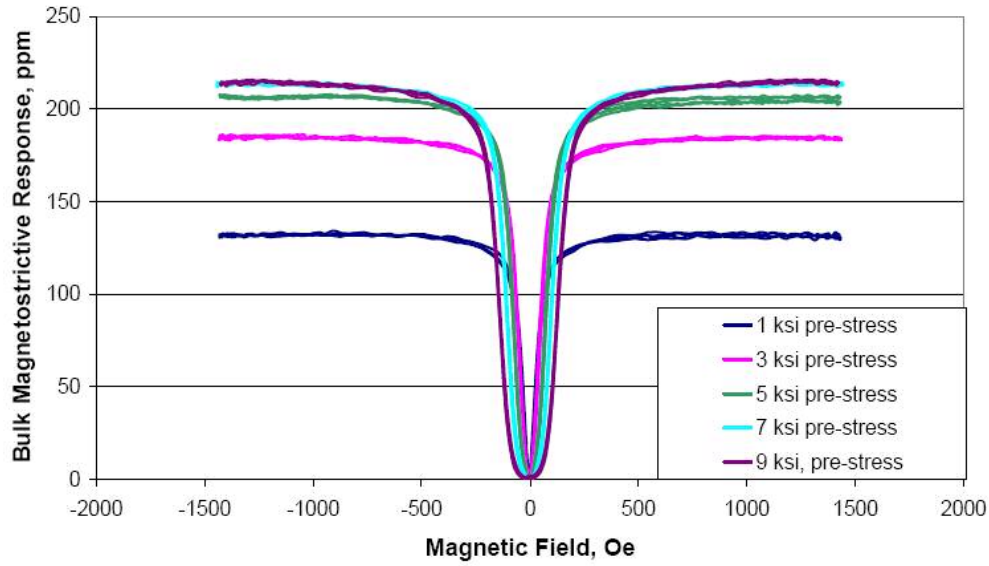


Figure 1.3: Magnetostriction vs Magnetic field curves of 18.4% production grade polycrystal Galfenol for various stress level [56].

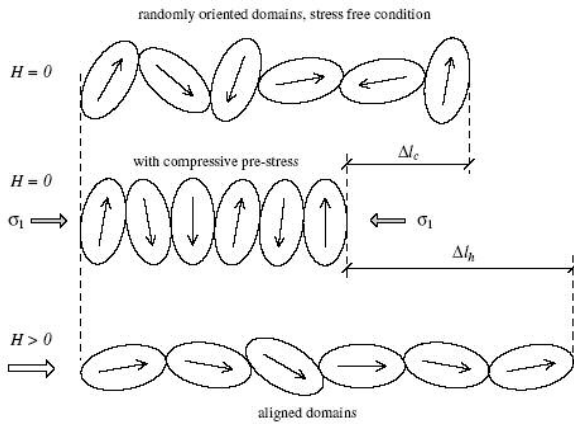


Figure 1.4: Effect of compressive pre-stress on magnetostriction [12].

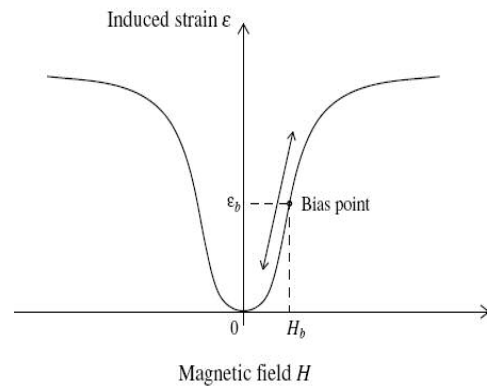


Figure 1.5: Range of application when using a bias magnetic field to operate in a linear region [12].

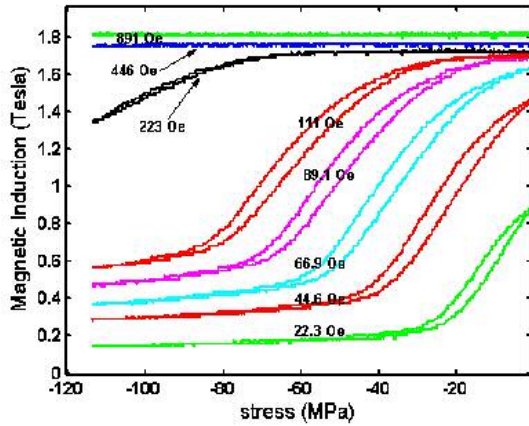


Figure 1.6: Sample magneto-mechanical sensor characterization curves of a 19% Gallium Galfenol sample [22].

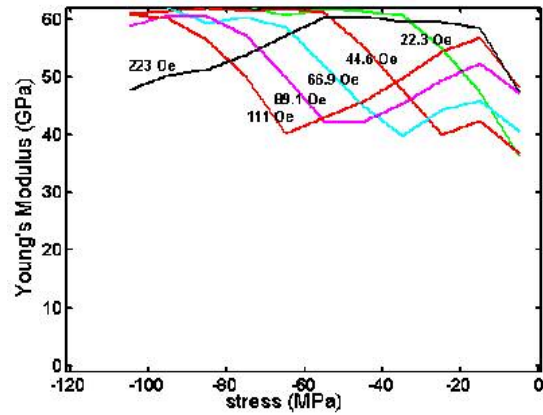


Figure 1.7: Illustration of the Delta-E effect in magnetostrictive Galfenol provided by [22].

B-H curves, M-H curves and Hysteresis

It is very common to see associated with the λ -H curves a magnetic induction, B , versus magnetic field, H , sharing the same x-axis. Since magnetic induction and magnetization are related one to another by

$$\mathbf{B} = \mu_0 \mathbf{H} + \mu_0 \mathbf{M} \quad (1.5)$$

where μ_0 is the permeability of vacuum, the magnetic characterization curve can also be plotted as the magnetization with respect to the magnetic field, in other word an M-H curve. The magnetization is directly linked to the magnetic field by the relationship $\mathbf{M} = \chi_m \mathbf{H}$, where χ_m is the susceptibility. Substituting this equation in (1.5) one can introduce the permeability matrix, $\boldsymbol{\mu}$ such that

$$\mathbf{B} = \mu_0 (1 + \chi_m) \mathbf{H} = \mu_0 \boldsymbol{\mu}_r \mathbf{H} = \boldsymbol{\mu} \mathbf{H} \quad (1.6)$$

where μ_r is the relative permeability. Figure 1.8 is a typical B-H curve for Galfenol coming from the same set of curves as Figure 1.3 provided by [19].

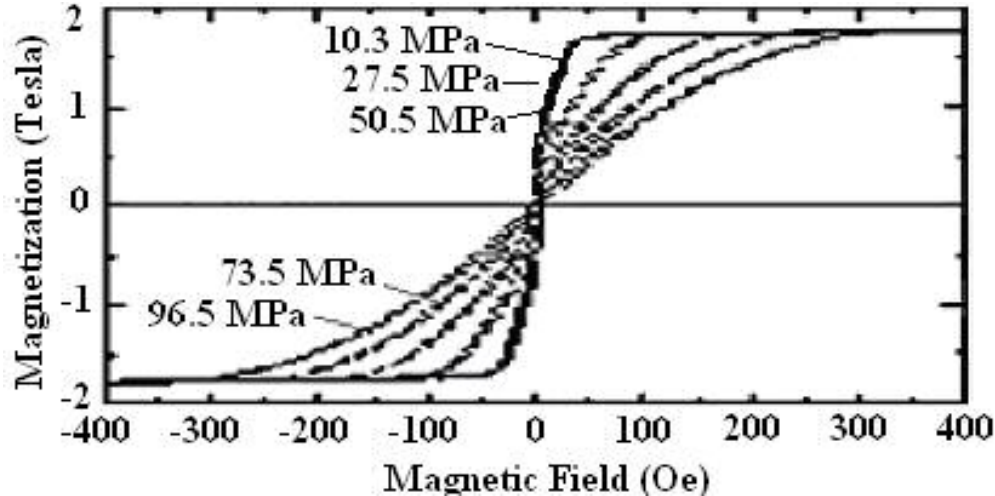


Figure 1.8: Sample magnetic characterization curves for a 19% Gallium Galfenol sample under various compressive stresses at 22°C [19].

When the material is fully magnetized (i.e. the magnetic moments are fully aligned with an applied magnetic field), the material has reached saturation magnetization. This can be observed on Figure 1.8 as the maximum magnetization magnitude. When characterizing the magnetic or magneto-mechanical behavior of a magnetostrictive material, the point at the origin corresponds to a demagnetized minimum length state for a given pre-stress. Then a field is applied up to saturation, beyond which increases in magnetic field do not cause increases in either magnetization or magnetostriction. Once saturation magnetization (and saturation magnetostriction) is reached, the magnetic field is lowered to its equivalent negative value and back to the positive value to complete the loop.

The very reproducible gap between the curves generated when increasing and decreasing the applied magnetic field is commonly named hysteresis loops & is associated with irreversible losses. The main source of hysteresis losses in an M-H or B-H curve is the work necessary to reorient the magnetic domains in the magnetostrictive material. Along with internal damping, this loss mechanism is another significant source of hysteresis in magneto-mechanical characterization curves (see area between the top and bottom λ -H curves for a single pre-stress on Figure 1.3 to visualize hysteresis). This type of hysteresis is independent of the bandwidth at which the material is driven. Under dynamic conditions, an additional type of hysteresis associated with eddy currents, occurs in all magnetizable materials including magnetostrictive materials. This will be discussed in more detail later in this section.

Other important information contained in B-H curve and M-H curves are values for saturation or peak magnetic induction, \mathbf{B}_s , saturation magnetization, \mathbf{M}_s , remanent magnetic induction, \mathbf{B}_R , and remanent magnetization, \mathbf{M}_R . The remanent values are the value of the magnetic induction (or magnetization) where the curve going from positive to negative peak magnetic induction (or magnetization) crosses the $\mathbf{H}=0$ axis.

Magnetic circuit, electromagnetic coupling and the demagnetization effect

The physics of magnetic and electric phenomena are very similar and connected. The Maxwell equations govern both types of physics couple electric and magnetic fields of a magnetic circuit. The Maxwell equations are inseparable except under static conditions. For example, a magnetic circuit made of permanent magnets generates no electric field. Under any type of dynamic conditions (i.e. quasi-static, time-harmonic or simply dynamic), magnetic and electric fields are strongly coupled. The most common

electromagnetic coupling is the one used to drive any magnetostrictive-based actuator: a driving coil generates a sinusoidal magnetic field by applying a time-harmonic electrical current.

An important part of the design of a device using a magnetostrictive material is the design of the magnetic circuit. To get an efficient magnetic circuit, high permeability materials such as 1018 steel are used to complete a loop between both ends of the magnetostrictive rod. For example, a common actuator design is to have a magnetostrictive rod surrounded by a driving coil surrounded itself by a high-permeability material housing. End caps link each end of the magnetostrictive rod to the high-permeability housing. This way the path of the magnetic flux generated by the driving coil run through the magnetostrictive material and is directed through the end-caps and the high permeability housing, completing a magnetic loop. In a similar fashion to an electric circuit, the high-permeability material serves as a conductor for the magnetic flux path. The geometry of the magnetic circuit and the material used along with the driving coil design are important factors in the design of magnetostrictive-based applications.

Another type of electromagnetic coupling almost simultaneously generates losses. An example of this type of power loss is explained by an electrical current generated in circles on the plane around the direction of the applied field. This electrical current generates in turn an induced magnetic field that opposes the originally applied magnetic field. This induced magnetic field depends on the magnitude of the original field, the driving frequency, and, the shape and permeability of the material used. This effect

applies to magnetizable materials and therefore to magnetostrictive materials. It is called eddy current power losses.

A last consideration to take into account regarding magnetic circuits is the demagnetization effect. Consider two poles creating a magnetic field between the pole faces. The magnitude of this magnetic field depends on the pole strength, the distance between the poles and the permeability of the material between the poles. The introduction of a ferromagnetic material between the two poles that does not completely occupy the volume will result in a discontinuous magnetic field as the magnetic flux passes through both air and the ferromagnetic material. The magnetic field produced by this new material will alter the previously existing magnetic field. This phenomenon arises because of demagnetization effects and depends on the shape and the permeability of the material added to the system.

The most common unit systems that exist to define magnetic quantities are the Gaussian system or CGS system and the SI-Kennelly system. Both types of units for magnetic quantities are given with their conversion factors in Table 1.4.

Quantity	CGS Units	Conv. factor	SI Units
Field H	Oersted (Oe)	79.58	(A/m)
Induction B	Gauss	$1 \cdot 10^{-4}$	Tesla (T)
Magnetization M	emu/cc	1000	(A/m)
Flux Φ	Maxwell	$1 \cdot 10^{-8}$	Weber (W_b)

Table 1.4: Unit system and conversion factors for magnetic quantities.

Temperature dependence and electro-magneto-mechanical coupling

A very common unidirectional coupling effect is the generation of mechanical strain in elastic materials undergoing a temperature change. The relationship is generally linear. The slope of a plot of thermally induced mechanical strain with respect to temperature is

called coefficient of thermal-expansion. This effect may be relevant when the material undergoes a temperature change. Temperature changes are often created in magnetostrictive actuators by the driving coil through resistive heating. Resistive heating is a thermo-electric coupling explained by the reluctance of the material to carrying an electric current. Therefore, although the resistivity of the copper used in a coil is quite low, a certain amount of the electrical energy is transformed into thermal energy through this phenomenon. The effect of resistive heating in a driving coil often results in operating the magnetostrictive material at temperature significantly higher than room temperature. This contributes to the design parameters of a driving coil. Since magnetostriction is sensitive to temperature change as well [14, 23], during measurements of characterization curves, a cooling system is used to counter coil induced increases in temperature. Other forms of thermo-coupling that could potentially affect the design of a magnetostrictive-based application include coupling between material properties and temperature (i.e.: permeability, resistivity and modulus of elasticity). Figure 1.9 shows the temperature dependence of the magnetostrictive effect for Terfenol-D [23].

The coupled behavior of magnetostrictive materials between mechanical, magnetic, electric and thermal fields has various origins. Some of the couplings between the various fields are unidirectional (i.e. thermal expansion: heat induces mechanical strain but strain does not induce heat) and some are bidirectional (i.e. piezoelectric effect). Various coupling effects were described in the previous subsection, some applicable to magnetizable materials and others more specific to magnetostrictive materials. A schematic displaying each type of coupling and their origin is given in Figure 1.10.

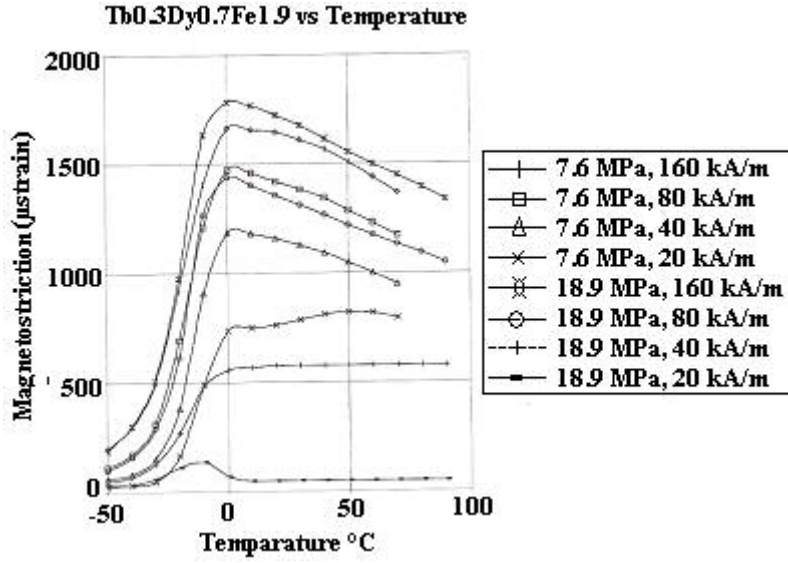


Figure 1.9: Sample λ - T° curves at various temperatures for a Terfenol-D sample [23].

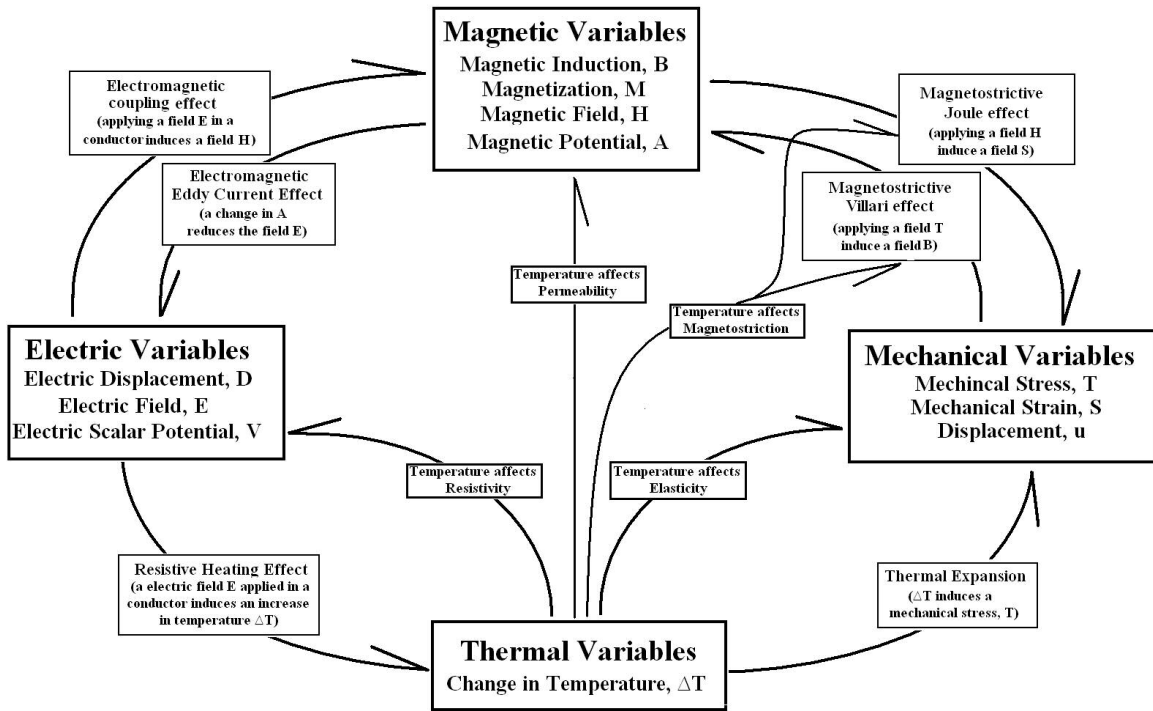


Figure 1.10: Coupling diagram

1.3.2. Terfenol-D, Galfenol and other magnetostrictive materials

Terfenol-D and other Rare-Earth Alloys

The most popular giant magnetostrictive material is the crystalline form of Terfenol-D, an alloy made of iron (Fe) and two rare earth elements terbium (Tb) and dysprosium (Dy). Discovered in the early seventies by Clark and coworkers, it generated a large interest because of its large magnetostriction of up to $2000\mu\text{strain}$ (second best after SMA) over a broad range of application frequencies combined with a low magnetic anisotropy. The stoichiometry of Terfenol-D can be represented as $\text{Tb}_x\text{Dy}_{1-x}\text{Fe}_y$, where $0.27 \leq x \leq 0.30$ and $1.9 \leq y \leq 1.95$. Small changes in stoichiometry have a major influence on the magnetic, elastic and magnetostrictive properties of the alloy. A small decrease in Iron content reduces brittleness significantly but also decreases the magnetostriction. Increasing x above 0.27 improves magnetostriction at lower fields and results in more efficient energy transduction. Terfenol-D's magnetostriction comes from the rare earth alloys which are very magnetostrictive but have low Curie temperatures, below room temperature. The iron is used to raise the Curie temperature to a reasonable level for application in the industry. The Curie temperature of rare-earth magnetostrictive materials averages 380°C .

The mechanical properties of the polycrystalline form of Terfenol-D are also a limiting design factor. The brittleness of the material and the low ultimate tensile strength requires the material to be used in compression only. Finally, Terfenol-D exhibits a fairly large hysteresis mostly due to magnetic wall friction. Other rare-earth magnetostrictive alloys include TbFe_2 and DyFe_2 but their large magnetic anisotropies limit their practical

applications. The two most common manufacturing processes used to manufacture Terfenol-D are the Free Standing Zone Melt (FSZM) Bridgman (BG) method. The material is available in multiple forms including solid and laminated rods, powder or thin films. Original work on these binary and ternary magnetostrictive alloys includes many papers by Clark [24-28] and are resumed and discussed in the “Handbook of Giant Magnetostrictive Material” by Engdahl [14].

Galfenol

Neither Terfenol-D, Iron nor Nickel possesses the combined desired properties of mechanical toughness and appreciable magnetostriction capability simultaneously. The large gap in saturation magnetostriction (15 μ strain for Iron, 45 μ strain for Nickel, 2000 for Terfenol-D) and the low tensile strength of Terfenol-D (~28MPa) has motivated recent research on magnetostrictive materials to principally focus on a fairly new promising material, Galfenol. Galfenol is a Gallium substituted α -Iron alloy exhibiting a peak magnetostriction of up to 420 μ strain capable of handling tensile stresses up to 440 MPa [19, 29]. Its crystallographic structure is body centered cubic where the Gallium atoms are randomly distributed among the Iron atoms.

The attractive features of Galfenol include: a ‘ductile’ behavior (although brittle fracture may occur under certain condition), a low magnetic field requirement (~200 Oe) to achieve saturation magnetostriction [19], very limited temperature dependence of properties between 20° C and 80° C, a high Curie temperature (~675°C) [19,30,31], the possibility of build-in pre-stress to operate in tension [32] and “in plane” auxetic properties in the <110> direction (i.e. negative poisson ratio) [19]. Moreover, Galfenol is not toxic and does not require special handling during the manufacturing process. The

most common manufacturing process of Galfenol is the Bridgman technique but investigation on more efficient production method are currently under investigation at ETREMA products, Inc., DRDC, and the University of Maryland [33].

Since Galfenol has a relatively high permeability, the material is easy to fully magnetize but is also susceptible to eddy current power losses occurring under dynamic operations. The low hysteresis exhibited by Galfenol under quasi-static conditions suggest that most of the hysteresis witnessed under dynamic operating conditions can be attributed to eddy current power losses. Therefore, in the design of a Galfenol-based application, measures are taken to limit eddy current power losses. Laminating the material and designing an optimized magnetic circuit, are often the key to optimal dynamic performance.

Characterization curves for magnetostrictive materials are typically measured by holding one independent variable constant while slowly varying the other (i.e. stress is held constant as field varies to generate λ -H curves). The amount of data necessary to fully characterize a material is large. Moreover, the optimal stoichiometry of Galfenol has not yet been determined and will probably vary with different applications. Therefore, part of the research effort consists of measuring characterization curves for various stoichiometries and crystal structures. The data points in Figure 1.11 represent magnetostriction measured for different stoichiometries of Galfenol with 10 to 35% atomic Gallium content single crystal. Most of the figures presented in this section are for a 19% Gallium Galfenol samples.

ETREMA products, Inc., now produces two types of polycrystal Galfenol, a “research grade” and a “production grade”. The main difference between the two types of

polycrystalline Galfenol is that the research grade was grown slower and therefore orientation of the crystal structures are closer to the preferred axis of magnetostriction. Additionally, current efforts on the metallurgy side of the research on Galfenol include various visualization techniques of domain orientations [34] and optimization of rolling techniques [35].

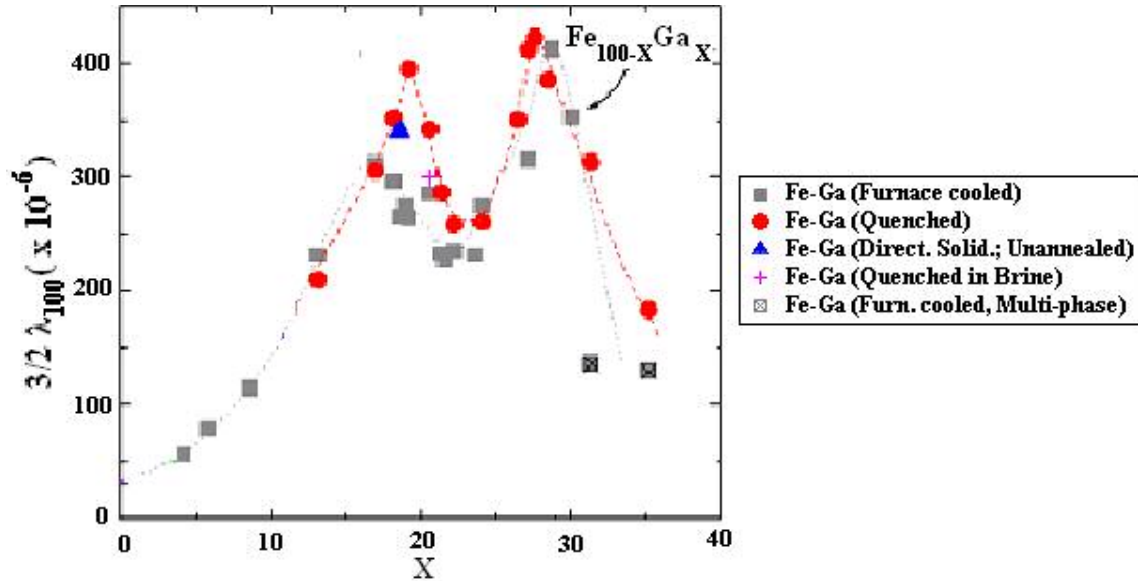


Figure 1.11: Magnetostriction versus Gallium content in single crystal Galfenol [17].

1.3.3. Applications

There are two types of applications for magnetostrictive materials: actuators or sensors. Magnetostrictive-based actuators usually have an electrical coil shaped in a solenoid form around a magnetostrictive rod. The coil transforms electrical energy into magnetic energy and the magnetostrictive rod is use to convert magnetic energy into mechanical energy. Optimization of the design of a magnetostrictive actuator includes the design of the magnetic circuit and driving coil. Generally, a driving coil is used to provide a superposition of the appropriate uniform bias field and time-harmonic applied field in the

sample. Sometimes permanent magnets are preferred to provide the bias field. The driving coil must also be properly design with respect rated voltage and current and with respect to the dielectric strength of comprising insulation materials. A good magnetic circuit must provide a uniform distribution of the magnetic field passing through the magnetostrictive rod as well as limited eddy current power losses. This is done by completing the magnetic circuit using a housing made of a high-permeability material as mentioned in section 1.3.1. The stiffness of the force outlet, mechanical transmission, and, actuator fixture and pre-stress system, have to be designed to optimize the structural performance of the application. A cooling system is also generally required to match the overall heat generation and internal heat transfer during operation. Finally, the total weight of the actuator is often an issue.

Magnetostrictive-based sensors use a piece of magnetostrictive material to transform a mechanical strain into a change in magnetization permeability and reluctance of the material as well as a change in the surrounding magnetic field. A pick-up or sensing coil, a GMR sensor or a Hall probe can be used to read the change in magnetic state. As with actuators, a good magnetic circuit design can be very beneficial. Modeling tools can prove to be very handy to correlating the magnetic field read by the pick-up coil, GMR sensor or Hall probe to the magnetic state of the magnetostrictive material, and in turn correlating that for strain and force applied to produce the magnetic state change.

Magnetostrictive-based applications are extensively detailed in the ‘Handbook on Giant Magnetostrictive Material’ by Engdahl [14] and can be grouped as followed:

- Sound and vibration sources systems including:

- Acoustic underwater systems using magnetostrictive transducers (such as the Tonpilz transducer design) are found in geophysical surveying and exploration, ocean tomography, mine clearance, underwater information exchange, underwater sonar systems.
- Sound systems using magnetostrictive transducers as broadband vibration sources are found in speakers and laboratory and industrial shakers.
- Vibration control systems using either the infinitely soft or the infinitely stiff modes of vibration control take advantage of the controllability of the magnetostrictive material.
- Direct motional control systems use the high strain and force capability of magnetostrictive, ideal for in micromotional control, in applications including: diesel engine fuel injectors, laser optical scanning systems, astronomical image stabilizing platform, movie film pin registration, and ¼ inch magnetic tape head positioner.
- Non-direct motional control systems take advantage of the possibility of applying a magnetic field from a distance with no wire or structure connected to the magnetostrictive material. Applications include linear motors, fast-response valve actuator, fast servo valves, pumps, and rotary motors.
- Material processing systems can use either direct interaction of a magnetostrictive actuator or sound penetration. Ultrasonics high-frequency, high-power actuator used in medical, dental, petrochemical, sonochemical applications. Application includes:

- Physical treatment such as ultrasonic cleaning, cell disruption and sterilization systems, ultrasonic friction welding, emulsification, deemulsification, and foaming systems, and, mixing, vibration and boundary layer control systems.
- Chemical treatment such as petroleum production and processing, chemical reaction, sonochemistry processes (i.e. chemical synthesis, emulsification, emulsion breaking, catalysis, food processing).
- Electromechanical converter such as energy-harvester systems used the magneto-mechanical coupling to transform one form of energy to another.
- Sensor systems include various type compressive force, moment and torque non-contact sensors and also sonar systems. The possibility to extend the various types of sensors to applications in tension using the capabilities of Galfenol is currently under investigation [36].

1.4. Modeling Magnetostrictive Materials

Several models of various complexity have been developed based on the linearized piezomagnetic coupled constitutive equations, (1.3) and (1.4). Early models were based on finite difference approaches, a simple method that is very compliant and suitable for use in modeling structures made of dissimilar materials such as most smart structures. Engdahl and Svensson [37] introduced a simple, uncoupled finite difference analysis to predict steady response of magnetostrictive rod due to an applied sinusoidal magnetic field using linear material characteristic. Kvarnsjo and Engdahl [38] developed a 2-D

finite difference transient analysis for modeling responses to a magnetic field using nonlinear material characteristics.

The effective dynamic coupling constants of a magnetostrictive actuator were established by Claeysen *et al.* [39] using a three-dimensional, coupled, linear finite element analysis based on an empirical representation of the material characteristics. Carman and Mitrovic [40] formulated a coupled one-dimensional non-linear finite element analysis using a phenomenological constitutive model for magnetostrictive actuator that showed good agreement with test data for high preload. However, it did not take into account saturation effects. These type of effects were incorporated along with thermal effects in a more comprehensive models by Hom and Shanker [41], and Duenas *et al.* [42]. Dapino *et al.* [43] developed a coupled nonlinear and hysteretic magneto-mechanical model for magnetostrictives providing an accurate representation of the bi-directional coupling between the magnetic and elastic states. The magnetostrictive effect is modeled by taking into account the Jiles-Atherton model of ferromagnetic hysteresis in combination with a quartic magnetostriction law.

3-D magneto-mechanical FEM models have been developed for static and ultrasonic applications of Terfenol-D using commercial codes such as ATILA and using personal FEM codes. The formulations currently available in commercial codes do not seem to properly capture the behavior of the active material [44, 45]. Stillesjö and Engdahl [45] proposed a 3-D model for a laminated rod that uses an effective magnetic field and magnetic induction accounting for the eddy currents power loss. Kannan [46] introduced the effect of the Maxwell stress tensor and modeled the material behavior by incremental constitutive equations based on the magnetic field. Perez-Aparicio and Sosa [1]

developed a fully coupled, dynamic, 3-D FEM model that uses the displacement vector, the magnetic vector potential and the electric scalar potential as independent variables, and includes eddy current power losses. This FEM is proposed in the Galerkin form and is implemented on commercially available software, FEAP.

More application-specific models include Anjanappa *et al.* [47, 48] who introduced a simple 1-D model simulating the behavior of a magnetostrictive mini-actuator. Wu and Anjanappa [49] and Krishnamurthy *et al.* [50] developed a simple rule of mixture model to calculate the response of magnetostrictive particulate composite. Flatau *et al.* [51] discussed on the effect of material characterization, design consideration, underlying physical processes that occurs during fabrication and structural health sensing, in magnetostrictive composites. In addition, Pradhan *et al.* [52] developed “first shear deformation theory” to study vibration control of laminated composite plate with embedded magnetostrictive layers. The effects of the material properties and placement of magnetostrictive layers on vibration suppression were examined.

1.5. Outline of Approach and thesis

Work presented in this thesis is based on existing structural, electromagnetic and coupled models at the macroscopic continuum level. All models are implemented in the commercial software FEMLAB 3.1 ©. The interest of using FEMLAB© is that the user can integrate application specific equations that describe the physics of the problem by modifying the FEM code using a MATLAB© language interface to add the desired formulation. Pre-existing modules of structural mechanics and electromagnetics (along with many others) are available and can be used in the construction of multi-physics

problems. Generally, multi-physics problems are implemented using the weak form of the boundary value problems.

All BVP formulations used in this thesis are presented in chapter 2 in the direct form. The formulation differs for various conditions so more than one formulation is given for each type of model. Implementations of multi-physics problems capturing the behavior of magnetostrictive material on FEMLAB 3.1 require “weak” form formulations of the BVPs. This is introduced in Chapter 3. The weak form formulation of the fully coupled electro-magneto-mechanical models is close to the one developed by Aparicio and Sosa [1], but the FEM used in this thesis is not based on the Galerkin form. Note that the coupled model presented in this thesis is intended for magnetostrictive materials that exhibit low hysteresis as it currently does not account for losses due to effects other than those due to eddy currents. Chapter 4 explains how to implement the presented models on FEMLAB, what kind of data can be obtained and how to process the results. Sample models for each formulation introduced are given in Chapter 5 and compared to experimental results. Finally, Chapter 6 summarizes the work presented and concludes with possible suggestions for future work on the three-dimensional and time-dependent modeling of magnetostrictive-based applications.

Chapter 2: Differential Formulation of the Governing Equations

This chapter's goal is to provide the Boundary Value Problem (BVP) governing the mechanical field in structurally involved transducer components and the electric and magnetic fields in the magnetic circuit at the macroscopic continuum level. A BVP captures a physical behavior of a material with a set of differential equations (i.e. mechanical, magnetic, and thermic). The set of differential equations consists of a governing equation, subsidiary condition(s), constitutive relation(s) and boundary condition(s). The various BVPs are given in their most general form, usually for applications under dynamic conditions, and then simplified to capture applications under other conditions (i.e. static). Similarly, modifications based on different types of materials (i.e. magnetizable materials) are introduced to obtain simpler, more efficient BVPs. Therefore, more than one BVP is presented for each type of physics. Eventually, in order to obtain a BVP capturing the coupled electro-magneto-mechanical behavior of a magnetostrictive material, mechanical and electromagnetic BVPs are modified and magneto-mechanical coupled constitutive equations are introduced. As explained in the last chapter, a coupled BVP can later be modified into a weak form suitable to implement a Finite Element model (FEM) on FEMLAB 3.1. This will be the topic of Chapter 3. All equations provided in this chapter are given in three-dimensions, often simplified in matrix form.

2.1. The Mechanical Governing Equation

2.1.1. The non-coupled, purely mechanical, Boundary Value

Problem

The mechanical BVP includes various independent and dependant variables. The independent variables are the “x”, “y”, and, “z” components, u , v and w , of the displacement vector,

$$\mathbf{u} = \begin{bmatrix} u \\ v \\ w \end{bmatrix} = [u \quad v \quad w]^t \quad (2.1)$$

In this thesis, the variables in *italic* are scalars and the variables given in **bold** are vectors or matrices. As for the superscript notation “t”, it is to denote the transpose of the matrix concerned. The mechanical dependent variables used in the equations of the BVP are the components of the strain tensor, \mathbf{S} , and the stress tensor, \mathbf{T} . Both the stress tensor and strain tensor are symmetric 3x3 matrices, which can be written as

$$\mathbf{T} = \begin{bmatrix} T_1 & T_{12} & T_{13} \\ T_{21} & T_2 & T_{23} \\ T_{31} & T_{32} & T_3 \end{bmatrix}; \quad T_{12} = T_{21}; \quad T_{13} = T_{31}; \quad T_{23} = T_{32} \quad (2.2)$$

where the indices 1, 2, and 3 refers to the direction of the “x”, “y”, and, “z” axis. A common form of the stress and strain tensors are 6 by 1 matrices written as

$$\begin{cases} \mathbf{T} = [T_1 & T_2 & T_3 & T_{23} & T_{13} & T_{12}]^t \\ \mathbf{S} = [S_1 & S_2 & S_3 & S_{23} & S_{13} & S_{12}]^t \end{cases} \quad (2.3)$$

This is the form which is referred to when the symbol \mathbf{S} and \mathbf{T} are used. Other dependent variables can be computed post-processing such as the mechanical energies.

The Mechanical BVP consists of:

- One governing equation, also called equation of motion,
- One subsidiary condition, also called strain-displacement relationship,
- One constitutive equation, also called Hooke's law, and,
- Two boundary conditions types.

The BVP presented in this section along with other more specific structural mechanics BVPs can be found in the FEMLAB structural mechanics module manual [4] or in books on solid mechanics (i.e. [5]).

The Equation of motion

First, consider the governing equation of all continuum mechanics problems, the equation of motion. It is derived from Newton 2nd Law, i.e. the sum of forces (in this case the internal stress and the externally applied forces) equals the product of mass and acceleration (in this case the density since the other terms are per unit of volume). It can be written as

$$\nabla \cdot \mathbf{T} + \mathbf{b} = \rho \frac{d^2 \mathbf{u}}{dt^2} \quad (2.4)$$

where \mathbf{b} is the elastic body force per unit of volume (i.e. gravity), ρ is the mass density, and, d^2/dt^2 is the second order time derivative where t is the time, not to be confused with the transpose superscript notation "t". The symbol, ∇ is define by

$$\nabla = \left[\frac{d}{dx} \quad \frac{d}{dy} \quad \frac{d}{dz} \right]^t \quad (2.5)$$

and is commonly called gradient. The expanded form of the equation of motion can be written as

$$\begin{cases} \frac{\partial T_1}{\partial x} + \frac{\partial T_{12}}{\partial y} + \frac{\partial T_{13}}{\partial z} + b_1 = \rho \frac{\partial^2 u}{\partial t^2} \\ \frac{\partial T_{12}}{\partial x} + \frac{\partial T_2}{\partial y} + \frac{\partial T_{23}}{\partial z} + b_2 = \rho \frac{\partial^2 v}{\partial t^2} \\ \frac{\partial T_{13}}{\partial x} + \frac{\partial T_{23}}{\partial y} + \frac{\partial T_3}{\partial z} + b_3 = \rho \frac{\partial^2 w}{\partial t^2} \end{cases} \quad (2.6)$$

Since equation (2.4) includes a second order time derivative in this governing equation, one may introduce the velocity \mathbf{v} given by

$$\mathbf{v} = \frac{\partial \mathbf{u}}{\partial t} \quad (2.7)$$

By using equation (2.7), one can write an expanded equation of motion of the form

$$\nabla \cdot \mathbf{T} + \mathbf{b} = \rho \frac{d\mathbf{v}}{dt} \quad (2.8)$$

Generally, equation (2.7) associated with equation (2.8) are preferred to equation (2.4) alone to implement mechanical BVP in FEM software like FEMLAB 3.1©, which does not solve second order time differential terms directly. In the case of the study of a structure under static loading, the velocity vector vanishes and equation (2.8) can be reduced to

$$\nabla \cdot \mathbf{T} + \mathbf{b} = \mathbf{0} \quad (2.9).$$

The strain-displacement and stress-strain relationships

The strain-displacement relationship is the subsidiary condition of the continuum mechanic BVP. Under the assumption of small deformation, it can be written as

$$\begin{aligned}
S_1 &= \frac{\partial u}{\partial x} & S_{12} &= \frac{1}{2} \left(\frac{\partial u}{\partial y} + \frac{\partial v}{\partial x} \right) \\
S_2 &= \frac{\partial v}{\partial y} & S_{23} &= \frac{1}{2} \left(\frac{\partial v}{\partial z} + \frac{\partial w}{\partial y} \right) \\
S_3 &= \frac{\partial w}{\partial z} & S_{13} &= \frac{1}{2} \left(\frac{\partial u}{\partial z} + \frac{\partial w}{\partial x} \right)
\end{aligned} \tag{2.10}.$$

When modeling deformations in a solid mechanics application, the design of the application is made such that the stress level remains small enough to stay in the elastic region everywhere in the structure [5]. In this case, a purely elastic material can be modeled using a linear relationship between stress and strains. Post-processing, one will verify that the maximum stress level has not exceeded the material's yield stress, the stress level above which plastic deformation would occur in a non-linear fashion. The stress-strain relationship, a 3-D version of Hooke's law, $T_1 = E_1 S_1$, where E_1 is the modulus of elasticity along the x axis for a 1D problem, can be written as

$$\mathbf{T}_{\text{mech}} = \mathbf{c} \mathbf{S}_{el} = \mathbf{c} (\mathbf{S} - \mathbf{S}_{th} - \mathbf{S}_0) \tag{2.11}$$

where \mathbf{c} is the 6 by 6 stiffness matrix, \mathbf{S} is the total strain, \mathbf{S}_{el} is the elastic strain, \mathbf{S}_{th} is the thermal strain and \mathbf{S}_0 is the initial strain. Note that the term, \mathbf{T}_{mech} denote the stress level induced by a deformation, \mathbf{S}_{el} only. If other sources of strain exist, a structural mechanics problem must be treated by separating the strain into term for each source as was done in the right hand side of equation (2.11). The stiffness matrix can be anisotropic, orthotropic, transversely isotropic, or isotropic depending on the number of planes of symmetry in the material modeled. For example, Aluminum is isotropic (same properties in all direction) and Galfenol is transversely isotropic (isotropic in the 12 plane and anisotropic in the 3 direction). Except for isotropic materials, it is important to use

rotation matrix to orient the material properties correctly in a structural mechanic problem. More detail on rotation matrix and planes of symmetry in materials can be found in “Elasticity in engineering Mechanics” by Boresi [5]. Other source of stress such as the application of an initial pre-stress or magnetic stress will be discussed later in this chapter. Equation (2.11) is usually the constitutive law used in the non-coupled purely mechanical BVP.

Boundary conditions

The boundary conditions (BC) can be of three forms, essential, natural or initial. The essential mechanical BC is formulated as a prescribed displacement \mathbf{u}^* on the surface, $\partial\Omega_u$ whereas the natural is formulated as an applied traction \mathbf{f}^* on the surface, $\partial\Omega_f$. The total surface $\partial\Omega$ is equal to $\partial\Omega_u \cup \partial\Omega_f$ (where the symbol \cup stands for “union” or “+”). The mechanical boundary condition can be written as

$$\mathbf{u}^* = \mathbf{u} \quad \text{on } \partial\Omega_u \quad (2.12)$$

$$\mathbf{f}^* = \mathbf{T} \cdot \mathbf{n} \quad \text{on } \partial\Omega_f$$

(2.13).

where \mathbf{n} is a unit normal vector. Initial BCs are used for time varying problems. They take the form of essential or natural BC but for a specific time such as $\mathbf{u}^*|_{t=0} = \mathbf{u}$. To sum up, Equations (2.7) and (2.8), (2.10), (2.11), (2.12) and (2.13) are respectively the governing equations, the subsidiary condition, the constitutive relation, and the boundary conditions of the mechanical BVP.

Principle of Virtual Work

The principle of virtual work states the virtual work from any variation in internal strain and external load are zero. The total stored energy, W , from external and internal strain and load is

$$W = \int_V \left(\frac{1}{2} (-S_1 T_1 - S_2 T_2 - S_3 T_3 - 2S_{12} T_{12} - 2S_{23} T_{23} - 2S_{13} T_{13}) + \mathbf{u}^t \mathbf{b} \right) dv \quad (2.14)$$
$$+ \int_S \mathbf{u}^t \mathbf{b}_s ds + \int_L \mathbf{u}^t \mathbf{b}_L dl + \mathbf{U}^t \mathbf{b}_p$$

where the subscript V, S, L and P stands for Volume, Surface, Line, and Point. The principle of virtual work states that $dW = 0$ where the “dW” is the variation of W. This will be derived in chapter 3 along with other weak form formulations of BVPs introduced in the chapter [5].

2.1.2. Modified Hooke's Law for Elastic Materials under Pre-stress

In many magnetostrictive devices, an axial pre-stress is applied along the active strain direction of the magnetostrictive materials. To model pre-stresses on a magnetostrictive material, Perez-Aparicio and Sosa [1] used the ‘theory of small displacement superposed upon large’. This method was developed by Hughes [53] and consists of modifying the stiffness matrix \mathbf{c} into a modified stiffness matrix whereby the mechanical stress tensor accounts for the stress due to the strain \mathbf{S} and due to the pre-stress \mathbf{T}_0 . Applied to the constitutive law of the non-coupled mechanical BVP of a purely elastic material, the modified stiffness matrix could be defined by

$$\mathbf{T} = \mathbf{T}_{\text{mech}} + \mathbf{T}_0 = \mathbf{c}\mathbf{S} + \mathbf{T}_0 = \mathbf{c}_{\text{modified}}\mathbf{S} \quad (2.15).$$

In such case, one must use a new 9x1 stress tensor that includes symmetric and skew-symmetric components (i.e. $\{T_1, T_2, T_3, T_{23}, T_{13}, T_{12}, T_{32}, T_{31}, T_{21}\}^t$). The “extra” three rotational components, T_{32}, T_{31}, T_{21} , are added to model the pre-stresses such that the modified stiffness matrix is given by

$$\mathbf{c} = \begin{bmatrix} c_{11} & c_{12} & c_{13} & 0 & 0 & 0 & 0 & 0 & 0 \\ & c_{11} & c_{13} & 0 & 0 & 0 & 0 & 0 & 0 \\ & & c_{33} & 0 & 0 & 0 & 0 & 0 & 0 \\ & & & c_{44} & 0 & 0 & 0 & 0 & 0 \\ & & & & c_{44} & 0 & 0 & 0 & 0 \\ & & & & & c_{66} & 0 & 0 & 0 \\ & & & & & & 0 & 0 & 0 \\ & & & & & & & 0 & 0 \\ & & & & & & & & 0 \end{bmatrix} + \frac{1}{4} \begin{bmatrix} 4T_{01} & 0 & 0 & 0 & 2T_{05} & 2T_{06} & 0 & 2T_{05} & 2T_{06} \\ & 4T_{02} & 0 & 2T_{04} & 0 & 2T_{06} & -2T_{04} & 0 & -2T_{06} \\ & & 4T_{03} & 0 & 0 & 0 & 0 & 0 & 0 \\ & & & T_{02} + T_{03} & 0 & 0 & T_{03} - T_{02} & 0 & 0 \\ & & & & T_{01} + T_{03} & 0 & 0 & T_{03} - T_{01} & 0 \\ & & & & & T_{01} + T_{02} & 0 & 0 & T_{02} - T_{01} \\ & & & & & & T_{02} + T_{03} & 0 & 0 \\ & & & & & & & T_{01} + T_{03} & 0 \\ & & & & & & & & T_{01} + T_{02} \end{bmatrix} \quad (2.16)$$

where the “0” included in the subscript of the pre-stress components serves to differentiate them from the stress component (i.e. T_{03} is the “z”-component of the applied pre-stress). Note that the stiffness matrix in equation (2.16) is transversely isotropic but could very well be anisotropic. For most applications, the only non-zero pre-stress component is T_{03} which significantly simplifies equation (2.16). In the case where no pre-stress is applied, the traditional form of the stiffness matrix can be used. In the rest of this thesis, when pre-stress is non-zero, \mathbf{c} will refer to the modified stiffness matrix given in

(2.16), and \mathbf{T}_{mech} , will refer to the mechanical stress tensor accounting for both strain induced stress and pre-stress (9x1 tensor).

Now, consider the mechanical subsidiary condition, also known as the ‘strain-displacement relationship for small displacement’. To stay consistent with the mechanical stress tensor accounting for the pre-stress in the stiffness matrix, the strain vector \mathbf{S} includes irrotational strain components and rotational strain components, making the strain tensor a 9x1 matrix. The strain-displacement relationship can be written as

$$\begin{bmatrix} S_1 \\ S_2 \\ S_3 \\ S_{23} \\ S_{13} \\ S_{12} \\ S_{32} \\ S_{31} \\ S_{21} \end{bmatrix} = \nabla^s \mathbf{u} = \begin{bmatrix} \partial/\partial x & 0 & 0 \\ 0 & \partial/\partial y & 0 \\ 0 & 0 & \partial/\partial z \\ 0 & \partial/\partial z & \partial/\partial y \\ \partial/\partial z & 0 & \partial/\partial x \\ \partial/\partial y & \partial/\partial x & 0 \\ 0 & \partial/\partial z & \partial/\partial y \\ \partial/\partial z & 0 & \partial/\partial x \\ -\partial/\partial y & -\partial/\partial x & 0 \end{bmatrix} \begin{bmatrix} u \\ v \\ w \end{bmatrix} \quad (2.17)$$

where ∇^s is an operator defined as above and previously used for purely elastic material [53] and for magnetostrictive material [1]. Note that if no pre-stress is applied the rotational strains may be neglected.

2.2. The Electromagnetic Governing Equations

There are many different types of macroscopic electromagnetic boundary value problems. Different types of couplings between the electric and magnetic fields can

occur. The most common is described by a wire with an electric current passing through it that generates a circular magnetic field in the plane perpendicular to the wire. Another common type occurs in dynamic cases and has to do with power losses associated with the formation of a small electric current that opposes to the one originally applied. The only two cases where they can be treated separately are ‘electrostatics’ and ‘magnetostatics’. This is when, respectively, no current, and no magnetic flux, moves inside the volume concerned.

In this section, the most general form of Maxwell’s equations is introduced. Solving them subjected to certain application conditions and boundary condition constitutes the problem of electromagnetic analysis. In this chapter, three main BVPs are introduced: one for the dynamic case, one for the quasi-static, time-harmonic case and one for the magnetostatic case. Many others exist but they are beyond the scope of this thesis. The BVP presented in this section along with other more specific electromagnetic BVP can be found in the FEMLAB electromagnetic module manual [4].

2.2.1. The dynamic electromagnetic boundary value problem

The Maxwell’s Equations

Maxwell’s equations are a set of equations stating the relationship between the fundamental electromagnetic quantities [6]. The governing equation of electro-magnetic phenomena is generally one of the four Maxwell’s equations which can be written, in their most general form, as

$$\nabla \times \mathbf{H} = \mathbf{J} + \frac{\partial \mathbf{D}}{\partial t} \quad (2.18)$$

$$\nabla \times \mathbf{E} = -\frac{\partial \mathbf{B}}{\partial t} \quad (2.19)$$

$$\nabla \cdot \mathbf{D} = q \quad (2.20)$$

$$\nabla \cdot \mathbf{B} = 0 \quad (2.21)$$

where \mathbf{E} is the electric field intensity vector, \mathbf{D} is the electric displacement or electric flux density, \mathbf{H} is the magnetic field intensity, \mathbf{B} is the magnetic flux density, \mathbf{J} is the current density and q is the electric charge density [54]. Equations (2.18) and (2.19) are respectively known as the Maxwell-Ampere's law and Faraday's law. Equations (2.20) and (2.21) are respectively the electric form and the magnetic form of Gauss' law. A fifth equation is generally presented with the Maxwell's equation, the equation of continuity given by

$$\nabla \cdot \mathbf{J} = -\frac{\partial q}{\partial t} \quad (2.22).$$

Electric and Magnetic Constitutive Relations

The general constitutive equations generally associated with the Maxwell's equations are given by

$$\mathbf{D} = \varepsilon_0 \mathbf{E} + \mathbf{P} \quad (2.23)$$

$$\mathbf{B} = \mu_0 (\mathbf{H} + \mathbf{M}) \quad (2.24)$$

$$\mathbf{J} = \sigma \mathbf{E} \quad (2.25)$$

where ε_0 is the permittivity of vacuum, μ_0 is the permeability of vacuum, and σ is the conductivity [4,6]. The permittivity of vacuum and the permeability of vacuum in the S.I. unit system are chosen to be, respectively, $\frac{1}{36\pi} \cdot 10^{-9}$ F/m and $4\pi \cdot 10^{-7}$ H/m. The electric polarization vector, \mathbf{P} , describes how the material is polarized when an electric field, \mathbf{E} ,

is applied. Similarly, the magnetization vector, \mathbf{M} , describes how the material is magnetized when a magnetic field, \mathbf{H} , is applied. Both can be interpreted as volume density of respectively electric and magnetic dipole moments. The electric polarization and magnetization have usually a range in which a linear relationship to, respectively, electric fields and magnetic fields, can be assumed. Certain materials however have non-zero electric polarization and magnetization for no electric or magnetic field applied. A good example of non-zero magnetization for no applied field is a permanent magnet. To accommodate these behaviors the constitutive equations can be rewritten as

$$\mathbf{D} = \varepsilon_0 \varepsilon_r \mathbf{E} + \mathbf{D}_r \quad (2.26)$$

$$\mathbf{B} = \mu_0 \mu_r \mathbf{H} + \mathbf{B}_r \quad (2.27)$$

$$\mathbf{J} = \sigma \mathbf{E} + \mathbf{J}^e \quad (2.28)$$

where ε_r is the relative permittivity, μ_r is the relative permeability, \mathbf{D}_r is the remanent current displacement, \mathbf{B}_r is the remanent magnetic flux density and \mathbf{J}^e is the externally generated current density [4,6]. The constitutive relations used for magnetostrictive materials are coupled with mechanical fields. They will be addressed in the last section of this chapter.

Definition of Electrical and Magnetic Potentials

Subsidiary conditions are equations that relate the independent variables to higher order dependant variables. In a dynamic electromagnetic BVP, it is convenient to use the potential equations as subsidiary conditions. These link the magnetic flux density \mathbf{B} and the electric field \mathbf{E} to a magnetic vector potential \mathbf{A} and an electric scalar V potential as follows:

$$\mathbf{B} = \nabla \times \mathbf{A} \quad (2.29)$$

$$\mathbf{E} = \nabla V - \frac{\partial \mathbf{A}}{\partial t} \quad (2.30)$$

Equations (2.29) and (2.30) are direct consequences of Gauss' Law and Faraday's law [1]. Equation (2.30) couples the electric field to both the electric and magnetic independent variables. The magnetic vector potential \mathbf{A} is a useful computing tool for electromagnetic BVP.

Electric and Magnetic Boundary Conditions

The magnetic BC are either formulated as a prescribed magnetic potential \mathbf{A}^* on the surface $\partial\Omega_A$ or as a prescribed magnetic flux density \mathbf{B}^* on the surface $\partial\Omega_B$. As with the mechanical boundary conditions, $\partial\Omega$ is equal to $\partial\Omega_A \cup \partial\Omega_B$. The magnetic BC can be written as

$$\mathbf{A}^* = \mathbf{A} \quad \text{on } \partial\Omega_A \quad (2.31)$$

$$\mathbf{B}^* = \mathbf{B} \mathbf{n} \quad \text{on } \partial\Omega_B \quad (2.32).$$

Finally, the electrical BC are either formulated as a prescribed electric potential V^* on the surface $\partial\Omega_V$ or as a prescribed surface charge density \mathbf{D}^* on the surface $\partial\Omega_D$, with $\partial\Omega$ equal to $\partial\Omega_V \cup \partial\Omega_D$. The electrical boundary condition can be written as

$$V^* = V \quad \text{on } \partial\Omega_V \quad (2.33)$$

$$\mathbf{D}^* = \mathbf{D} \mathbf{n} \quad \text{on } \partial\Omega_D \quad (2.34).$$

2.2.2. Additional electromagnetic variables

The following electromagnetic quantities may be calculated during post-processing: the magnetization vector, \mathbf{M} , the polarization vector, \mathbf{P} , the magnetic and electric

energies, W_e and W_m , the electric, magnetic, radiative and resistive power, P_e , P_m , P_h and P_r , and the time-average dissipated energy in the magnetostrictive material Q . The first two quantities can be computed using

$$\mathbf{M} = \left(\frac{\boldsymbol{\mu}}{\mu_0} - \mathbf{B} \right) \mathbf{H} \quad (2.35)$$

and,

$$\mathbf{P} = \mathbf{D} - \boldsymbol{\epsilon} \mathbf{E} \quad (2.36)$$

where \mathbf{I} is a 3x3 identity vector [1].

Electric and magnetic energies, W_e and W_m , can be expressed as

$$W_e = \int_V \left(\int_0^{\mathbf{D}} \mathbf{E} \cdot \partial \mathbf{D} \right) dv = \int_V \left(\int_{t_0}^{t_1} \mathbf{E} \cdot \frac{\partial \mathbf{D}}{\partial t} dt \right) dv \quad (2.37)$$

$$W_m = \int_V \left(\int_0^{\mathbf{B}} \mathbf{H} \cdot \partial \mathbf{B} \right) dv = \int_V \left(\int_{t_0}^{t_1} \mathbf{H} \cdot \frac{\partial \mathbf{B}}{\partial t} dt \right) dv \quad (2.38).$$

One may get the electric and magnetic power, P_e and P_m , by taking the time derivative of, respectively, the electric and magnetic energies such that

$$P_e = \int_V \mathbf{E} \cdot \frac{\partial \mathbf{D}}{\partial t} dv \quad (2.39)$$

$$P_m = \int_V \mathbf{H} \cdot \frac{\partial \mathbf{B}}{\partial t} dv \quad (2.40).$$

These energies are related to the resistive and radiative energy by Poynting's theorem [4].

The resistive and radiative energy are respectively given by

$$P_h = \int_V \mathbf{J} \cdot \mathbf{E} dv \quad (2.41)$$

$$P_r = \int_S (\mathbf{E} \times \mathbf{H}) \cdot \mathbf{n} dv \quad (2.42).$$

The Poynting's theorem states

$$-\int_V \left(\mathbf{E} \cdot \frac{\partial \mathbf{D}}{\partial t} + \mathbf{H} \cdot \frac{\partial \mathbf{B}}{\partial t} \right) dv = \int_V \mathbf{J} \cdot \mathbf{E} dv + \int_S (\mathbf{E} \times \mathbf{H}) \cdot \mathbf{n} dv \quad (2.43).$$

The quantity $\mathbf{S} = \mathbf{E} \times \mathbf{H}$ is called the Poynting vector. Using (2.26) and (2.27),

$$\mathbf{E} \cdot \frac{\partial \mathbf{D}}{\partial t} = \mathbf{E} \cdot \left(\frac{\partial \mathbf{D}}{\partial \mathbf{E}} \cdot \frac{\partial \mathbf{E}}{\partial t} \right) = \epsilon \mathbf{E} \cdot \frac{\partial \mathbf{E}}{\partial t} = \frac{\partial}{\partial t} \left(\frac{1}{2} \epsilon \mathbf{E} \cdot \mathbf{E} \right) \quad (2.44)$$

$$\mathbf{H} \cdot \frac{\partial \mathbf{B}}{\partial t} = \mathbf{H} \cdot \left(\frac{\partial \mathbf{B}}{\partial \mathbf{H}} \cdot \frac{\partial \mathbf{H}}{\partial t} \right) = \frac{1}{\mu} \mathbf{H} \cdot \frac{\partial \mathbf{H}}{\partial t} = \frac{\partial}{\partial t} \left(\frac{1}{2\mu} \mathbf{H} \cdot \mathbf{H} \right) \quad (2.45).$$

Therefore equation (2.43) can be rewritten as

$$-\frac{\partial}{\partial t} \int_V \left(\frac{1}{2} \epsilon \mathbf{E} \cdot \mathbf{E} + \frac{1}{2\mu} \mathbf{H} \cdot \mathbf{H} \right) dv = \int_V \mathbf{J} \cdot \mathbf{E} dv + \int_S (\mathbf{E} \times \mathbf{H}) \cdot \mathbf{n} dv \quad (2.46)$$

using (2.44) and (2.45) [1,4,6].

Eddy current power losses

Eddy currents are one of several loss mechanisms in magnetostrictive materials. Eddy currents occur when a dynamic magnetic field is applied to a ferromagnetic material. This electric current forms in planes perpendicular to the magnetic field vectors. In turn, this current creates an opposing smaller magnetic field that ultimately cancels a portion of the originally applied magnetic field. The time-average dissipated energy in the magnetostrictive material Q quantifies the eddy current power losses and is given by

$$Q = \mathbf{J} \cdot \mathbf{E} = \mathbf{J}^e \cdot \left(\nabla V + \frac{\partial \mathbf{A}}{\partial t} \right) + \sigma \cdot \left(\nabla V + \frac{\partial \mathbf{A}}{\partial t} \right) \otimes \left(\nabla V + \frac{\partial \mathbf{A}}{\partial t} \right) \quad (2.47)$$

[1].

Lamination of the ferromagnetic material reduces the cross-sectional area and therefore reduces the eddy current power losses. An alternative to laminations is to increase the electrical resistivity. A magnetostrictive actuator is often comprised of the actuating material surrounded by successively a coil and a highly permeable housing. To complete the magnetic circuit, end caps link the actuating material to the housing. As with lamination, a slit in the housing of a transducer can be used to reduce the strength of eddy currents in the housing by reducing the cross sectional area in which a current can circulate. To sum up by laminating the active material and by introducing a slit in the housing as shown in Figure 2.1, one may drastically reduce the eddy current power losses for device operating at high frequency.

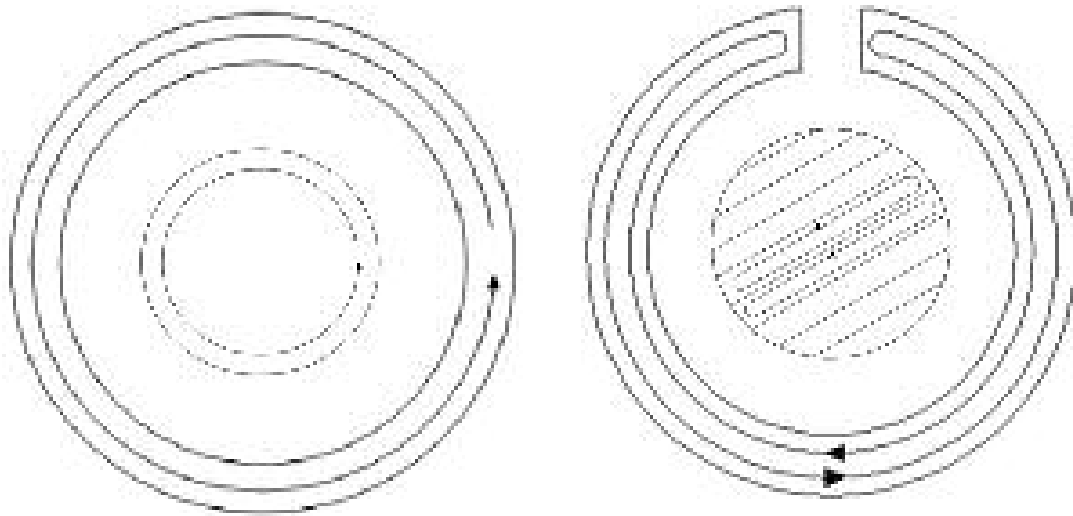


Figure 2.1: Illustration of the effect of reducing the cross sectional area of a magnetizable material to limit eddy current power losses (left: cross section view of a circular rod surrounded by hollow cylinder, right: cross section view of a laminated rod surrounded by a slit hollow cylinder).

2.2.3. Simplification for the magnetostatic and time-harmonic applications

The Magnetostatic cases

There are two approaches to the magnetostatic cases. First one can reduce the Maxwell's equations by removing the time derivatives of the magnetic induction \mathbf{B} and electric displacement \mathbf{D} and the electric field \mathbf{E} . This will eliminate coupling between the magnetic BVP and the electric BVP (i.e. no eddy current power losses) and equation (2.71) becomes $\nabla \times \mathbf{H} = 0$. A new formulation based on a scalar magnetic potential V_m may be defined such that

$$\mathbf{H} = -\nabla V_m \quad (2.48).$$

consequently, the boundary conditions (2.31) become

$$V_m^* = V_m \quad \text{on } \partial\Omega_{V_m} \quad (2.49).$$

In this case the model only applies the magnetostatic case with no current [4,6].

If static current is applied, the second alternative consists of keeping the magnetic vector potential and the electric vector potential. Since it is a static case, any time derivative is equal to zero, which reduces the Maxwell-Ampere's law and the continuity equation to

$$\nabla \times (\mu_0^{-1} \nabla \times \mathbf{A} - \mathbf{M}) - \sigma \mathbf{v} \times (\nabla \times \mathbf{A}) + \sigma \nabla V = \mathbf{J}^e \quad (2.50)$$

$$-\nabla \cdot (\sigma \mathbf{v} \times (\nabla \times \mathbf{A}) + \sigma \nabla V - \mathbf{J}^e) = 0 \quad (2.51)$$

[4]. Note the term $\sigma \mathbf{v} \times (\nabla \times \mathbf{A})$ represents the current generated by a static magnetic field in constant motion. The term $-\sigma \nabla V$ represents the current generated by a static electric field. One may solve (2.50) independently from other equations.

The Quasi-Static approximation

In the Maxwell's equation, the time rate of change of the electric charge density, $\partial \rho / \partial t$, and the time rate of change of the electric displacement, $\partial \mathbf{D} / \partial t$, represent the lag between the changes of the fields induced by a change in sources. This describes the physical phenomenon of a finite speed of propagation of electromagnetic waves. The Quasi-Static approximation considers the speed of propagation to be infinite. In term of quantities, this means $\partial \rho / \partial t$ and $\partial \mathbf{D} / \partial t$ are assumed to be zero. This is equivalent to calculating electromagnetic fields for stationary currents at every instant.

Assuming a geometry moves at a velocity \mathbf{v} relative to a fixed reference system, the force \mathbf{F} per charge q is given by

$$\mathbf{F} / q = \mathbf{E} + \mathbf{v} \times \mathbf{B} \tag{2.52}$$

Therefore the current density is given by

$$\mathbf{J} = \sigma (\mathbf{E} + \mathbf{v} \times \mathbf{B}) + \mathbf{J}^e \tag{2.53}$$

where \mathbf{J}^e is the externally applied current density [4,6, and 54].

The Maxwell's Equations under Quasi-Static Conditions

Setting $\partial \rho / \partial t$ and $\partial \mathbf{D} / \partial t$ to zero in the Maxwell equations and using (2.53),

$$\nabla \times \mathbf{H} = \mathbf{J} = \sigma (\mathbf{E} + \mathbf{v} \times \mathbf{B}) + \mathbf{J}^e \tag{2.54}$$

$$\nabla \times \mathbf{E} = - \frac{\partial \mathbf{B}}{\partial t} \quad (2.55)$$

$$\nabla \cdot \mathbf{D} = \rho \quad (2.56)$$

$$\nabla \cdot \mathbf{B} = 0 \quad (2.57).$$

Using (2.27), (2.29) and (2.30), one can rewrite Ampere's law and the continuity equation as

$$\sigma \frac{\partial \mathbf{A}}{\partial t} + \nabla \times (\mu_0^{-1} \nabla \times \mathbf{A} - \mathbf{M}) - \sigma \mathbf{v} \times (\nabla \times \mathbf{A}) + \sigma \nabla V = \mathbf{J}^e \quad (2.58)$$

$$-\nabla \cdot \left(\sigma \frac{\partial \mathbf{A}}{\partial t} - \sigma \mathbf{v} \times (\nabla \times \mathbf{A}) + \sigma \nabla V - \mathbf{J}^e \right) = 0 \quad (2.59)$$

[4,6].

The Gauge transformation

Before rewriting Maxwell-Ampere's law and the constitutive equation for a quasi-static time harmonic model, one must introduce the concept of Gauge fixing. This is simply a new form of potentials defined as

$$\tilde{\mathbf{A}} = \mathbf{A} + \nabla \psi \quad (2.60)$$

$$\tilde{V} = V - \frac{\partial \psi}{\partial t} \quad (2.61)$$

where ψ can be called the gauge function. The same magnetic and electric field can be obtained from this formulation as that from (2.29) and (2.30):

$$\mathbf{B} = \nabla \times \mathbf{A} = \nabla \times (\tilde{\mathbf{A}} - \nabla \psi) = \nabla \times \tilde{\mathbf{A}} \quad (2.62)$$

$$\mathbf{E} = -\nabla V - \frac{\partial \mathbf{A}}{\partial t} = -\nabla \left(\tilde{V} + \frac{\partial \psi}{\partial t} \right) - \frac{\partial (\tilde{\mathbf{A}} - \nabla \psi)}{\partial t} = -\nabla \tilde{V} - \frac{\partial \tilde{\mathbf{A}}}{\partial t} \quad (2.63).$$

This formulation allows placement of constraints on ψ making the solution unique[4,54].

Whenever a problem is time-harmonic the field can be written using a phasor. The electrical field is therefore given by

$$\mathbf{E}(\mathbf{r}, t) = \hat{\mathbf{E}}_{(\mathbf{r})} \cos(\omega t + \phi) = \text{Re}\left(\hat{\mathbf{E}}_{(\mathbf{r})} e^{j\phi} e^{j\omega t}\right) = \text{Re}\left(\tilde{\mathbf{E}}_{(\mathbf{r})} e^{j\omega t}\right) \quad (2.64)$$

where $\tilde{\mathbf{E}}_{(\mathbf{r})}$ is a phasor that contains the field amplitude and phase information. Note this equation is independent of time. This formulation simplifies the form of the derivative which is

$$\frac{\partial \mathbf{E}}{\partial t}(\mathbf{r}, t) = \text{Re}\left(j\omega \tilde{\mathbf{E}}_{(\mathbf{r})} e^{j\omega t}\right) \quad (2.65)$$

[4,54].

2.3. The Mechanical and Electromagnetic Governing

Equations for Magnetostrictive Materials

2.3.1. Electromagnetic Stress Tensor and Modified Equilibrium

Equation for Magnetizable Material

For a magnetostrictive material, the stress tensor, \mathbf{T} , must include the strain induced stress tensor, the stress tensor due to pre-stress and the stress tensor due to the magnetic field, \mathbf{T}_M , also know as Maxwell's stress tensor. An important issue encountered when modeling a magnetostrictive material is to include an electromagnetic stress tensor \mathbf{T}_M to account for the stress due to the electromagnetic force induced by a magnetic field, \mathbf{H} [36]. In order to account for this force in the equation of motion(2.8), one must split the volumetric body force, \mathbf{b} , into a mechanical volumetric body force, \mathbf{b}_{mech} and an

electromagnetic volumetric body force, \mathbf{b}_{mag} , which, depending of the type of material (i.e. polarizable, magnetizable), can take different forms. Magnetostrictive materials are magnetizable magnetic materials. Therefore, the electromagnetic body force is expressed as,

$$\mathbf{b}_{\text{mag}} = \mathbf{J} \times \mathbf{B} + \nabla \mathbf{H} \cdot \mu_0 \mathbf{M} \quad (2.66).$$

By substituting equation (2.66) into the mechanical equation of motion (2.8), the Maxwell stress tensor can be written as

$$\mathbf{T}_M = \mathbf{H} \otimes \mathbf{B} - \frac{\mu_0}{2} (\mathbf{H} \cdot \mathbf{H}) \mathbf{I} \quad (2.67)$$

where the operator \otimes is the dyadic tensor product. Using equation (2.66), one can rewrite the equation of motion (2.8) as

$$\nabla \cdot (\mathbf{T}_{\text{mech}} + \mathbf{T}_M) + \mathbf{b}_{\text{mech}} = \rho \frac{d\mathbf{v}}{dt} \quad (2.68).$$

A full derivation on how to get (2.67) is given in Kannan [46].

2.3.2. Simplified Maxwell's Equations

A few simplifications can be made for the modeling of magnetostrictive materials. First, because of a lack of capacitance in magnetostrictive material, the electric free charge density q can be dropped when applying Maxwell's equations to the magnetostrictive material. Therefore equation (2.20) reduces to

$$\nabla \cdot \mathbf{D} = 0 \quad (2.69)$$

Note however that the modeling of the magnetic circuit surrounding the magnetostrictive material other parts of the design (i.e. a coil) may require to use equation (2.20) instead of equation(2.69). Second, the electric current density can be separated into

$$\mathbf{J} = \mathbf{J}^e + \sigma \mathbf{E} \quad (2.70)$$

where \mathbf{J}^e is the externally applied volumetric current density and σ is the electrical conductivity [10,12]. Using equation (2.70) in equation (2.18), one gets

$$\nabla \times \mathbf{H} = \sigma \mathbf{E} + \frac{\partial \mathbf{D}}{\partial t} \quad (2.71).$$

The externally applied volumetric current density in equation (2.70) is equal to zero for magnetostrictive material but can be non-zero in the rest of the magnetic circuit (i.e. the induction coil in an actuator design) [1].

2.3.3. The Linearized Coupled Constitutive Equations

The constitutive equations describing a magnetostrictive material are a coupled set of equations linking the mechanical stress and strain tensors to the magnetic field and flux density. These relationships, although nonlinear, can be approximated to a linear formulation for small increments of these quantities. The linearized form of the constitutive equation is given by

$$\mathbf{S} = \mathbf{c}^H \mathbf{T}_{\text{mech}} + (\mathbf{d}^T)^t \mathbf{H} \quad (2.72)$$

$$\mathbf{B} = \mathbf{d}^H \mathbf{T}_{\text{mech}} + \boldsymbol{\mu}^T \mathbf{H} \quad (2.73)$$

where \mathbf{c} is the stiffness matrix introduced in section 2.1, \mathbf{d} is the magneto-mechanical coupling matrix, $\boldsymbol{\mu}$ is the permeability and the superscript t continues to indicate the transpose of the matrix with the superscript. It is a common notation to use the superscript ‘H’, ‘B’, ‘T’ and ‘S’ to indicate that the values inside this matrix reflect conditions under which the parameter in the superscript is a known constant (i.e. \mathbf{c}^H is the stiffness matrix in presence of a constant magnetic field of magnitude \mathbf{H}). These

equations also known as the piezomagnetic constitutive equations for a magnetostrictive material, may be expressed in many ways. Although equations (2.72) and (2.73) are the most common form found in publications on the subject, it may be more convenient to express the mechanical stress and the magnetic field in terms of the strain and the magnetic induction. To do so, one must first rearrange (2.72) into

$$\mathbf{T}_{\text{mech}} = \mathbf{c}^H \left[\mathbf{S} - (\mathbf{d}^T)^t \mathbf{H} \right] = \mathbf{c}^H \mathbf{S} - \mathbf{g} \mathbf{H} \quad (2.74)$$

where $\mathbf{g} = \mathbf{c}^H (\mathbf{d}^T)^t$ the stiffness matrix \mathbf{c}^H is a symmetric matrix. Then, by introducing equation (2.74) in (2.73), the magnetic induction can be written as

$$\mathbf{B} = \mathbf{d}^H \mathbf{c}^H \mathbf{S} + (\boldsymbol{\mu}^T - \mathbf{d}^H \mathbf{g}) \mathbf{H} = \mathbf{g}' \mathbf{S} + \boldsymbol{\mu}^S \mathbf{H} \quad (2.75).$$

where $\mathbf{g}' = \mathbf{d}^H \mathbf{c}^H = \mathbf{d} \mathbf{c}^H = (\mathbf{c}^H \mathbf{d}^t)^t = \mathbf{g}^t$ if $\mathbf{d}^H = (\mathbf{d}^T)^t = \mathbf{d}$, which is a valid assumption for small increment of the independent variables. Similarly, by isolating the magnetic field \mathbf{H} in equation (2.75), one gets

$$\mathbf{H} = -(\boldsymbol{\mu}^S)^{-1} \mathbf{g}' \mathbf{S} + (\boldsymbol{\mu}^S)^{-1} \mathbf{B} = \mathbf{h}^t \mathbf{S} + (\boldsymbol{\mu}^S)^{-1} \mathbf{B} \quad (2.76)$$

where $\mathbf{h}^t = -(\boldsymbol{\mu}^S)^{-1} \mathbf{g}'$. Finally, by introducing equation (2.76) in equation (2.74), one gets

$$\mathbf{T}_{\text{mech}} = \left[\mathbf{c}^H - \mathbf{g} \mathbf{h}^t \right] \mathbf{S} - \mathbf{g} (\boldsymbol{\mu}^S)^{-1} \mathbf{B} = \mathbf{c}^B \mathbf{S} - \mathbf{h} \mathbf{B} \quad (2.77)$$

where $\mathbf{c}^B = \left[\mathbf{c}^H - \mathbf{g} \mathbf{h}^t \right]$. Equations (2.76) and (2.77) are the two forms of the constitutive equations that will be used in the weak form formulation of the coupled problems. An additional constitutive equation linking the electrical field to the electric displacement is necessary for the dynamic model.

2.3.4. Summary of the BVP capturing the behavior of a Magnetostrictive Material

To conclude this chapter let me sum up the equations used in the BVP capturing the macroscopic behavior of a magnetostrictive material under dynamic applications. The Mechanical governing equations used for magnetostrictive materials or any other type of elastic materials are the equation of motion (2.8), which is often associated to (2.7) get a first order differential equations. The mechanical subsidiary condition is also the same as for a regular elastic material. It is the strain-displacement relationship introduced in equations (2.10). The electric and magnetic governing equations for magnetostrictive materials under dynamic application are, respectively, equations (2.69) and (2.71) as introduced earlier in this section. Electric and magnetic subsidiary conditions are the potentials equations (2.29) and (2.30). Finally the coupled constitutive relations used are equation (2.76) and (2.77). Figure 2.2 shown below sums up this paragraph.

	Mechanic PDEs	Magnetic PDEs	Electric PDEs
Governing Equations	$\nabla \cdot (\mathbf{T}_{\text{mech}} + \mathbf{T}_M) + \mathbf{b} = \rho \ddot{\mathbf{u}}$	$\nabla \times \mathbf{H} = \sigma \mathbf{E} + \frac{\partial \mathbf{D}}{\partial t}$	$\nabla \cdot \mathbf{D} = 0$
Subsidiary Conditions	$\mathbf{S} = \nabla^s \mathbf{u}$	$\mathbf{B} = \nabla \times \mathbf{A}$	$\mathbf{E} = \nabla V - \frac{\partial \mathbf{A}}{\partial t}$
Boundary Conditions	$\mathbf{u}^* = \mathbf{u}$ on $\partial\Omega_u$ $\mathbf{f}^* = \mathbf{T} \cdot \mathbf{n}$ on $\partial\Omega_f$	$\mathbf{A}^* = \mathbf{A}$ on $\partial\Omega_A$ $\mathbf{B}^* = \mathbf{B} \cdot \mathbf{n}$ on $\partial\Omega_B$	$V^* = V$ on $\partial\Omega_v$ $\mathbf{D}^* = \mathbf{D} \cdot \mathbf{n}$ on $\partial\Omega_D$
Constitutive Equations	$\mathbf{T}_{\text{mech}} = \mathbf{c}^B \mathbf{S} - \mathbf{h} \mathbf{B}$ $\mathbf{H} = \mathbf{h}^t \mathbf{S} + (\boldsymbol{\mu}^S)^{-1} \mathbf{B}$		$\mathbf{D} = \boldsymbol{\epsilon} \mathbf{E}$

Figure 2.2: Summary of the differential form of the electro-magneto-mechanical BVP for magnetostrictive material under dynamic application.

Simplification to Static

The static version of the BVP displayed in Figure 2.3 consist of using equations (2.9) and (2.21) as, respectively, the mechanical and magnetostatic governing equations, equations (2.10) and (2.48) as the subsidiary conditions, equations (2.74) and (2.75) as the coupled constitutive law and, finally, equations (2.12), (2.13), (2.32) and (2.49) as boundary conditions.

	Continuum Mechanic PDEs	Magnetostatic PDEs
Governing equations	$\nabla \mathbf{T} + \mathbf{b} = \mathbf{0}$	$\nabla \cdot \mathbf{B} = \mathbf{0}$
Subsidiary conditions	$\mathbf{S} = \frac{1}{2} \left((\nabla \cdot \mathbf{u})^T + \nabla \cdot \mathbf{u} \right)$	$\mathbf{H} = -\nabla V_m$
Boundary conditions	$\mathbf{u}^* = \mathbf{u}$ on $\partial\Omega_u$ $\mathbf{f}^* = \mathbf{T} \cdot \mathbf{n}$ on $\partial\Omega_f$	$V_m^* = V_m$ on $\partial\Omega_{V_m}$ $\mathbf{B}^* = \mathbf{B} \cdot \mathbf{n}$ on $\partial\Omega_B$
Rearrange coupled constitutive equations	$\mathbf{T}_{\text{mech}} = \mathbf{c}^H \left[\mathbf{S} - (\mathbf{d}^T)^t \mathbf{H} \right] = \mathbf{c}^H \mathbf{S} - \mathbf{g} \mathbf{H}$ $\mathbf{B} = \mathbf{d}^H \mathbf{c}^H \mathbf{S} + (\boldsymbol{\mu}^T - \mathbf{d}^H \mathbf{g}) \mathbf{H} = \mathbf{g}' \mathbf{S} + \boldsymbol{\mu}^S \mathbf{H}$	

Figure 2.3: Summary of the differential form of the magneto-mechanical BVP for magnetostrictive material under static application.

Chapter 3: Weighted-Residual Formulations

In chapter 2, different sets of BVP were introduced to capture the mechanical and electromagnetic behavior of all sorts of pieces that could be involved in a magnetostrictive-based application. For the structurally involved pieces, the dynamic and static BVPs in their differential form are based on the equilibrium equations. To model the electromagnetic circuit, BVPs, based on the Maxwell's equations, were introduced for dynamic, quasi-static time-harmonic and the static conditions. Using these BVPs of continuum mechanics and electromagnetics under dynamic applications, a fully coupled, electro-magneto-mechanical BVP was developed for magnetostrictive materials. Using a similar approach, a static, fully coupled, magneto-mechanical BVP was introduced as well.

On FEMLAB 3.1 ©, most BVPs are easier to implement in the differential form. However, coupled BVPs, especially the dynamic set, requires being in the weighted-residual form, also known as “weak form”. This type of method is the common basis of most FEM schemes. It consists of taking the variation of the governing equation and boundary conditions and expressing it in an integral form, using subsidiary conditions and constitutive relation to write this new form in terms of the independent variables.

The static, fully coupled, magneto-mechanical BVP for magnetostrictive material as well as purely mechanical BVPs (static and dynamic) are examples of models commonly implemented using the “weak” form. The common appellation of the “weak” form in structural mechanics problem is Principle of Virtual Work (PVW), the weighted-residual form of the equilibrium equation. It is used to implement structural mechanics FEM

schemes based on the Galerkin Method. FEMLAB offers to implement either form but the method used by the software to solve a structural mechanic model is the PVW.

Coupled pre-implemented models such as the piezoelectric model (similar to the static magnetostrictive model), uses either the “weak” form or an alternate form of implementation, close to the differential form, called the “coefficient” form. This type of formulation uses a very general partial differential equation where coefficients are placed in front of some of strategic terms. This alternate formulation will not be discussed in detail because it is difficult to put coupled BVP in this form. FEMLAB © software technical engineers strongly advise use of the “weak” form for BVPs with numerous independent variables. This requires inputting all the coupling coefficients between each of independent variables. Models with more than one type of coupling such as in the dynamic electro-magneto-mechanical BVP, are almost impossible to implement in the differential or “coefficient” form for that reason.

Chapter 3 introduces the weighted residual form for various BVPs: the dynamic and static structural mechanics BVPs, the static, fully coupled, magneto-mechanical BVP (and at the same time the static piezoelectric BVP), and, finally, the dynamic, fully coupled, electro-magneto-mechanical BVP, the most complicated kind. In the next chapter, the method to implement such kind of formulations on FEMLAB along with implementation method for the BVPs in there differential form will be addressed.

3.1. The “Weak” Form Formulation of the Structural Mechanics BVPs

First let me recall the equations involved in the static and dynamic structural mechanics BVPs for purely elastic material. Note that these BVPs do not account for the Maxwell stress tensor introduced in section 2.3.1.

	Dynamic BVP	Static BVP
Governing Equation	$\nabla \cdot \mathbf{T} + \mathbf{b} = \rho \frac{d^2 \mathbf{u}}{dt^2}$	$\nabla \cdot \mathbf{T} + \mathbf{b} = 0$
Subsidiary Condition	$\mathbf{S} = \nabla^s \mathbf{u}$	
Constitutive Equation	$\mathbf{T} = \mathbf{s}_{\text{modified}} \mathbf{S}$	
Boundary Conditions	$\mathbf{u}^* \Big _{t=0} = \mathbf{u}$ on $\partial\Omega_u$ $\mathbf{T} \cdot \mathbf{n} \Big _{t=t_0} = \mathbf{f}^*$ on $\partial\Omega_f$	$\mathbf{u} = \mathbf{u}^*$ on $\partial\Omega_u$ $\mathbf{T} \cdot \mathbf{n} = \mathbf{f}^*$ on $\partial\Omega_f$

Figure 3.1: Summary of Structural mechanics BVPs for purely elastic material.

There are two ways to get a “weak” form formulation: start from the energy terms and start from the governing equation and the natural BCs. In this thesis, the second method will be used and instead of using matrix notation and all terms will be introduced in indicial notation to make this chapter easier to understand. Consider the equations of motion with suitable boundary conditions. Multiplying them by the variation of the displacement vector and putting them into integral form, respectively, over the volume and over the surface, and finally equating the sum to zero, one obtains:

$$\iiint_{\Omega} \left(T_{\beta\alpha,\beta} + b_{\alpha} - \rho \frac{\partial^2 u_{\alpha}}{\partial t^2} \right) \delta u_{\alpha} dv + \iint_{\partial\Omega} (T_{\alpha\beta} n_{\beta} - f_{\alpha}^*) \delta u_{\alpha} ds = 0 \quad (3.1)$$

where α and β successively equal 1, 2 and 3 [2,3,4,5,55]. The coma in the subscript of the term $T_{\alpha\beta,\beta}$ means that the coefficient of the stress matrix $T_{\alpha\beta}$ is differentiated with respect to x_{β} , where x_{β} successively equal x, y, z for β equal to 1, 2 and 3. In terms of energy variation terms, one can separate equation (3.1) such that

$$\delta W_b = \iiint_{\Omega} \left(b_{\alpha} - \rho \frac{\partial^2 u_{\alpha}}{\partial t^2} \right) \delta u_{\alpha} dv \quad (3.2),$$

$$\delta W_s = \iint_{\partial\Omega} (T_{\beta\alpha} n_{\beta}) \delta u_{\alpha} ds - \iint_{\partial\Omega} f_{\alpha}^* \delta u_{\alpha} ds \quad (3.3).$$

where δW_b is the virtual work due to externally applied body forces and inertial forces, and, δW_s is the virtual work due to surface stresses. Now, before starting the derivation of the variation of the total energy by modifying the way equations (3.2) and (3.3) are written, let me introduce simple variational calculus. The linearity (hence interchangeability) of the derivative of the variation of a term can be written in the three following forms

$$\frac{\partial \delta u_{\alpha}}{\partial x_{\beta}} = (\delta u_{\alpha})_{,\beta} = \delta (u_{\alpha,\beta}) \quad (3.4).$$

Another mathematical tool used in “weak” form formulations is the divergence theorem, which can be written as

$$\iiint_{\Omega} \frac{\partial F_i}{\partial x_i} dv = \iint_{\partial\Omega} F_i n_i ds \quad i=1,2,3 \quad (3.5).$$

Using the divergence theorem, one can rewrite equation (3.3) as

$$\begin{aligned}
\delta W_s &= \iint_{\partial\Omega} (T_{\beta\alpha} n_\beta) \delta u_\alpha ds - \iint_{\partial\Omega} f_\alpha^* \delta u_\alpha ds \\
&= \iiint_{\Omega} \frac{\partial}{\partial x_\beta} (T_{\beta\alpha} \delta u_\alpha) dv - \iint_{\partial\Omega} f_\alpha^* \delta u_\alpha ds \\
&= \iiint_{\Omega} \left(\frac{\partial T_{\beta\alpha}}{\partial x_\beta} \delta u_\alpha + T_{\beta\alpha} \frac{\partial \delta u_\alpha}{\partial x_\beta} \right) dv - \iint_{\partial\Omega} f_\alpha^* \delta u_\alpha ds
\end{aligned} \tag{3.6}.$$

The next step is to introduce the virtual strain term, $\delta S_{\alpha\beta}$ associated with a virtual displacement, δu_α , which can be written

$$\delta S_{\alpha\beta} = \delta \left[\frac{1}{2} (u_{\alpha,\beta} + u_{\beta,\alpha}) \right] = \frac{1}{2} (\delta (u_{\alpha,\beta}) + \delta (u_{\beta,\alpha})) \tag{3.7}.$$

Using equation (3.7), one may see that the term $T_{\beta\alpha} \delta S_{\alpha\beta}$ can be expressed as

$$T_{\beta\alpha} \delta S_{\alpha\beta} = T_{\alpha\beta} \frac{\partial \delta u_\alpha}{\partial x_\beta} \tag{3.8}.$$

Then, equation (3.6) can be written

$$-\delta W_s = -\iiint_{\Omega} (T_{\beta\alpha,\beta} \delta u_\alpha + T_{\beta\alpha} \delta S_{\alpha\beta}) dv + \iint_{\partial\Omega} f_\alpha^* \delta u_\alpha ds \tag{3.9}.$$

Now, the variation of the term $\nabla \cdot \mathbf{T} = T_{\alpha\beta,\beta}$ can be introduced as such

$$\delta W_i = \iiint_{\Omega} T_{\beta\alpha,\beta} \delta u_\alpha dv \tag{3.10}.$$

Then equation (3.1) can be written as the sum of equation (3.2), (3.9) and (3.10), such that

$$\begin{aligned}
\delta W_i + \delta W_b + \delta W_s &= + \iiint_{\Omega} T_{\beta\alpha,\beta} \delta u_{\alpha} dv + \iiint_{\Omega} \left(b_{\alpha} - \rho \frac{\partial^2 u_{\alpha}}{\partial t^2} \right) \delta u_{\alpha} dv \\
&\quad - \iiint_{\Omega} \left(T_{\beta\alpha,\beta} \delta u_{\alpha} + T_{\beta\alpha} \delta S_{\alpha\beta} \right) dv + \iint_{\partial\Omega} f_{\alpha}^* \delta u_{\alpha} ds \\
&= - \iiint_{\Omega} T_{\beta\alpha} \delta S_{\alpha\beta} dv + \iiint_{\Omega} \left(b_{\alpha} - \rho \frac{\partial^2 u_{\alpha}}{\partial t^2} \right) \delta u_{\alpha} dv + \iint_{\partial\Omega} f_{\alpha}^* \delta u_{\alpha} ds = 0
\end{aligned} \tag{3.11}$$

where $\delta \bar{U} = \iiint_{\Omega} T_{\beta\alpha} \delta S_{\alpha\beta} dv$ is the variation of the internal energy term and

$\delta \bar{W} = \delta W_b + \delta W_s$ is the total virtual work due to body forces, inertial forces and surface stresses [2,3,4,5, and 55].

The last line of equation (3.11) constitutes the “weak” form generally input into FEMLAB 3.1 along with the subsidiary condition and the constitutive equation in order to allow the software to express the variation of the internal energy in terms of the compliance matrix, the displacement vector and the variation of the displacement vector. Since this task is not required by the software and is not necessary to implement FEM schemes in the Galerkin form, it will not be carried through in this thesis but additional derivation can be found in any FEM or advanced structural mechanics books [5,55]. To conclude this section, let me introduce the equivalent form for static application where the inertial force term vanishes:

$$- \iiint_{\Omega} T_{\beta\alpha} \delta S_{\alpha\beta} dv + \iiint_{\Omega} b_{\alpha} \delta u_{\alpha} dv + \iint_{\partial\Omega} f_{\alpha}^* \delta u_{\alpha} ds = 0 \tag{3.12}.$$

3.2. The “Weak” Form Formulation of Static fully coupled electro-mechanical and magneto-mechanical BVPs

In this section, the “weak” form formulation of two very similar BVP is introduced, one capturing the static behavior of a piezoelectric material and one capturing the static behavior of a magnetostrictive material. One might ask why the interest in piezoelectric? Well simply because the latest version of FEMLAB 3.1 Structural Mechanics module and MEMS module includes a built in model for piezoelectric materials. This model was previously suggested by using the “coefficient” form of a structural mechanics model coupled with an electrostatic model. And therefore, one may be able to look up such a model from the library of the FEMLAB software and compare it to the fully coupled, static, magneto-mechanical model developed later in this section.

One main issue to discuss however is the role of the Maxwell stress tensor. As explained in the last section, the Maxwell stress tensor is a non linear contribution of the magnetic field to the mechanical stress in a magnetostrictive material. Kannan [46] (magnetostrictive) and Hom and Shankar [41] (electrostrictive) appear to be the only ones to have attempted to include the effects of a body force of electromagnetic origin in a computational analysis of the deformation of a polarized or magnetized coupled material. Both use an incremental scheme based on the Galerkin method. They seem however to have approaches which only partially account for the effect of body forces and moments due to the difficulty of incorporating the effect of the antisymmetric part of the stress tensor in the linearized constitutive equations.

All the implementations in this thesis use linear constitutive equations. They are only applied for applications where changes in deformation and in magnetic field are sufficiently small to assume the constitutive equation to be linear. Kannan [46] used incremental coupled constitutive equations to capture the effect of saturation in the magnetostrictive effect. This approach is achievable, although quite difficult, because of assumptions such as the quasi-static simplification of the Maxwell's equations.

Both derivations presented in this section were developed by the author during the completion of a class on variational methods in structural mechanics. Both might not look like anything reference on the topic but the results seem to be the same. Note however that the piezoelectric formulation does not account for body forces of electromagnetic origin whereas the magnetostrictive formulation may.

3.2.1. The Static fully coupled electro-mechanical “weak” form formulation for piezoelectric material

Piezoelectric materials exhibit a naturally occurring coupling effect between their electrical and mechanical properties. The coupling works both ways: electric polarization is produced by mechanical strain (the ‘direct’ piezoelectric effect) and, inversely, an electrical current induce mechanical strain (the ‘converse’ piezoelectric effect).

Electro-mechanical static BVP

There are two sets of governing equations, mechanical and electrical. The mechanical governing equation and subsidiary condition are the same as the one introduced in Chapter 2 and in the first section of this chapter. The electrical governing equation, also

known as the Maxwell's equations, under the assumption of quasi-static electrical field can be reduced to

$$\nabla \mathbf{D} = q \quad (3.13)$$

$$D_{i,i} = q \quad i = 1,2,3 \quad (3.14)$$

and

$$\mathbf{E} = -\nabla V \quad (3.15)$$

$$E_i = -V_{,i} \quad i = 1,2,3 \quad (3.16)$$

[3,4]. Weak form formulation of an electrical problem generally uses (3.13) as the governing equation and (3.15) as the subsidiary condition. Note that q is zero inside the electrically insulating dielectric. The electrical BCs were introduced in Chapter 2 for the electro-magneto-mechanical model.

Using the same approach as with previously introduced BCs, the electrical BC are either formulated as a prescribed electric potential, V^* , on the surface $\partial\Omega_V$ or as a prescribed surface charge density, Q^* , on the surface $\partial\Omega_Q$. Note that $\partial\Omega$ is equal to $\partial\Omega_Q \cup \partial\Omega_V$ and the electrical BC can be written as

$$V = V^* \quad \text{on } \partial\Omega_V \quad (3.17)$$

and

$$D_i n_i = -Q^* \quad \text{on } \partial\Omega_Q \quad (3.18)$$

[3,4]. Under the assumption that the thickness of the electrode bounded to the piezoelectric material is negligible, the free charge on the surface electrodes can be represented by a prescribed charge density, Q^* .

For a normal elastic solid, the mechanical constitutive equation used is Hooke's law ($T_{ij} = s_{ijkl}S_{kl}$ where s is a 4th order compliance tensor). Similarly, the electrical constitutive relation linearly links the electric displacement to the electric field ($D_i = e_{ij}E_j$ where e is the dielectric tensor). For piezoelectric materials, the constitutive relations used are an extension of the linear mechanical and electrical constitutive equation. In indicial form, the linear piezoelectric constitutive relation introduced in the introduction chapter, can be written

$$T_{ij} = C_{ijkl}S_{kl} - h_{kij}E_k \quad (3.19)$$

$$D_i = h_{ijk}S_{jk} + e_{ij}E_j \quad (3.20)$$

where h is the 3rd order coupling tensor [3,4].

Weak form derivation

In a similar way to what was done for a purely mechanical problem, a variation principle approach can be derived from the governing equations. The weak form can be obtained by expanding the principle of virtual work with the electrical governing equation and boundary conditions. The weak form obtained is

$$\begin{cases} -\int_{\Omega} (T_{ij,j} + b_i) w_i dv + \int_{\partial\Omega_T} (T_{ij}n_j - T_i^*) w_i ds = 0 \\ -\int_{\Omega} D_{k,k} \omega dv + \int_{\partial\Omega_Q} (D_i n_i + Q^*) \omega ds = 0 \end{cases} \quad (3.21)$$

where w_i and ω are weight functions that satisfy the mechanical and electrical boundary conditions respectively [3]. Both the equation of motion and Maxwell's electrostatic equations are self-adjoint problems. Therefore, we can rewrite (3.21) using variation of

the displacement, δu_i (which vanish on $\partial\Omega_u$), and of the scalar potential, δV (which vanishes on $\partial\Omega_Q$), and obtain

$$\begin{cases} -\int_{\Omega} (T_{ij,j} + b_i) \delta u_i dv + \int_{\partial\Omega_T} (T_{ij} n_j - T_i^*) \delta u_i ds = 0 \\ -\int_{\Omega} D_{k,k} \delta V dv + \int_{\partial\Omega_Q} (D_i n_i + Q^*) \delta V ds = 0 \end{cases} \quad (3.22).$$

Now, by adding both equation in (3.22) and using the strain-displacement relationship and equation (3.15) as subsidiary conditions, using partial integration and applying the divergence theorem, (3.22) can be rewritten as

$$\int_{\Omega} (T_{ij} \delta S_{ij} - D_k \delta E_k) dv - \int_{\Omega} b_i \delta u_i dv - \int_{\partial\Omega_T} T_i^* \delta u_i ds + \int_{\partial\Omega_Q} Q^* \delta V ds = 0 \quad (3.23)$$

where δS_{ij} is the variation of the strain field produced by the compatible displacement field δu_i , and similarly δE_k is the electric field produced by the compatible electric potential $\delta\phi$ [3]. The first term of (3.23) is the variation of the electric enthalpy density, H . It is an energy term defined as

$$\delta H = \int_{\Omega} (T_{ij} \delta S_{ij} - D_k \delta E_k) dv \quad (3.24).$$

Note that the first section, development stopped at the stage of (3.22) but for coupled problems of this sort, it might be interesting to pull out the variation component to get a functional. To do so, first, one needs to pull the variation out of each term in (3.24) to obtain

$$\delta H = \int_{\Omega} (\delta (T_{ij} S_{ij}) - S_{ij} \delta T_{ij} - \delta (D_k E_k) + E_k \delta D_k) dv \quad (3.25).$$

Using the variation of the constitutive equation (3.19) and (3.20), one gets

$$\delta H = \int_{\Omega} (\delta (T_{ij} S_{ij}) - S_{ij} (C_{ijkl} \delta S_{kl} - h_{kij} \delta E_k) - \delta (D_k E_k) + E_k (h_{kij} \delta S_{ij} + e_{ki} \delta E_i)) dv \quad (3.26).$$

Rearranging (3.26), one gets

$$\delta H = \int_{\Omega} \left(\delta(T_{ij}S_{ij}) - \delta(D_k E_k) - S_{ij}C_{ijkl}\delta S_{kl} + E_k e_{ki}\delta E_i + S_{ij}h_{ijk}\delta E_k + E_k h_{kij}\delta S_{ij} \right) dv \quad (3.27).$$

In Equation (3.27), the 3rd term shows the necessity of having a symmetric 4th order compliance tensor. Similarly, the 4th term shows the necessity of having a symmetric 2nd order permittivity tensor. And finally, the last two terms show the necessity of having a symmetric 3rd order coupling tensor. By factoring out the coupling tensor in the last two terms, the last term of equation (3.27) reduces to $h_{kij} (S_{ij}\delta E_k + E_k\delta S_{ij})$ where the term inside the parenthesis is equivalent to the variation of $(E_k S_{ij})$. This manipulation is only achievable thanks to the symmetry of the coupling tensor. Additionally, by using the rule of variational calculus on the 3rd and 4th terms of (3.27), one may obtain

$$\delta H = \int_{\Omega} \left(\delta(T_{ij}S_{ij}) - \delta(D_k E_k) - \frac{1}{2}\delta(S_{ij}C_{ijkl}S_{kl}) + \frac{1}{2}\delta(E_k e_{ki}E_i) + h_{kij}\delta(E_k S_{ij}) \right) dv \quad (3.28).$$

By regrouping the last 3 terms of (3.28), the variation of the electric enthalpy can be rewritten as

$$\delta H = \int_{\Omega} \left(\delta(T_{ij}S_{ij}) - \delta(D_k E_k) + \frac{1}{2}\delta(-S_{ij}C_{ijkl}S_{kl} + E_k e_{ki}E_i + 2E_k h_{kij}S_{ij}) \right) dv \quad (3.29)$$

and by rearranging the last term of (3.29), one gets

$$\delta H = \int_{\Omega} \left(\delta(T_{ij}S_{ij}) - \delta(D_k E_k) + \frac{1}{2}\delta\left(\left(-S_{ij}C_{ijkl}S_{kl} + E_k h_{kij}S_{ij}\right) + \left(E_k e_{ki}E_i + E_k h_{kij}S_{ij}\right)\right) \right) dv \quad (3.30)$$

or

$$\delta H = \int_{\Omega} \left(\delta(T_{ij}S_{ij}) - \delta(D_k E_k) + \frac{1}{2}\delta\left(S_{ij}\left(-C_{ijkl}S_{kl} + h_{kij}E_k\right) + E_k\left(e_{ki}E_i + h_{kij}S_{ij}\right)\right) \right) dv \quad (3.31).$$

By using the constitutive relations (3.19) and (3.20) respectively in the 3rd and 4th term of (3.31), one gets

$$\delta H = \int_{\Omega} \left(\delta(T_{ij}S_{ij}) - \delta(D_k E_k) + \frac{1}{2}\delta(-S_{ij}T_{ij} + E_k D_k) \right) dv \quad (3.32).$$

Finally, grouping all the terms of (3.32) under the same variation sign we get

$$\delta H = \int_{\Omega} \left(\delta \left(T_{ij} S_{ij} - D_k E_k - \frac{1}{2} S_{ij} T_{ij} + \frac{1}{2} E_k D_k \right) \right) dv \quad (3.33)$$

which reduces to

$$\delta H = \delta \left(\int_{\Omega} \frac{1}{2} (S_{ij} T_{ij} - E_k D_k) dv \right) \quad (3.34)$$

[3]. Similarly, the last three terms of (3.23) can be grouped to form the work due to an external load, W , such that,

$$\delta W = \int_{\Omega} b_i \delta u_i dv + \int_{\partial\Omega_T} T_i^* \delta u_i ds - \int_{\partial\Omega_Q} Q^* \delta V ds \quad (3.35)$$

By pulling the variation out of the integral, one may rewrite (3.35) as

$$\delta W = \delta \left(\int_{\Omega} b_i u_i dv + \int_{\partial\Omega_T} T_i^* u_i ds - \int_{\partial\Omega_Q} Q^* V ds \right) \quad (3.36)$$

where ϕ is the surface potential where charge is prescribed [3]. One may rewrite (3.23) as

$$\delta I = \delta H - \delta W = 0 \quad (3.37)$$

where I , is called the functional. Consequently,

$$I = \int_{\Omega} \left(\frac{1}{2} T_{ij} S_{ij} - \frac{1}{2} D_k E_k \right) dv - \left(\int_{\Omega} b_i u_i dv + \int_{\partial\Omega_T} T_i^* u_i ds - \int_{\partial\Omega_Q} Q^* V ds \right) \quad (3.38).$$

3.2.2. The static fully coupled magneto-mechanical “weak” form formulation for magnetostrictive material

The static fully coupled magneto-mechanical BVP consists of using equations displayed in figure 2.3. Note however that the equilibrium equation, equation (2.9), must be rewritten in the form of equation (2.70) in order to account for the Maxwell stress tensor.

The electric variables do not appear in the static model and the magnetic vector potential \mathbf{A} is replaced by a magnetic scalar potential V_m which reduces the BVP

independent variables from $\{u, v, w, A_x, A_y, A_z, V\}$ for the dynamic PDE, to $\{u, v, w, V_m\}$ for the static PDE. Then, by using the same method of derivation as the one used for the electro-mechanical BVP, one gets, in vector form,

$$\int_{\Omega} (\delta \mathbf{S})^t \mathbf{T} dv - \int_{\Omega} \mathbf{b} \delta \mathbf{u} dv - \int_{\partial \Omega_f} \mathbf{f}^* \delta \mathbf{u} ds = 0 \quad (3.39)$$

and

$$-\int_{\Omega} (\delta \mathbf{H})^t \mathbf{B} dV + \int_{\partial \Omega_q} (\delta V_m)^t \mathbf{B}^* dS = 0 \quad (3.40).$$

Now, as one may recall from the piezoelectric derivation, up to this point the constitutive equation were not used. Only governing equations and subsidiary conditions are necessary to get up to this point. Adding equation (3.39) and (3.40), a functional can be derived for magnetostrictive material by following the same derivation as for piezoelectric. Note however, that to get this functional the constitutive equations must not include the effect of the Maxwell stress tensor. They must be of the form of equations (2.74) and (2.75). Therefore, the functional formulation is not a fully coupled implementation and consequently may not be the best way to proceed for these types of models. The functional obtained is of the form

$$F = \int_{\Omega} \frac{1}{2} \left((\mathbf{S})^t \mathbf{T} - (\mathbf{H})^t \mathbf{B} \right) dV - \int_{\Omega} \mathbf{u}^t \mathbf{b} dV - \int_{\partial \Omega_f} \mathbf{u}^t \mathbf{f}^* dS + \int_{\partial \Omega_q} (V_m)^t \mathbf{B}^* dS \quad (3.41)$$

where the first integral can also be called the magnetic enthalpy and the rest of the integral term can be seen as work due to external load.

To get a fully coupled model accounting for the electromagnetic body forces and moments, one must keep the “weak” form formulation given by equations (3.39) and (3.40), and use constitutive equations accounting for the Maxwell stress tensor, \mathbf{T}_M ,

introduced in last chapter. The coupled constitutive equations used therefore consists of equation (2.74) and a fully coupled stress constitutive equation which may be written as

$$\mathbf{T} = \mathbf{T}_{\text{mech}} + \mathbf{T}_{\text{M}} = \mathbf{c}^{\text{H}}\mathbf{S} - \mathbf{g}\mathbf{B} + \mathbf{H} \otimes \mathbf{B} - \frac{\mu_0}{2}(\mathbf{H} \cdot \mathbf{H})\mathbf{I} \quad (3.42).$$

3.3. The “weak” formulation of dynamic fully coupled electro-magneto-mechanical BVP

A well-posed set of PDEs describing the dynamic behavior of a magnetostrictive material has been introduced in section 2.3. The equations involved are summarized in table 2.2 provided at the end of chapter 2. To derive a weak form formulation of this BVP, one must first derive an integral form of the multi-physic BVP. This can be done by multiplying the governing equations and the natural boundary conditions with weight functions (say $\delta\mathbf{u} = \{\delta u, \delta v, \delta w\}^t$ for the mechanical sets of PDEs, δV for the electrical set of PDEs, and $\delta\mathbf{A} = \{\delta A_1, \delta A_2, \delta A_3\}^t$ for the magnetic set of PDE) and by integrating the governing equations over a subdomain Ω and the BC over the boundary $\partial\Omega$. Then, to go from an integral form to a weak form, one must used the subsidiary conditions and mathematical tools such as integration by parts, the divergence theorem and Stokes theorem such as the one derived in the previous sections. The weak form obtained is

$$-\int_{\Omega} (\delta\mathbf{S})^t \mathbf{T} dV + \int_{\Omega} (\delta\mathbf{u})^t \mathbf{b} dV + \int_{\partial\Omega} (\delta\mathbf{u})^t \mathbf{f}^* dS + \int_{\Omega} (\delta\mathbf{u})^t \rho \ddot{\mathbf{u}} dV = 0 \quad (3.43),$$

$$-\int_{\Omega} (\nabla \delta V)^t \mathbf{D} dV + \int_{\Omega} (\delta V)^t \mathbf{D}^* dS = 0 \quad (3.44),$$

$$\begin{aligned}
& -\int_{\Omega} (\delta \mathbf{B})^t \mathbf{H} dV + \int_{\Omega_h} (\delta \mathbf{A})^t \mathbf{H}^* dS + \int_{\Omega} (\delta \mathbf{A})^t \mathbf{J}^e dV \\
& - \int_{\Omega} (\delta \mathbf{A})^t \sigma \nabla V dV - \int_{\Omega} (\delta \mathbf{A})^t \sigma \dot{\mathbf{A}} dV = 0
\end{aligned} \tag{3.45}$$

where the term $\ddot{\mathbf{u}}$ is the 2nd order time differential of the displacement field \mathbf{u} and $\dot{\mathbf{A}}$ is the 1st order time differential of the magnetic vector potential \mathbf{A} [1]. By using central and forward finite differences approach, respectively, these terms can be approximated to

$$\ddot{\mathbf{u}}_{(t_{n+1})} = \frac{(\mathbf{u}_{(t_{n+1})} - 2\mathbf{u}_{(t_n)} + \mathbf{u}_{(t_{n-1})})}{\Delta t^2} \tag{3.46}$$

and,

$$\dot{\mathbf{A}} = \frac{\mathbf{A}_{(t_{n+1})} - \mathbf{A}_{(t_{n-1})}}{\Delta t} \tag{3.47}.$$

The software's solver, however, has a "time" solver which only treats first order time differential. Therefore, the only alternative to implement equation (3.43) is to start with equation (2.7) and (2.8). Then equation (2.7) can be expressed in the "weak" form as

$$\int_{\Omega} \mathbf{v} \delta \mathbf{v} dv = \int_{\Omega} \frac{\partial \mathbf{u}}{\partial t} \delta \mathbf{v} dv \tag{3.48}$$

and (2.8) can be rewritten as

$$-\int_{\Omega} (\delta \mathbf{S})^t \mathbf{T} dV + \int_{\Omega} (\delta \mathbf{u})^t \mathbf{b} dV + \int_{\partial \Omega_f} (\delta \mathbf{u})^t \mathbf{f}^* dS + \int_{\Omega} (\delta \mathbf{u})^t \rho \frac{\partial \mathbf{v}}{\partial t} dV = 0 \tag{3.49}.$$

So the final form of the "weak" form of the dynamic electro-magneto-mechanical BVP are the equations (3.49), (3.44) and (3.45), in conjunction with the constitutive equations (2.78), (3.42) and (2.23). Note that this weak form is in terms of variation of the field terms $\{\delta \mathbf{S}, \delta \mathbf{H}, \delta \mathbf{E}\}$ and variation of the variables $\{\delta \mathbf{u}, \delta \mathbf{v}, \delta \mathbf{A}, \delta V\}$ and the flux density term $\{\mathbf{T}, \mathbf{B}, \mathbf{D}\}$. Using FEMLAB, the weak form application mode requires using

equations in this form in any non-static models. Figure 3.2 is a summary of the direct and “weak” form of such type of BVP.

	Mechanic PDEs	Magnetic PDEs	Electric PDEs
Governing Equations	$\nabla \cdot \mathbf{T} + \mathbf{b} = \rho \frac{d\mathbf{v}}{dt} \quad \mathbf{v} = \frac{\partial \mathbf{u}}{\partial t}$	$\nabla \times \mathbf{H} = \sigma \mathbf{E} + \frac{\partial \mathbf{D}}{\partial t}$	$\nabla \cdot \mathbf{D} = 0$
Subsidiary Conditions	$\mathbf{S} = \nabla^s \mathbf{u}$	$\mathbf{B} = \nabla \times \mathbf{A}$	$\mathbf{E} = \nabla V - \frac{\partial \mathbf{A}}{\partial t}$
Boundary Conditions	$\mathbf{u}^* = \mathbf{u} \text{ on } \partial\Omega_u$ $\mathbf{f}^* = \mathbf{T} \cdot \mathbf{n} \text{ on } \partial\Omega_f$	$\mathbf{A}^* = \mathbf{A} \text{ on } \partial\Omega_A$ $\mathbf{B}^* = \mathbf{B} \cdot \mathbf{n} \text{ on } \partial\Omega_B$	$V^* = V \text{ on } \partial\Omega_V$ $\mathbf{D}^* = \mathbf{D} \cdot \mathbf{n} \text{ on } \partial\Omega_D$
Constitutive Equations	$\mathbf{T} = \mathbf{T}_{\text{mech}} + \mathbf{T}_M = \mathbf{c}^B \mathbf{S} + \mathbf{h}^t \mathbf{B} + \mathbf{H} \otimes \mathbf{B} - \frac{\mu_0}{2} (\mathbf{H} \cdot \mathbf{H}) \mathbf{I}$ $\mathbf{H} = \mathbf{h} \mathbf{S} + (\boldsymbol{\mu}^s)^{-1} \mathbf{B}$		$\mathbf{D} = \boldsymbol{\epsilon} \mathbf{E}$
Weak Form Formulation	$-\int_{\Omega} (\delta \mathbf{S})^t \mathbf{T} dV + \int_{\Omega} (\delta \mathbf{u})^t \mathbf{b} dV + \int_{\partial\Omega_f} (\delta \mathbf{u})^t \mathbf{f}^* dS + \int_{\Omega} (\delta \mathbf{u})^t \rho \frac{\partial \mathbf{v}}{\partial t} dV = 0$ $\int_{\Omega} \mathbf{v} \delta \mathbf{v} dv = \int_{\Omega} \frac{\partial \mathbf{u}}{\partial t} \delta \mathbf{v} dv$ $-\int_{\Omega} (\nabla \delta V)^t \mathbf{D} dV + \int_{\Omega} (\delta V)^t \mathbf{D}^* dS = 0$ $-\int_{\Omega} (\delta \mathbf{B})^t \mathbf{H} dV + \int_{\partial\Omega_H} (\delta \mathbf{A})^t \mathbf{H}^* dS + \int_{\Omega} (\delta \mathbf{A})^t \mathbf{J}^e dV - \int_{\Omega} (\delta \mathbf{A})^t \sigma \nabla V dV - \int_{\Omega} (\delta \mathbf{A})^t \sigma \dot{\mathbf{A}} dV = 0$		

Figure 3.2: Summary of the differential form of the electro-magneto-mechanical BVP for magnetostrictive material under dynamic application.

Chapter 4: FEM Implementations on FEMLAB 3.1©

Chapter 2 and 3 defined, respectively, the differential and “weak” form formulation of the various BVPs that will be used to capture the electromagnetic, mechanic and coupled electro-magneto-mechanical behaviors of the different parts involved in modeling a magnetostrictive-based application under different application conditions. The goal for Chapter 4 is to present details that illustrate the implementation of 3-D FEM models based on these BVPs on FEMLAB 3.1©. Although a basic knowledge of the software is preferable, an unfamiliar user can use sections of this chapter as a tutorial manual to gain an understanding of steps needed to implement these equations. This chapter is separated into 3 sections. The first one introduces the software’s capabilities and limitations and focuses on the justification of the choice of commercial software used. The next two sections focus on implementation methods for the static and dynamics models.

4.1. Brief Overview of FEMLAB 3.1 ©

FEMLAB 3.1 © is a powerful interactive software which enable one to model and solve all kinds of scientific and engineering problems based on BVPs. The software includes pre-implemented BVPs of various types of physics including structural mechanics, electromagnetic, heat transfer, etc. Each type of physics BVP is implemented for different application conditions and is generally proposed in 1, 2 and 3 dimensions. Each model type is called an application mode. For example, “3-D, solid stress-strain, static analysis” or “Axial symmetry (2-D), Magnetostatic, Azimuthal Currents” are application

mode names. Application modes are split into modules (i.e. the “Electromagnetic module”) which may be purchased individually with the initial software package [4]. In this Chapter, application modes from the “Structural Mechanics Module” and “Electromagnetic Module” are used. If the application of the magnetostrictive material is MEMS related, one may also consider the “MEMS module”.

This software runs finite element analysis together with adaptive meshing and error control using a variety of numerical solvers. Although the solver types suggested for each type of BVP presented in this chapter will be mentioned, the mathematical and numerical foundations of each type of solver will not be addressed. One can find additional information on this topic and other implementation related topics in the FEMLAB manuals [4]. For those familiar with FEMLAB, the main types of solvers used in this thesis, are the “SPOOLES direct” solver, the “UMFPACK direct” solver, and the “GMRES iterative” solver (in combination with the “Incomplete LU” or “Algebraic multigrid” preconditioner). These can be set to solve “linear” or “non-linear” problems which may be time dependent as long as the BVPs have, at most, first order time derivatives. For the equation of motion, which has a 2nd order time derivative of the displacement vector, the software requires using an additional variable, the velocity vector [4]. This is why, in Chapter 2 and 3, the mechanical equation of motion was separated by introducing an additional governing equation defining the velocity vector. This way the software solves two governing equations with first order time-derivative instead of one with a 2nd order time-derivative.

With FEMLAB©, one may easily extend conventional models for one type of physic into multi-physics models capable of solving coupled physical phenomena. There are two

ways to solve coupled problems: “sequential” solving and “simultaneous” solving. The “sequential” method consists of solving one type of physics first and applying the results to the second type of physics before solving it. In other word, one solves a multi-physics problem in sequence. The limitation of this method is that it can only take into account unidirectional coupling meaning that coupling between say the mechanical and thermal fields can only occur such that only one field affect the other. This is the case for a thermal expansion problem where the mechanical fields are dependent on the temperature but not the other way around. In this case, we would solve the heat transfer problem first, save the temperature distribution obtained and use it to solve the unidirectional-coupled mechanical BVP.

The second way of solving coupled problem is to compute the solution for both types of physics simultaneously. The way the software treats such a problem is by setting multiple degrees of freedom to each node accounting for both types of physics. This way one can solve bidirectional-coupled problems such as the electromechanical BVPs for a piezoelectric material. Since there are more degrees of freedom in such a model, this alternate way of solving coupled problems generally requires significantly more computational time [4].

FEMLAB© was chosen among other FEM programs for its ability to implement and solve bidirectional-coupled multi-physic problems. Many FEM programs solve only one type of physics. Some are able to solve coupled BVPs such as thermo-mechanical or electromechanical BVPs. A good example of such software is ANSYS© which was originally a structural mechanics FEM software that allows the user to alter the code in order to solve coupled problems. The only real limitation of this software is that it is not

able to solve complex non-linear bidirectional-coupled BVPs such a dynamic electro-magneto-mechanical BVPs, nor can it solve the electromagnetic part necessary to predict the fields inside the magnetic circuit typical of the magnetostrictive-based application modeled. Recently, ANSYS© released a software that allows multi-physics problems to be solved in a similar manner to FEMLAB©. More information can be found on ANSYS© official webpage. Other than this new version of ANSYS©, the author is not aware of any other commercial FEM software can solve such multi-physics BVPs at this time. The capabilities of both softwares seem to be similar based on the respective webpage advertisement of their products.

4.2. Implementation of the static BVPs

This section focuses on 3-D FEM of the previously introduced static BVPs. The structural mechanics FEM of a purely elastic material will serve as a basic introduction to the software for readers who are not familiar with FEMLAB 3.1©. It uses a pre-implemented FEM codes there almost no programming is necessary to build such a model. The subsequent sub-section will be less detailed and might require unfamiliar users to refer to the FEMLAB manual now and then.

4.2.1. Structural mechanics FEM of a purely elastic material

Model definition and geometry drawing

In this section the implementation of a simple structural mechanics problem is described. The example chosen is the modeling of a rectangular beam, clamped on one end and with

an applied load on the other end. The first screen one may see when starting FEMLAB 3.1 is the one shown in Figure 4.1. It is the “model navigator” window, which allows the user to select the BVP to implement. The first step is to select the “space dimension”. Since 3-D analysis will be required to account for some phenomenon occurring in a magnetostrictive-based application such as eddy current power losses, all models are implemented in 3-D. Adapting the presented work to similar 2-D or axisymmetric analysis is possible but may require serious modifications of the equations used.

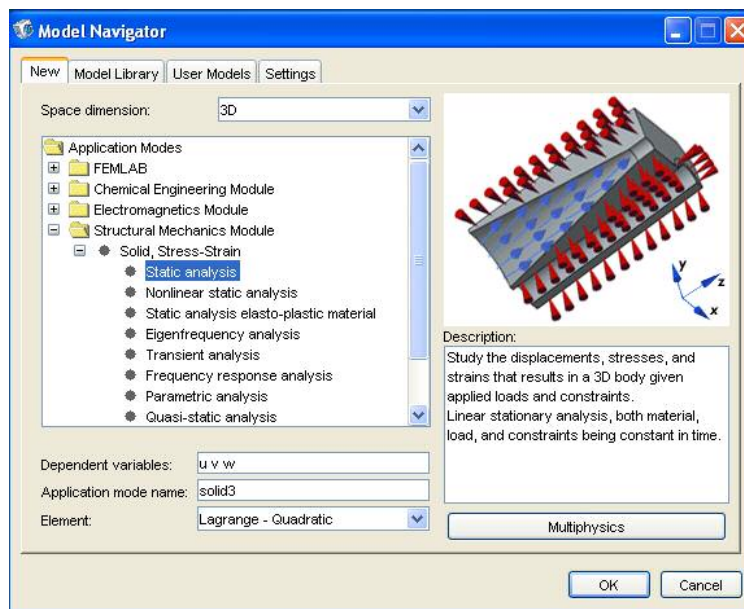


Figure 4.1: Model Navigator window.

The second step consists of defining the application mode. For this model, select the “Solid, Stress-Strain / Static analysis” in the “Structural Mechanics Module” folder. Note that in the model navigator one can set the application analysis mode name and can see the dependent variable names. The type of element suggested by the program is also displayed in the model navigator and may be changed at this point or later. Once you press “Ok”, the FEMLAB “geometry” screen appears. This is shown in Figure 4.2.

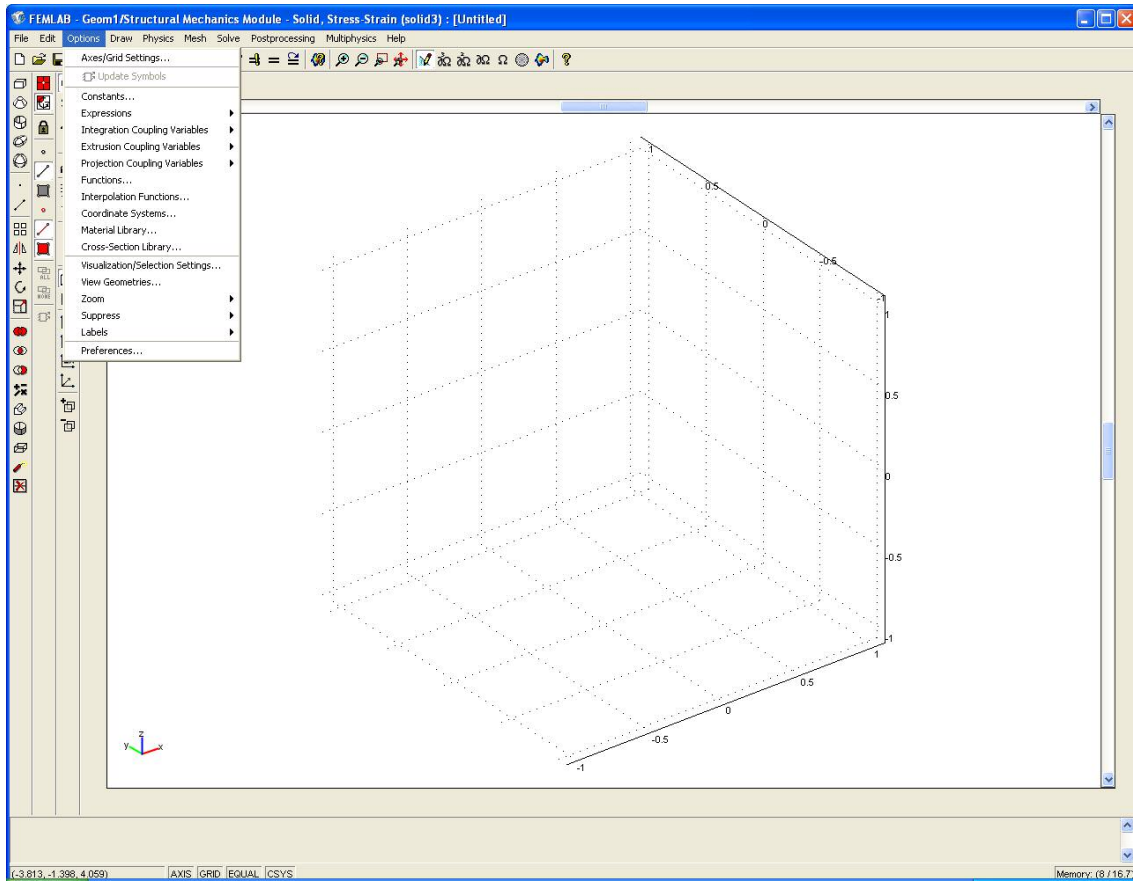


Figure 4.2: Option menu in the FEMLAB geometry window.

Drawing structures using the FEMLAB software is not very difficult but requires a certain amount of practice. Here, a simple rectangular beam modeled as a single “subdomain” is drawn, so that no major issues will be encountered while drawing the structure. “Subdomains”, “Boundaries”, “Edge”, and “Point” are the respective names for the volume, the boundary of the volume, a line on the boundary of the volume and a point in or on the volume. When drawing geometry with multiple subdomains, one must make sure that the common boundaries of each subdomains are correctly linked (i.e. no very small gaps between subdomains should appear in the geometry).

To set the Axis and grid, one must open the “draw” menu and select “Axis and Grid setting” as displayed in Figure 4.2 and 4.3. Note that the default units of FEMLAB are S.I. (although one could work in other unit systems [4]). Choose the minimum and maximum values of the axis as displayed in Figure 4.3. Then one must choose a “2-D work plane” to draw the cross-section of the beam in order to extrude it. Choose the y-z plane with no displacement from the x-axis. Similarly to the 3-D view, axis and grid settings can be done for the 2-D work plane. Choose the “y” axis minimum and maximum value to be $-3e-2$ and $3e-2$ ($e-2$ stands for $\times 10^{-2}$) and choose $5e-3$ for the grid spacing. The next step is to draw a 5 by 1 cm rectangle centered at the (0,0) point in the “y-z plane” as displayed and extrude it by $30e-3$ as displayed in Figure 4.4. The various drawing tools are found in the “draw” menu or in the vertical tool bars on the left of the screen. The link to the “extrude” window can be found in the “draw” menu as well.

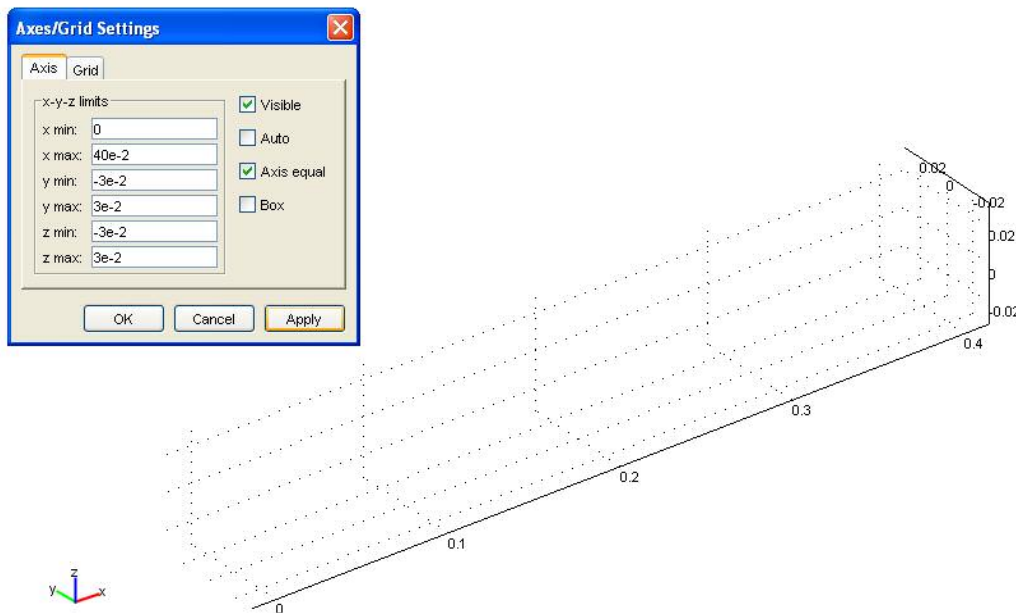


Figure 4.3: Axis and Grid setting window.

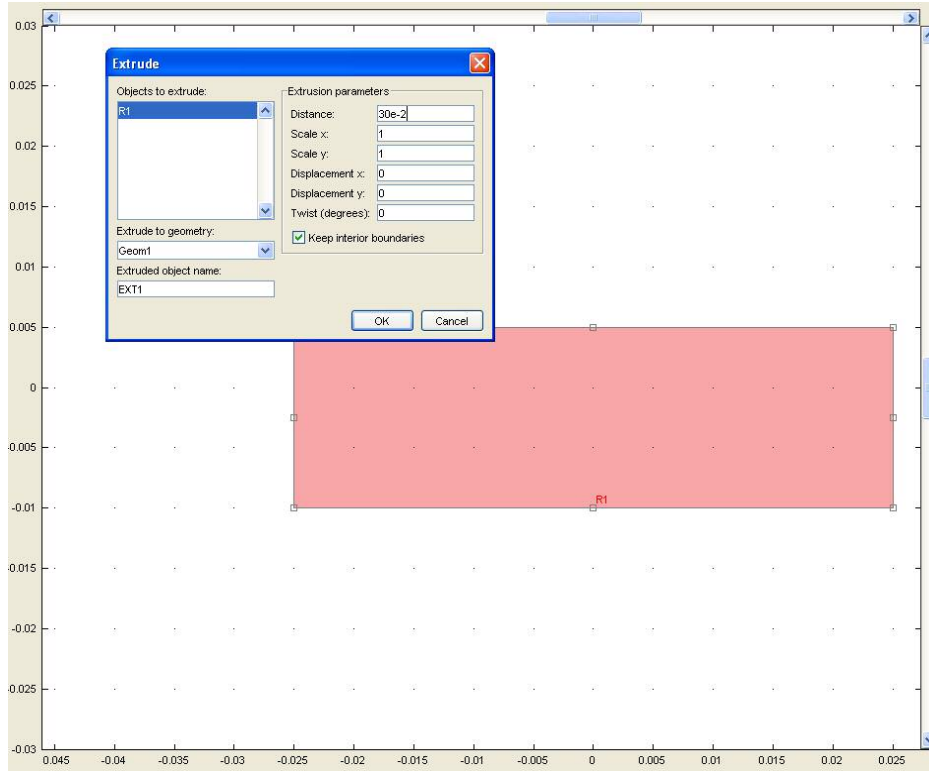


Figure 4.4: 2-D work plane with beam cross-section and “extrude” window.

Physics implementation

Now that the geometry is complete, let’s take a look at the physics of the pre-implemented module has set up. In order to be consistent with the work presented in Chapter 3, let’s work with “weak” form implementation. To set “weak” form formulation on FEMLAB, go to the “solve” menu, select “solver parameter”, and change the Solution form to “weak” as displayed in Figure 4.5. Then to visualize the equation system, go to the “Physics” menu and select “Equation System / Subdomain Settings”. Select the subdomain 1 (there should be only 1), and look at the “weak”, “dweak”, and, “variables” tabs as displayed in Figure 4.6. The equation displayed is

$$\begin{aligned}
 &-(ex_solid3_test*sx_solid3+ey_solid3_test*sy_solid3+ez_solid3_test*sz_solid3 \\
 &\quad +2*exy_solid3_test*sxy_solid3+2*eyz_solid3_test*syz_solid3 \\
 &\quad +2*exz_solid3_test*sxz_solid3)
 \end{aligned}$$

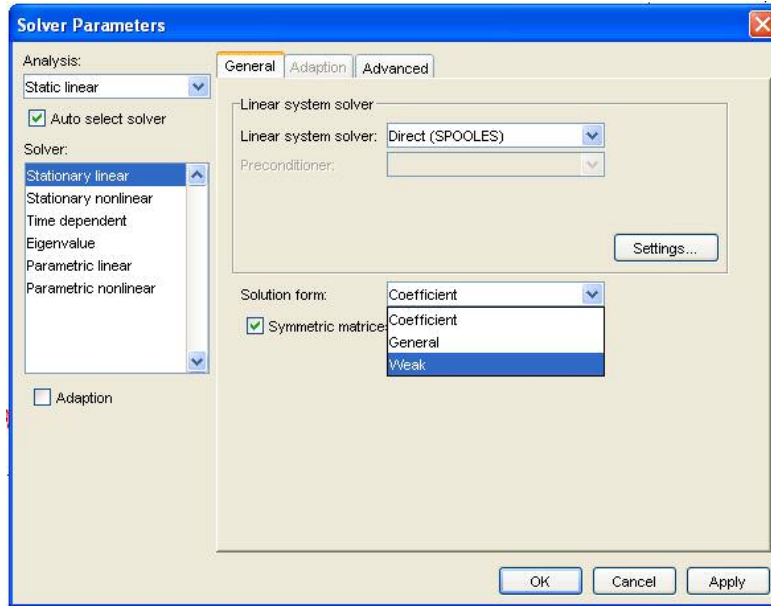


Figure 4.5: Setting “weak” form display of the equation system.

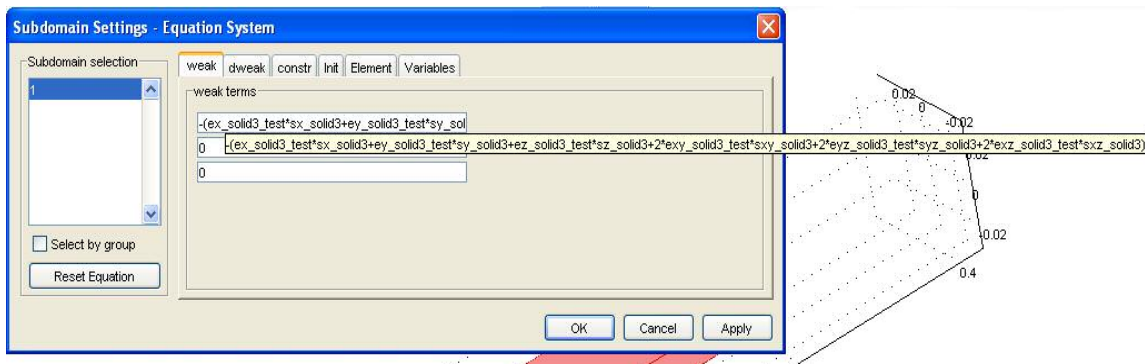


Figure 4.6: “weak” tab in the “Subdomain Setting / Equation System” window.

FEMLAB is written in a modified Matlab language, meaning that if we wanted to include a certain type of function in this equation we could use Matlab functions. The variables names follow a certain logic. For example, “ex_solid3_test” is the test function of the “x” component of the strain tensor. The “_solid3” is to indicate that this variable is solved by the application mode called “solid3”.

This application mode name can be changed in the model navigator (see Figure 4.1) and this nomenclature is very practical when dealing with multi-physics problem to identify which variables are solved by a certain application mode. The “_test” extension is to indicate that it is the variation of the “x” component of the strain. In this equation, only the stress components and the variation of the strain components are used. Every variables starting with “s” refers to a stress component and the variables starting with “e” refers to a strain component. Note that the equation displayed in this window is the content of the volume integral of the equilibrium equation (3.12) assuming no body forces are applied.

The “dweak” tab is non-zero everywhere only for time-dependent problems. This will be addressed in the section on dynamic models. The “variable” tab is very useful. It allows visualizing and potentially modifying the equations which define dependent variables. Recall that in the model navigator window (see Figure 4.1) the dependent variables are the “x”, “y”, and “z” components of the displacement vector, “u”, “v” and “w”. Figure 4.7 shows the “variable” tabs in which the equations for the body load, the total displacement, the stress tensor components, the strain tensor components, the strain energy density and the Von Mises and Tresca stress are provided. Note that “ux” stands for the first order derivative of “u” with respect to “x”. This type of shorthand notation only applies to the different degrees of freedom, which are in this case “u”, “v”, and “w”.

Now depending on the type of material modeled the variable equations will be automatically modified. Since for a simple model nothing needs to be changed in the “Subdomain Setting / Equation System” window, close the window by clicking “cancel”. To set the type of material go to the “Physics” menu and select “Subdomain Setting...”.

The “Material” tab allows you to define the material properties (see Figure 4.8). One can select different material models such as isotropic, orthotropic, anisotropic or even elastoplastic material to implement the compliance matrix and the thermal coefficient matrix. Another option is to select a material from the material library. To do so, click on the “load” button next to “material library” in the “Material” tab and, for example, “select Aluminum” (see Figure 4.9). Since it’s an isotropic material, no changes will occur in the “Variable” tab of the “Subdomain Setting / Equation System” window. However, if you select an anisotropic material, the equation for the stress and other dependent variables will be automatically modified.

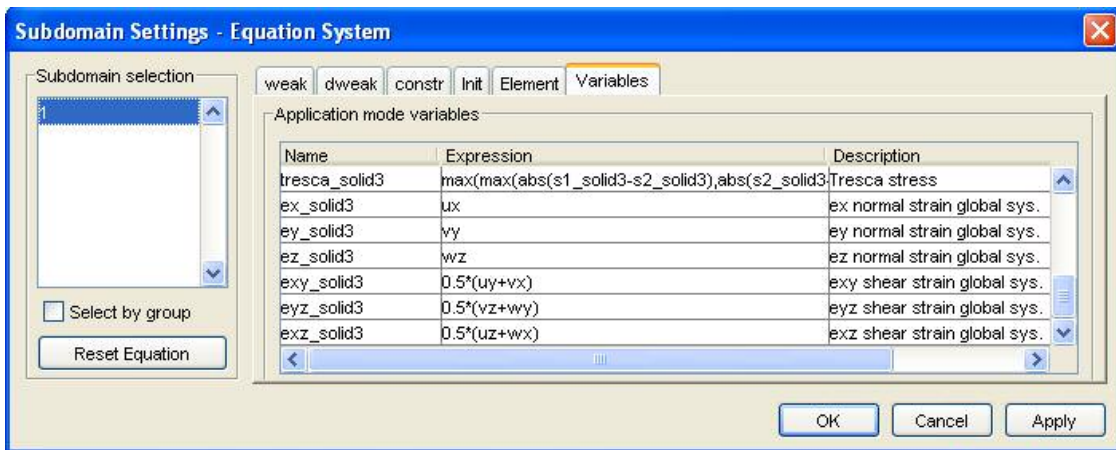


Figure 4.7: “Variable” tab in the “Equation setting / Subdomain” window.

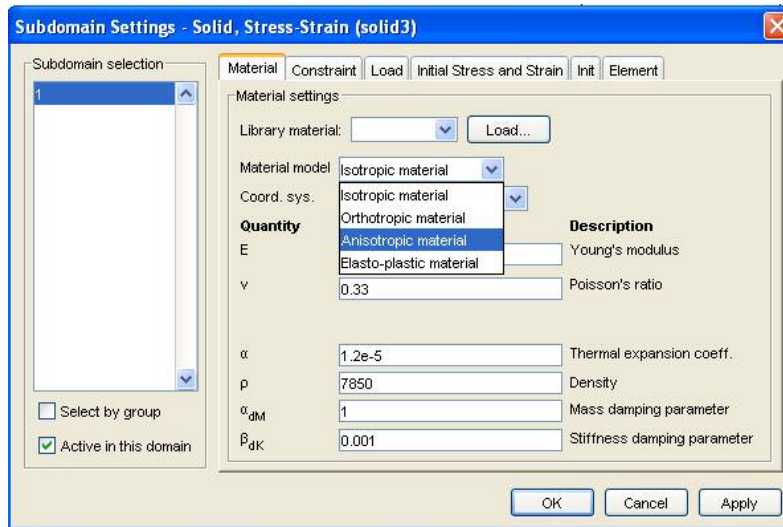


Figure 4.8: “Material” tab in the “subdomain setting” window.

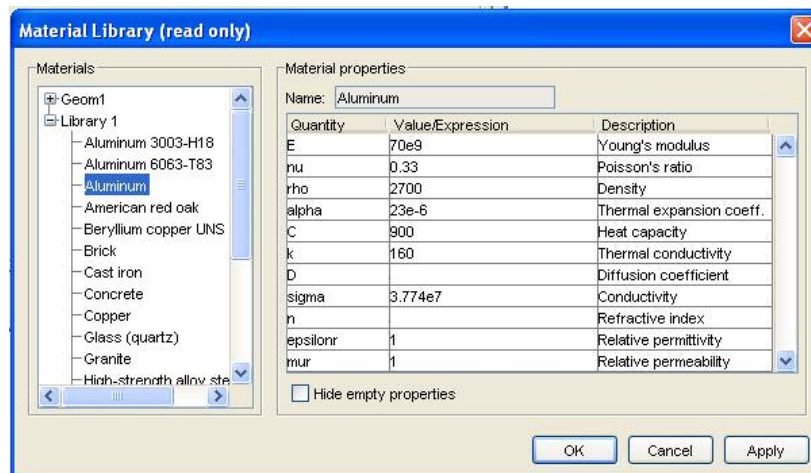


Figure 4.9: “Material library” window.

Note that in the “subdomain setting” window, there are tabs to define constraints on the subdomain, volumetric load, initial stress and strain and other tabs irrelevant for now. Since none of the mentioned applies to our simple model, these tabs will not be further discussed but information on how to set these can be found in the FEMLAB manual [4]. The “boundary condition setting” can be found in the “physics” menu. They allow the user to set constraints and to specify load on the boundary of the domain. In Figure 4.10,

the “constraint” tab displays the necessary setting to model clamped boundary conditions. In the “load” tab, the face load on the boundary at the other end can be set in force per unit of area. Since the area of this boundary is 5×10^{-4} ($5 \times 10^{-2} \times 1 \times 10^{-2}$), assuming a -50 N load in the “z” direction, the total force per unit of area in the “z” direction will be -100000 N/m². Figure 4.11 displays the “load” tab of the “boundary setting” window.

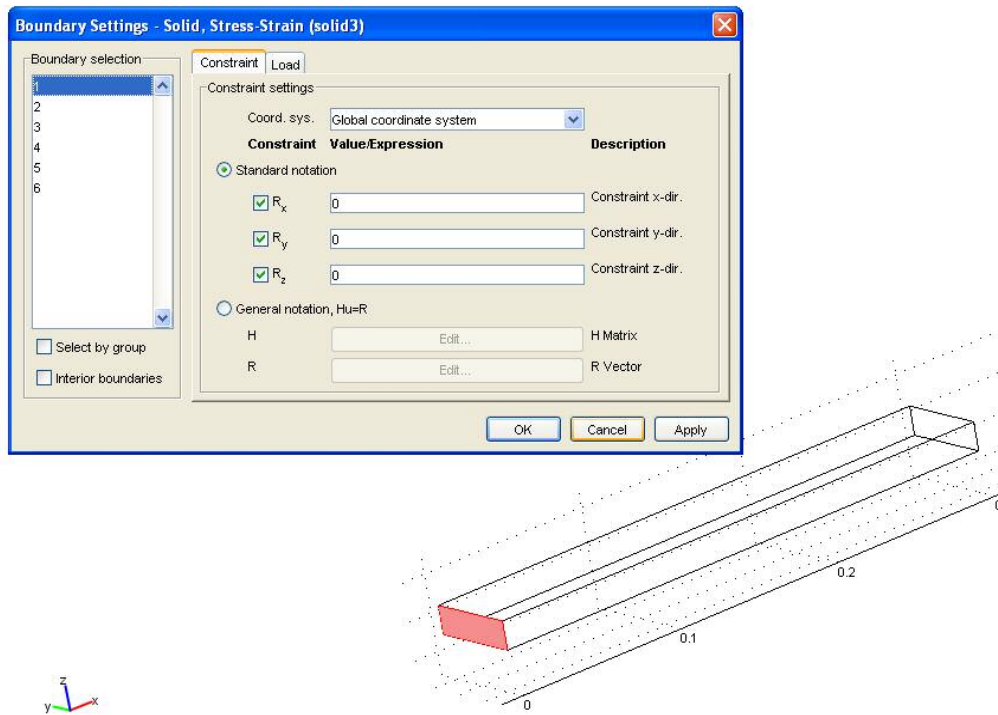


Figure 4.10: “Constraint” tab of the BC setting window.

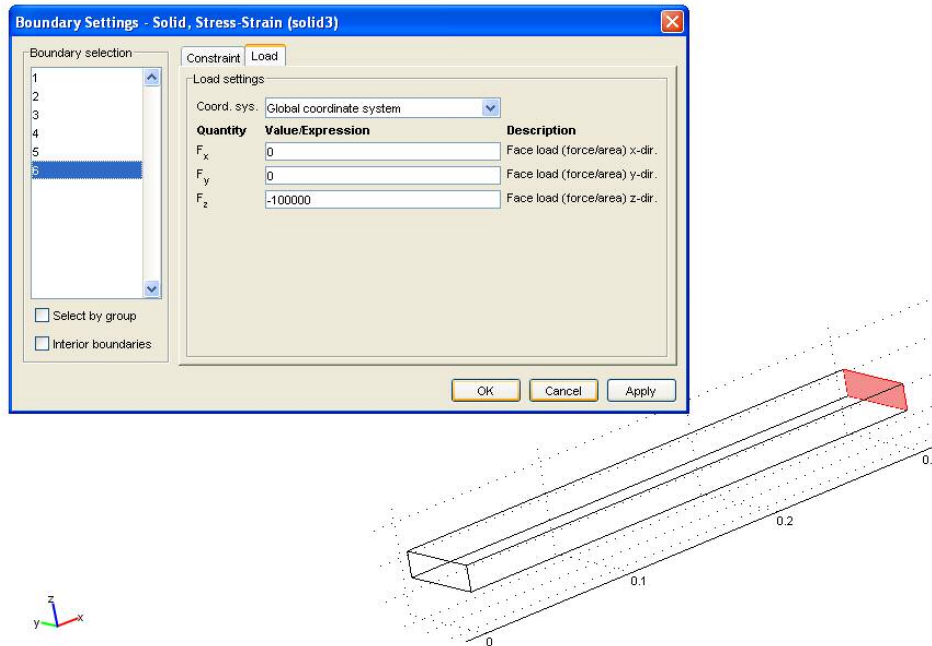


Figure 4.11: “Load” tab of the BC setting window.

Mesh and Solver Parameters

For a simple model with only one subdomain not much effort is required to get an appropriate meshing. One must go into the “mesh parameter” window by selecting it in the “mesh” menu. Then select a “predefined mesh size” such as “Coarse” and mesh. For complex geometries with various subdomains, a couple of the following tips may be useful:

- To focus the computation analysis on one subdomain, boundary, edge or point, such as the magnetostrictive material or one of its boundaries, one can choose in the respective tab of the “mesh parameter” window the maximum element size and growth rate. The maximum element size should be set smaller than $1/5^{\text{th}}$ of the thickness of the subdomain. This is to ensure that the field will be computed at least at 5 points in the smallest region. The element growth rate should be set to a large value (e.g. 2) in large subdomains where the fields changes slowly and does

not require much precision. It should be very close to 1 in the region of interest (i.e. 1.05). The element growth rate must be above 1.

- Narrow regions may require use of an advanced meshing option. In the “advance” tab, one can set the resolution of the narrow region to a higher value than 1 such as 1.5. The higher the length to thickness ratio the higher the resolution of the narrow regions needs to be.
- It is necessary when meshing a complex structure to make sure that the number of degrees of freedom is low enough. Since this is function of both the number of dependent variables (3 for a static mechanical FEM) and the number and type of elements. Some elements have more nodes than others but certain types of physics require quadratic or higher order elements to appropriately capture the phenomenon modeled.
- Finally, for better results, start your meshing one level coarser than you intend and refine it once. In Figure 4.12, a “coarser” mesh once refined is shown. Note that refining a mesh for a simple model triples the number of degree of freedom so it might not be wise to use this option in complicated geometry.

As mentioned earlier, there are many types of solvers which can be used for linear and non-linear models. For a structural mechanics model of a purely elastic material, SPOOLES seems to be the best one (also the recommended one by the software engineers). Generally, the software selects the best solver for the chosen application mode.

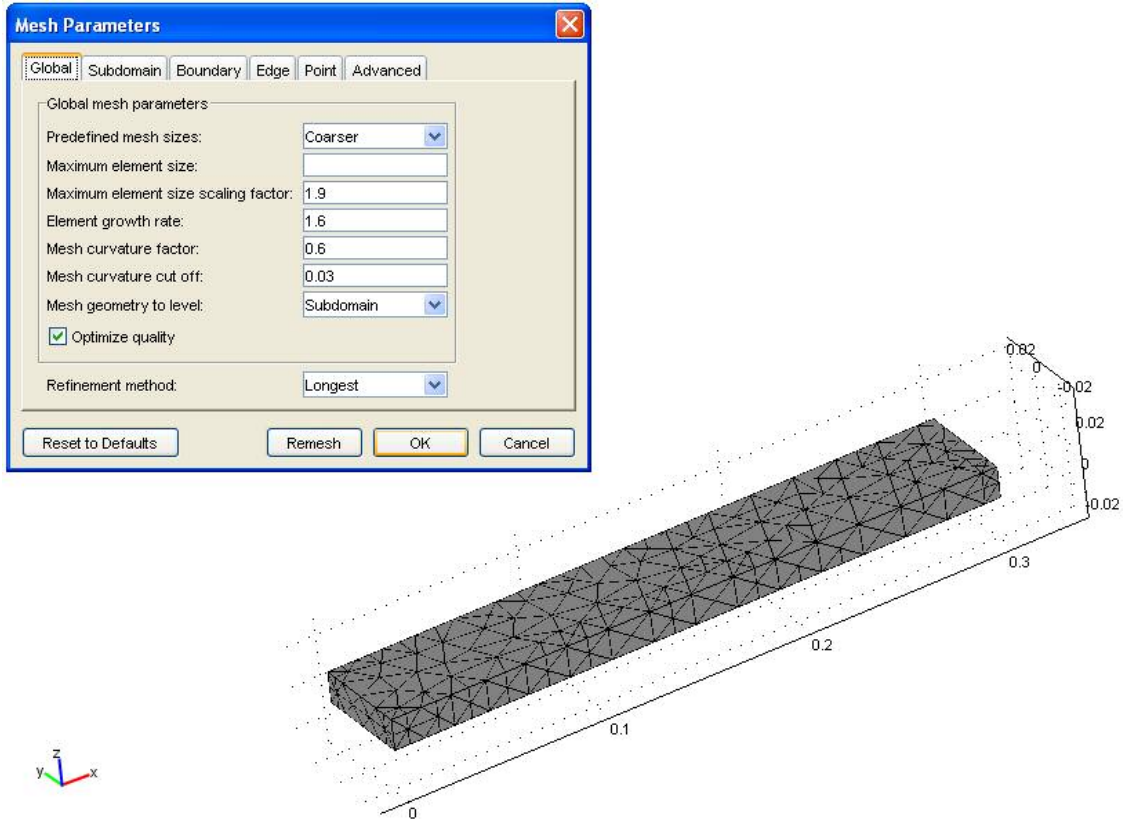


Figure 4.12: “Mesh parameters” window and meshed structure.

A couple of options may be set or unset before solving a model. For example coupled models tend to be unsymmetrical so in the “Solver Parameter” window, one must uncheck the symmetric matrix check box for coupled problems. In our case, this is not necessary. When a matrix is complex symmetric, which is common for harmonic analysis of structural mechanics and electromagnetic problems, one must clear the “Use Hermitian transpose” check box in the advance tab. Other than these two important check boxes, one must use common sense to set “non-linear” or “time-dependent” solver appropriately such models.

Finally before solving the model, one must open the “solver manager” window and select the “initial value expression” check box or eventually the “Initial value expression

evaluated using the current solution”. In the case of a sequential solving of a unidirectional coupled problem, one must first select the “initial value expression” check box to solve the first type of physics and then the “current solution” check box for the second type of physics where coupling occurs. Eventually, one must store the first solution in order to reuse it when solving for the dependent coupled field. This will allow the user not to recompute the first model solution before each attempt to solve the coupled dependent type of physics.

Once the model is solved, the post processing is quite simple. Depending on the type of modeled field, a slice plot, a boundary plot, a deformed shape plot, a streamline plot, etc. or a combination of some of the above may be used. For each type of post-processing used one must first check and uncheck the checkbox referring to the desired post-processing plot type and then go to the respective tab to set the predefined quantity to be plotted and the various options of each type of plots. Figure 4.13 shows the result of our model using a deform shape and a boundary plot of the displacement. The maximum displacement obtained is 6.76×10^{-4} m and occurs on the opposite surface to the clamped end as one could expect.

Since plotting using the various types of 3-D plots is not always ideal to read a precise value at one point in the geometry, one may find very useful to use the “cross-section plot parameter” window (in the post-processing menu). It allows plotting any variables on a chosen surface or along a specific line. For example, one may plot the “z” component of the strain along the neutral axis of the beam (from position (0,0,0) to (.3,0,0)). Figure 4.14 shows the results and the setting to obtain such a plot. Slice plots can be achieved by setting the coordinates of 3 points instead of 2.

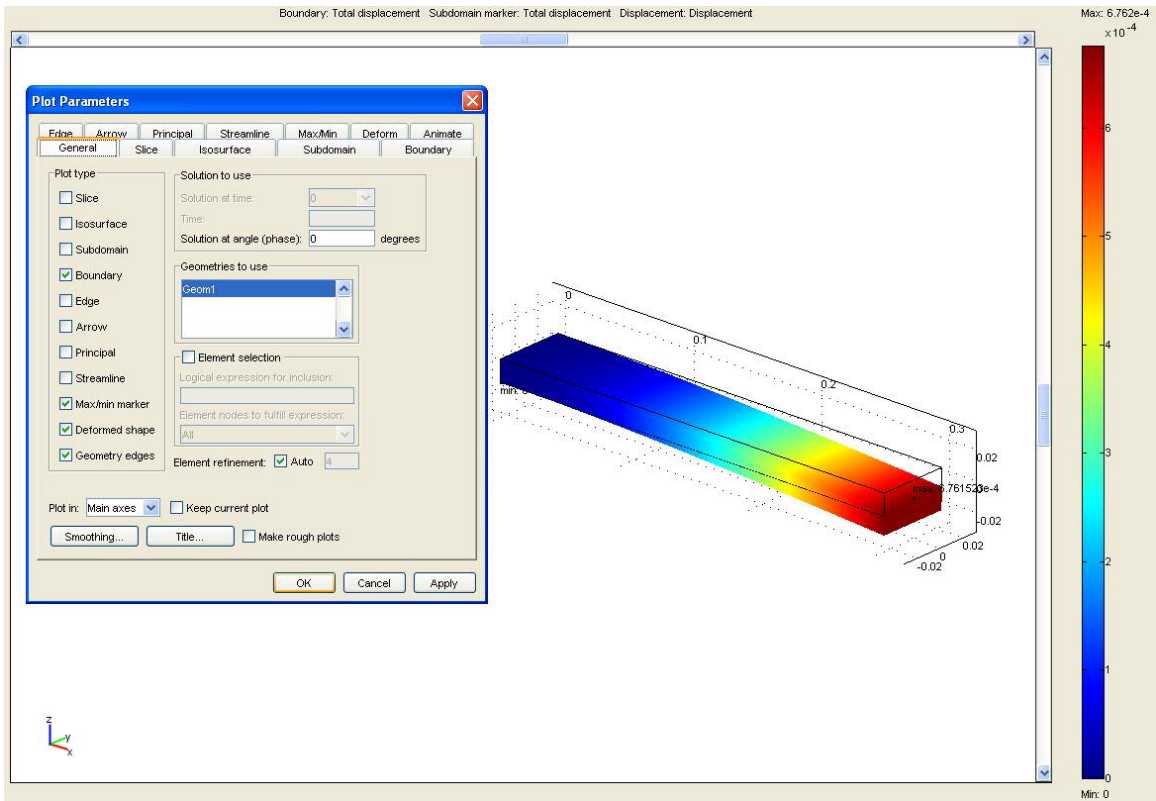


Figure 4.13: “Plot parameter” window and final solution.

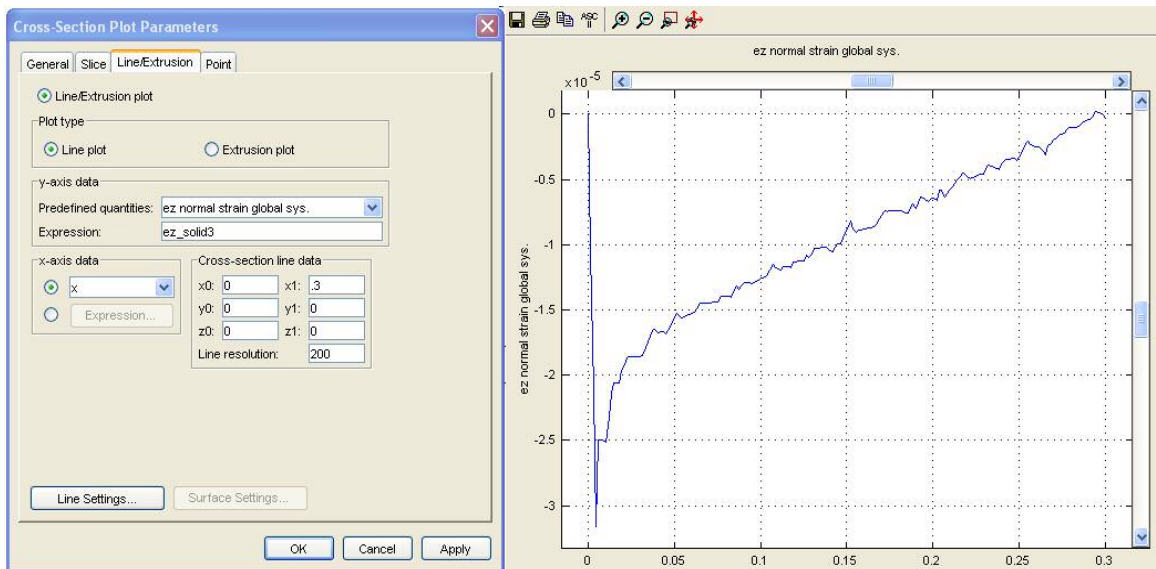


Figure 4.14: “Cross-section plot parameter” window and line plot of the “z” component of the strain along the neutral axis.

4.2.2. Magnetostatic FEM

There are two types of magnetostatic models. One is based on a vector magnetic potential and the other one on a scalar magnetic potential. In this section, only the implementation of the second type is covered. The implementation for the first type is a simplification of the magnetic equations used in the dynamic electro-magneto-mechanical models presented in the next section. The example presented in this section is a magnetic circuit using permanent magnets to apply a constant magnetic field over a small region. The purpose of this apparatus was to obtain in-plane magnetostriction measurements while applying a magnetic field at different angles with respect to the easy axis of the magnetostrictive sample. The sample was mounted on a rotating support keeping the magnetic circuit fixed while the sample rotates through 360° .

The magnetostatic model was used to quantify the magnetic induction inside the magnetostrictive sample. Figure 4.15 displays the apparatus magnetic circuit as modeled. The very small shaded volume in the middle is a Galfenol magnetostrictive plate with average relative permeability of 360. The two small cylinders on each side of the magnetostrictive plate are permanent magnets, magnetized to 100000 A/m each. The magnetization value of the permanent magnets is usually set based on experimental values obtained in air. Modeling only the permanent magnet in air, one can calibrate the magnetization of the permanent magnets such that it exactly reproduces the lab value. This way, when the magnetostrictive plate is added in the model, one can expect to get accurate modeling of the field. This technique is often used to calibrate coils models and permanent magnet models.

The rest of the magnetic circuit is made of magnetic steel 1018 of relative permeability of 2000. The last two subdomains are made of air with permeability of one. The first is the space between the two permanent magnets and surrounding the magnetostrictive plate and the second is the large brick surrounding the magnetic circuit. Note that among the pieces made of magnetic steel, the two pieces attached to the permanent magnet that pass through the main frame of the magnetic circuit can be moved such that the air gap between the two permanent magnets varies thereby allowing control of the applied magnetic field seen by the sample. The sample was $8 \times 8 \times 1 \text{ mm}^3$, therefore the minimum air gap needed to be above 12 mm wide to allow a 360 rotation of the sample. The magnetic induction obtained was around 0.8 Tesla at each end of the sample and around 1.4 Tesla in the center of the sample.

The first step necessary to implement this system include the drawing of the complex geometry along with a complex meshing emphasizing on the region near the magnetostrictive sample. This will not be covered here. The second step is to define the material types and properties in the “subdomain setting” windows. Since this is a purely magnetic model, the magnetostrictive material is considered as a simple magnetizable material with constant relative permeability. Note that FEMLAB allows implementing non-linear equations for permeability or other material properties but this option was not explored for the work presented in this thesis for two reasons. First, the non-linear models require more memory and memory use was already maximized for this 3-D geometry. Second, the applications generally operate in a limited range such that the change in magnetic field is small enough to assume a linear relationship between magnetic field and magnetic induction.

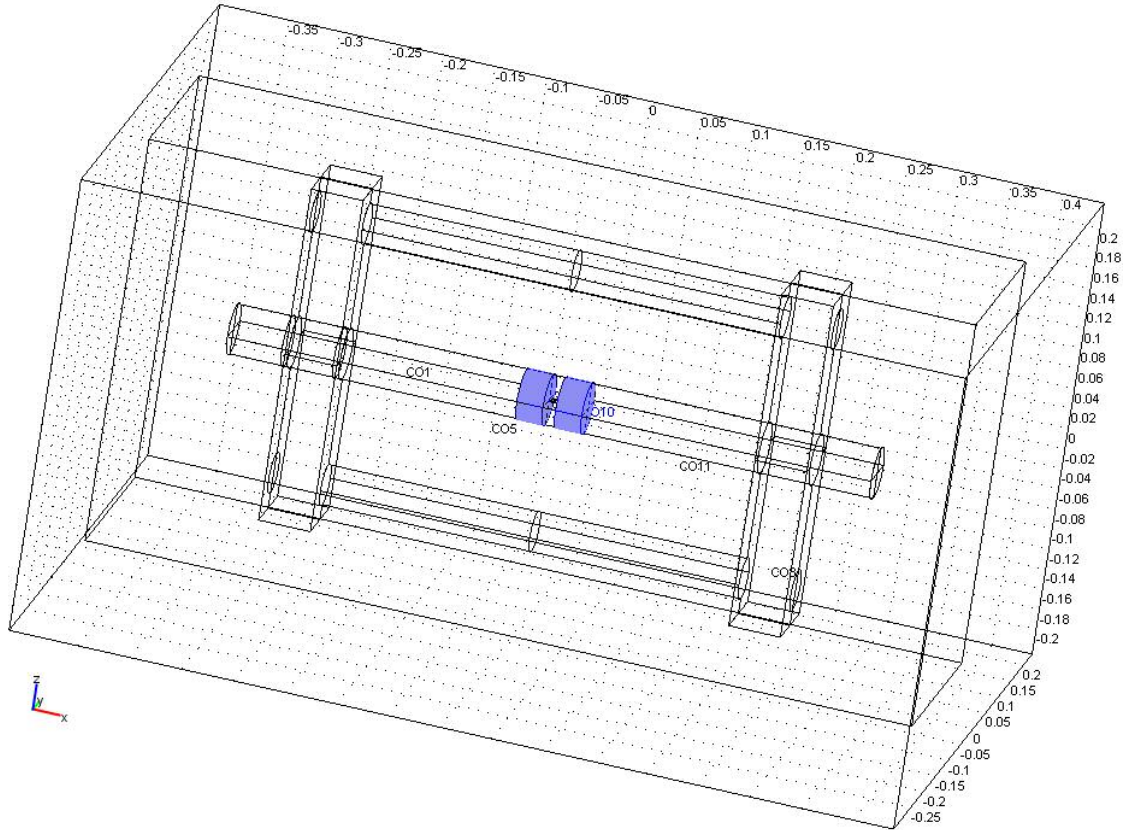


Figure 4.15: Geometry of the magnetic circuit

The other magnetizable material used in this model is the magnetic steel. The permanent magnets are magnetized material using a constitutive relation different from magnetizable materials. The constitutive relations of a magnetized material and magnetizable material were previously introduced as, respectively, equation (2.24) and equation (2.27) with a negligible remanent magnetic induction. Air uses equation (2.27) as well but the relative permeability is zero in this case.

The subdomain and boundary equation system was not modified like for the structural mechanics example. The BCs selected are “continuity” everywhere except on the boundaries of the air modeled around the system where “magnetic insulation” is chosen to insure that the magnetic flux path stays inside the “air” subdomain. The mesh needs to

use “Lagrange quadratic” elements but “Lagrange linear” elements will work if one is limited by memory requirements. To modify the element type, one must change the element type to Lagrange linear in the model navigator and potentially make sure that each subdomain has this type of element by going into the “element” tab of the “subdomain setting” window. As suggested by the software engineers for this application mode, the solver used was a GMRES solver with an “algebraic multigrid” preconditioner. Post-processing was done using a streamline plot for the magnetic flux density, a slice plot for the magnetic field distribution and a cross-section line plot to get numerical values of the magnetic field and magnetic flux density along the sample midline. Results obtained in this model as well as in subsequent models are presented in this chapter are discussed in Chapter 5.

4.2.3. Fully coupled magneto-mechanical FEM of a magnetostrictive material

Now that both the static structural mechanics and the magnetostatic application modes were introduced, one may consider a coupled magneto-mechanical model of a magnetostrictive material. The model presented in this section consists of two simple magnetostrictive plates attached to a beam. In this model the magnetostrictive material is used as sensors. The set-up consist of a $317.5 \times 24.85 \times 1.6 \text{ mm}^3$ Aluminum beam with two $25.1 \times 8.35 \times 1.57 \text{ mm}^3$, 18.4% polycrystalline production grade Galfenol plates (fairly new magnetostrictive material provided by ETREMA products, Inc.) attached symmetrically on the top and the bottom of the beam at 25mm from the clamped end. Figure 4.16 shows the model geometry.

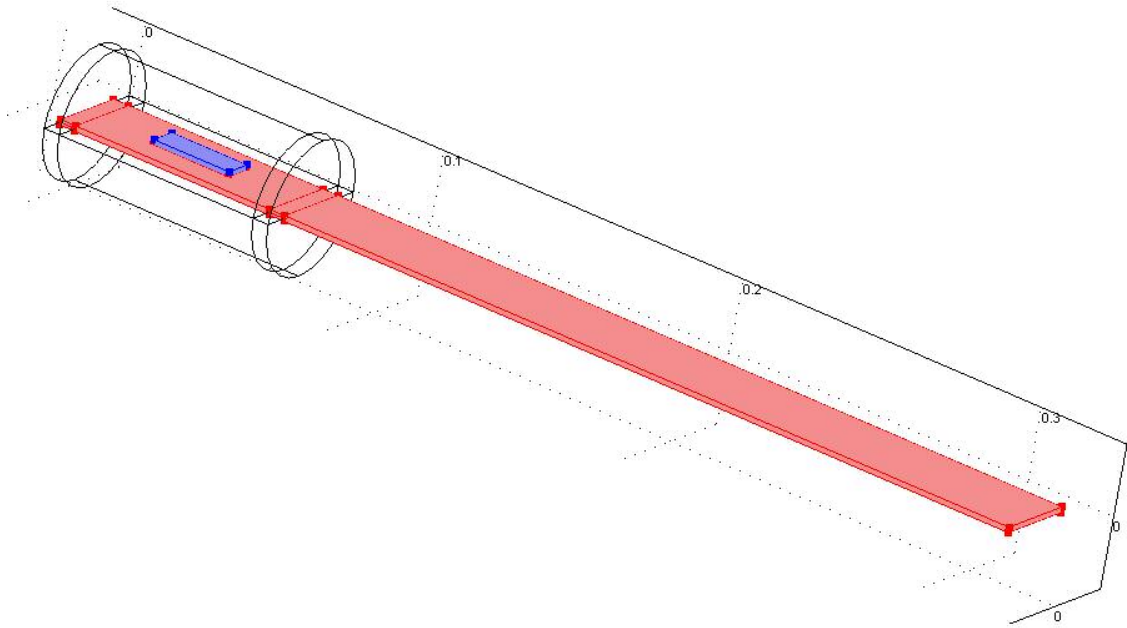


Figure 4.16: Geometry of the example implemented for the static coupled magneto-mechanical model.

The first step when implementing a multi-physics model is to select the type of physics involved in the “model navigator” window. One must first select in the model navigator the two types of application modes to couple. Here the primary application mode is “3-D, solid stress-strain, static analysis” and the secondary application mode is “3-D Magnetostatic, No Currents” (see Figure 4.16). In the experimental apparatus, a coil generated the magnetic field. To model the coil, one needs an application mode where the electric quantities are considered. A “3-D, Magnetostatic” application mode would allow us to model a coil but in order to save memory, modeling the magnetic field with permanent magnet provides a fairly equivalent result with a less complex and smaller geometry and a less computationally demanding application mode.

The second step consists of drawing and meshing your structure. This will not be discussed in more details since the topic has been covered in the last two subsections.

Once the geometry is finished and meshed one can set the equation system. The first issue to consider is that this model is made of elastic material (the aluminum beam), magnetic material (the permanent magnets), air and magnetostrictive material (the Galfenol plates) each of which does not necessarily require to be solved in both the structural mechanic application mode and the magnetic application mode. For example, the permanent magnets and the air do not need to be part of the solid mechanics application mode. The aluminum needs to be both in the mechanical and magnetic application modes but no coupling occurs for this subdomain. The Galfenol plates are also in both application mode but with modified equations. To determine which domains are active and which are non-active for a certain application mode, one must go in the “multiphysics” menu and select the “solid, stress-strain” for example. Then go to the “subdomain setting” window in the physic menu and uncheck the domain referring to the permanent magnet and the air. Similarly, after selecting the magnetostatic application mode, repeat the task in the “subdomain setting” window for the non-active material. For this model all subdomains are active for the magnetic FEM.

Recall the weighted-residual formulation described in section 3.2.2. Before implementing any equation one must open the “constant” window in the “Option” menu and add the following constants:

- The stiffness matrix components $\{c_{11}, c_{12}, c_{13}, c_{22}, c_{23}, c_{33}, c_{44}, c_{55}, c_{66}\}$,
- The coupling matrix components $\{g_{11}, g_{12}, g_{13}, g_{21}, g_{22}, g_{23}, \dots, g_{61}, g_{62}, g_{63}\}$ (also called “h” in some models),
- The permeability (constant strain) matrix components $\{\text{musr}_{11}, \text{musr}_{22}, \text{musr}_{33}\}$.

The value of each constant comes from the characterization curves of the magnetostrictive material being modeled. More on how to choose these is discussed in section 4.4. Figure 4.17 shows the “constants” window. Note that these constants may be added in the “Subdomain expression” window accessible from the “Option/Expression” menu. Selecting the Galfenol plate subdomains in this menu allows defining expressions and constants which will be taken into account only when referring to the concerned subdomains. Either way of adding the constant to the model is valid in this case.

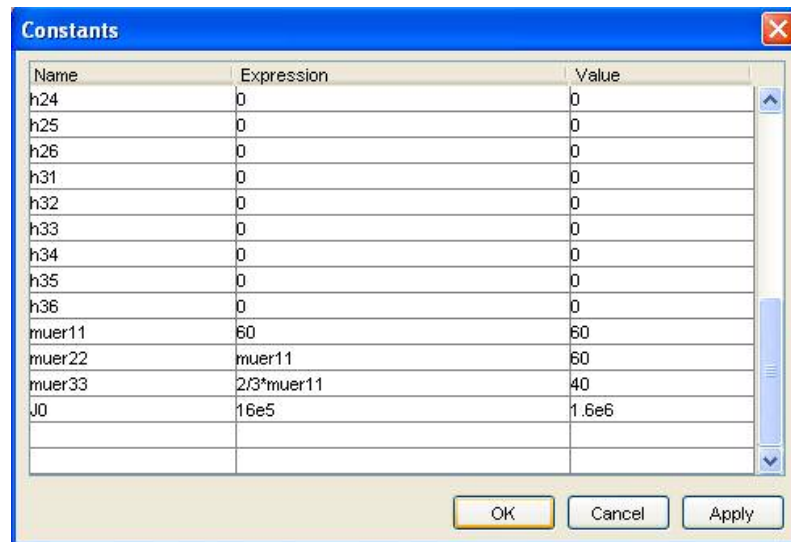


Figure 4.17: “Constants” window.

Now that the constants have been defined the equations for the subdomain of the Galfenol plates can be changed based on the weighted residual integral introduced in Chapter 3. To do so, first select the solid mechanics model in the “Multi-physics” menu and open the “Physics” tab of the “subdomain setting” window. For each type of material, chose the appropriate “material model”. Select anisotropic for the Galfenol plates subdomains and click on the “Edit” button next to the Quantity “D” to input the constants for the stiffness matrix. Figure 4.18 shows the “D” matrix window and the

“subdomain setting” window for an anisotropic material. Similarly, for the magnetostatic “subdomain setting” window select an anisotropic permeability matrix and input the constant names for the coefficient of the permeability matrix introduced earlier.

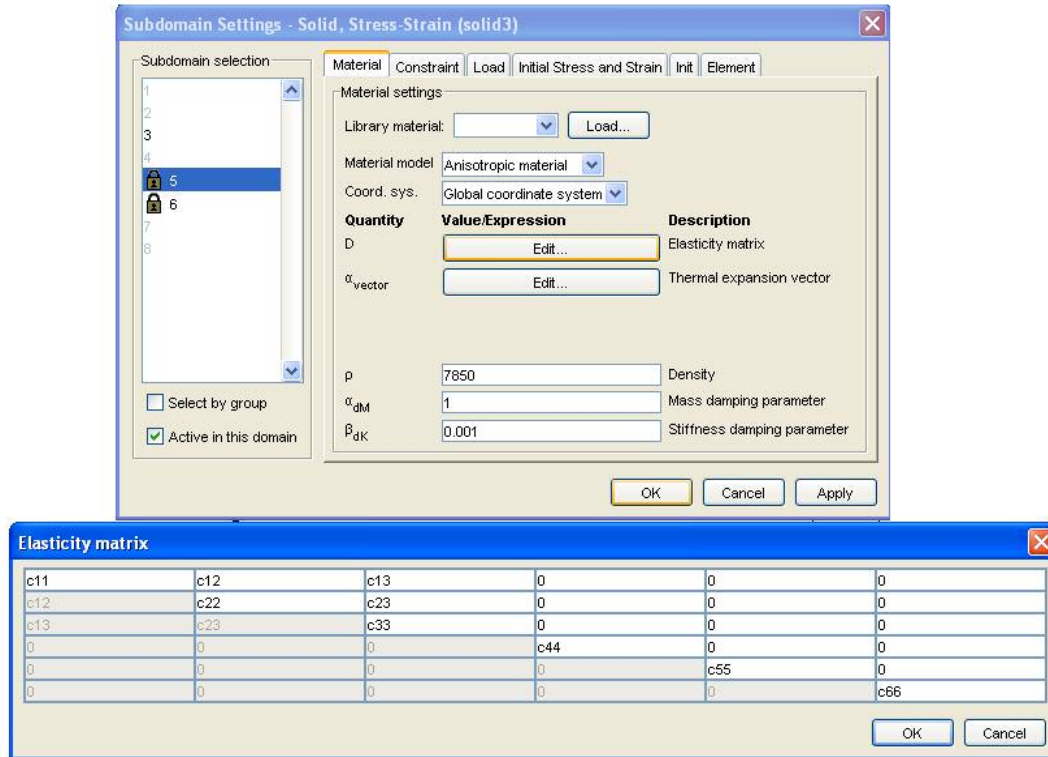


Figure 4.18: “D” matrix window and the “subdomain setting” window for an anisotropic material.

The next step consists of modifying the equation settings of the application modes. To do so, first change the solution form to “weak” in the “solver parameter” window and open the “Equation system/subdomain setting” window. The weak forms of the equation governing the purely magnetic and purely mechanical application mode are implemented in the subdomain active for these application modes. The subdomains referring to the Galfenol plates need to have equation (3.39) and (3.40) implemented. In the “variable” tabs, the formula for the stress and magnetic induction should be modified to account for

the anisotropy previously implemented earlier. Complete these equations to get (2.77) and (2.76). Table 4.1 summarizes the important variables of the implementation. The constitutive equations are the only changes from the original software equation set up.

The weak form may be expressed as the test function of the strain energy density for the mechanical application mode and the test function of the magnetic energy for the magnetic application mode. Note that here the three first slots refer to the displacement vector components (respectively, “u”, “v” and “w”) and the third refers to the magnetic scalar potential. If the magnetic application mode was selected first in the “model navigator” window, the first slot would correspond to the magnetic scalar potential and the last three slots to respectively “u”, “v” and “w”. See Figure 4.19 to see how the governing equations are implemented in the weak form on the “weak” tab of the “subdomain setting/ equations system” window. The solvers recommended for this type of problem are “non-linear SPOOLES” and “non-linear GMRES” with an “algebraic multigrid” preconditioner. Ideally, “Lagrange quadratic” elements are used but eventually linear elements may be used to limit the memory use. Results will be discussed in next chapter.

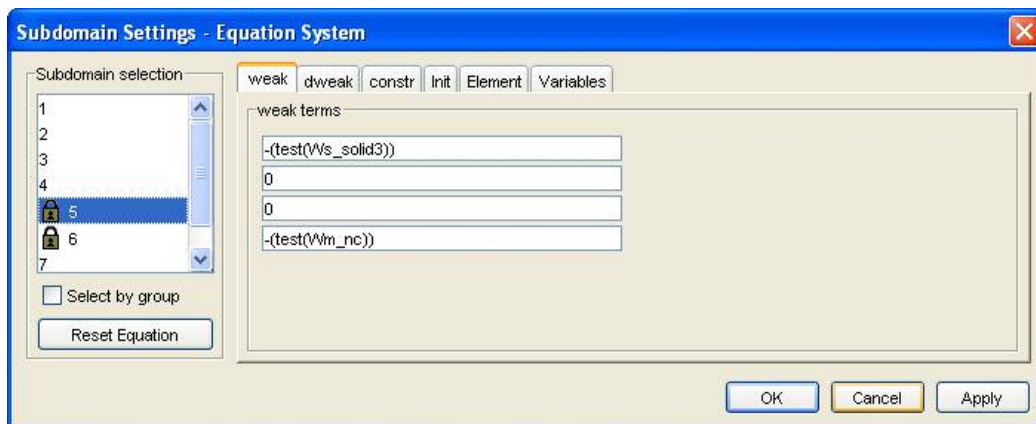


Figure 4.19: “weak” tab of the “subdomain setting/ equations system” window.

	Expression		Description
Name	Equation (2.17)		
ex_solid3	ux		Strain "x" component
ey_solid3	vy		Strain "y" component
ez_solid3	wz		Strain "z" component
exy_solid3	0.5*(uy+vx)		Strain "xy" component
eyz_solid3	0.5*(wy+vz)		Strain "yz" component
exz_solid3	0.5*(uz+wx)		Strain "xz" component
Hx_nc	-Vmx		Magnetic field "x" component
Hy_nc	-Vmy		Magnetic field "y" component
Hz_nc	-Vmz		Magnetic field "z" component
sx_solid3	(c11*ex_solid3+c12*ey_solid3+c13*ez_solid3)-(g11*Bx_nc+g12*By_nc+g13*Bz_nc) +Hx_nc*Ex_nc-0.5*mu0_nc*(Hx_nc*Hx_nc+Hy_nc*Hy_nc+Hz_nc*Hz_nc)		Stress "x" component
sy_solid3	(c12*ex_solid3+c22*ey_solid3+c23*ez_solid3)-(g21*Bx_nc+g22*By_nc+g23*Bz_nc) +Hy_nc*By_nc-0.5*mu0_nc*(Hx_nc*Hx_nc+Hy_nc*Hy_nc+Hz_nc*Hz_nc)		Constitutive equations (2.76) Stress "y" component
sz_solid3	(c13*ex_solid3+c23*ey_solid3+c33*ez_solid3)-(g31*Bx_nc+g32*By_nc+g33*Bz_nc) +Hz_nc*Bz_nc-0.5*mu0_nc*(Hx_nc*Hx_nc+Hy_nc*Hy_nc+Hz_nc*Hz_nc)		Note coeff (alpha, beta=1, 2, 3) are from c^H Stress "z" component
sxy_solid3	(c11*ex_solid3+c12*ey_solid3+c13*ez_solid3)-(g41*Bx_nc+g42*By_nc+g43*Bz_nc) +Hz_nc*Bz_nc-0.5*mu0_nc*(Hx_nc*Hx_nc+Hy_nc*Hy_nc+Hz_nc*Hz_nc)		Stress "xy" component
syz_solid3	(c11*ex_solid3+c12*ey_solid3+c13*ez_solid3)-(g51*Bx_nc+g52*By_nc+g53*Bz_nc) +Hz_nc*Bz_nc-0.5*mu0_nc*(Hx_nc*Hx_nc+Hy_nc*Hy_nc+Hz_nc*Hz_nc)		Stress "yz" component
sxz_solid3	(c11*ex_solid3+c12*ey_solid3+c13*ez_solid3)-(g61*Bx_nc+g62*By_nc+g63*Bz_nc) +Hz_nc*Bz_nc-0.5*mu0_nc*(Hx_nc*Hx_nc+Hy_nc*Hy_nc+Hz_nc*Hz_nc)		Stress "xz" component
Bx_nc	(mu0_nc*mustr11)*Hx_nc+(g11*ex_solid3+g12*ey_solid3+g13*ez_solid3 +g14*2*eyz_solid3+g15*2*exz_solid3+g16*2*exy_solid3)		Magnetic induction "x" component
By_nc	(mu0_nc*mustr22)*Hy_nc+(g21*ex_solid3+g22*ey_solid3+g23*ez_solid3 +g24*2*eyz_solid3+g25*2*exz_solid3+g26*2*exy_solid3)		Constitutive equations (2.77) Magnetic induction "y" component
Bz_nc	(mu0_nc*mustr33)*Hz_nc+(g31*ex_solid3+g32*ey_solid3+g33*ez_solid3 +g34*2*eyz_solid3+g35*2*exz_solid3+g36*2*exy_solid3)		Magnetic induction "z" component
Wm_nc	0.5*(Bx_nc*Hx_nc+By_nc*Hy_nc+Bz_nc*Hz_nc)		Magnetic energy density
Ws_solid3	0.5*(sx_solid3*ex_solid3+sy_solid3*ey_solid3+sz_solid3*ez_solid3 +2*sxy_solid3*exy_solid3+2*syz_solid3*eyz_solid3+2*sxz_solid3*exz_solid3)		Strain energy density

Table 4.1: Summary of the important variables displayed in the "Variables" tab of a magnetostriuctive subdomain.

4.3. Implementation of the Dynamic BVPs

4.3.1. Electromagnetic, time-harmonic, FEM

The electromagnetic, time harmonic FEM can be very practical in the design period of a magnetostrictive based transducer. The magnetic circuit of a transducer significantly affects the performance of the magnetostrictive material. One must make sure that the rod is uniformly and sufficiently penetrated by the magnetic field. The electromagnetic model was used to model the magnetic circuit of pump (see Figure 4.20).

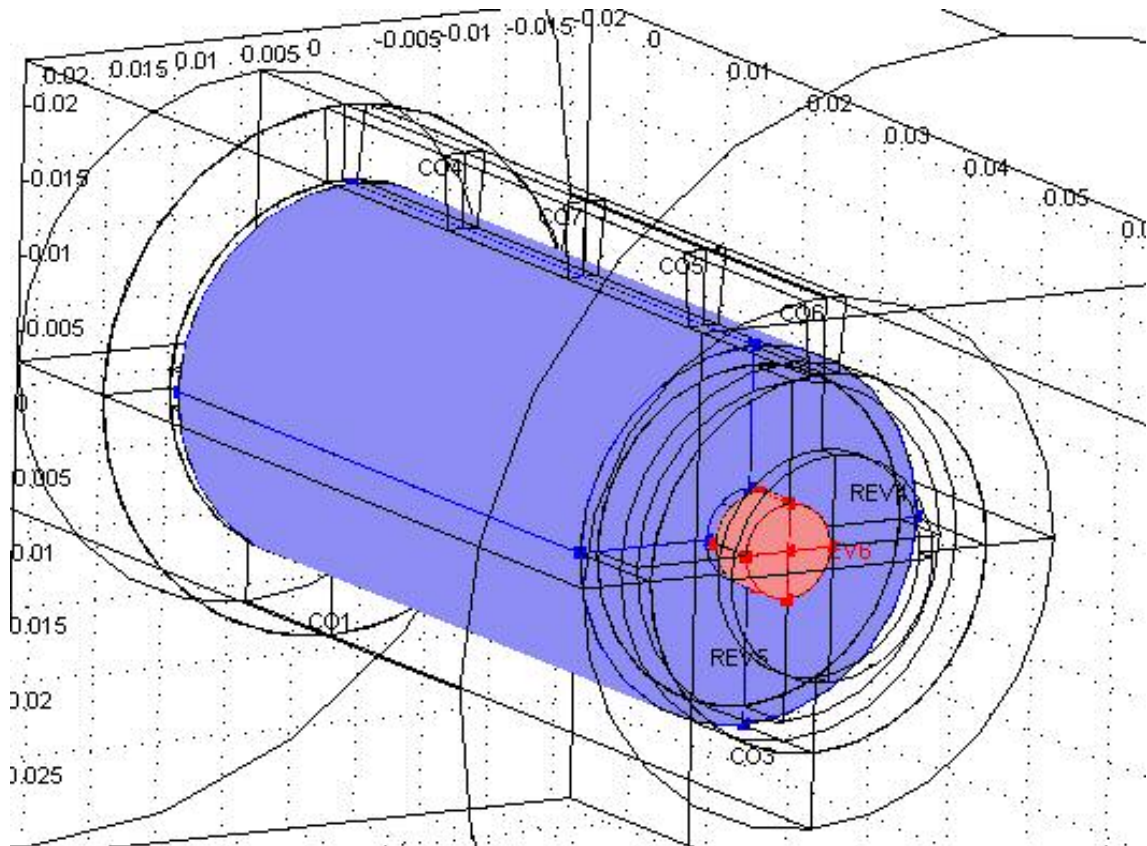


Figure 4.20: Pump model geometry.

The coil and the magnetostrictive rod can be observed in Figure 4.20 as well as the steel housing (transparent parts). On the top of the steel housing, four subdomains were created to model the effect of the slit in the housing length on the magnetic circuit performance at different frequencies. As explained in the introduction chapter, eddy current power losses can be significant in high frequency applications. The main goal of this model was to visualize the effect of eddy currents by varying the size of the slit of the housing and observing the distribution of the magnetic field inside the sample for different conditions. Since four subdomains were drawn to model the slit, one can go from a “full slit situation” by giving a relative permeability of 1 (in the “subdomain setting” window) to all four domains, to a “no slit situation” by giving those four subdomains a relative permeability of magnetic steel, the material used in the rest of the housing parts.

The main implementation issue of this model was to reproduce accurately the field generated by the coil. The best way to model a coil in 3-D analysis on FEMLAB3.1© is to use an “externally applied volumetric current density”, \mathbf{J}^e , applied inside a hollow cylinder. Depending on the axis of symmetry of the coil one can implement in the “electric parameter” tab of the “subdomain setting” window (see Figure 4.21), for the hollow cylinder subdomain:

- “x” axis is the coil symmetry axis:

$$J_{ex_qav} = 0, \quad J_{ey_qav} = -J_0 \cdot z / \sqrt{y^2 + z^2}, \quad J_{ez_qa} = J_0 \cdot y / \sqrt{y^2 + z^2},$$

- “y” axis is the coil symmetry axis:

$$J_{ex_qav} = -J_0 \cdot z / \sqrt{x^2 + z^2}, \quad J_{ey_qav} = 0, \quad J_{ez_qav} = J_0 \cdot x / \sqrt{x^2 + z^2},$$

- “z” axis is the coil symmetry axis:

$$J_{ex_qav} = -J_0 * y / \sqrt{x^2 + y^2}, \quad J_{ey_qav} = J_0 * x / \sqrt{x^2 + y^2}, \quad J_{ez_qav} = 0.$$

It is not suggested to use a random axis to model a coil but eventually similar equations can be implemented for any orientation.

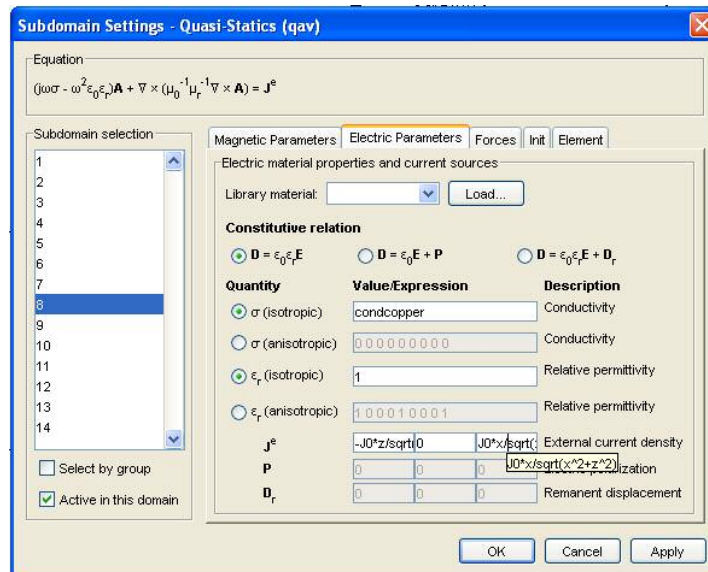


Figure 4.21: “Electric parameter” tab of the “subdomain setting” window.

Apart from the coil modeling there are no difficult issues with this application mode. The current frequency can be defined in the “Application scalar variables” window accessible from the “physics” menu under “scalar variables” (see Figure 4.22). No changes were done in the equation settings. The “application mode properties” are displayed in Figure 4.23. This window can be opened from the model navigator by selecting the application mode and clicking on “application mode properties”. Material properties and some constants such as J_0 , the magnitude of the externally applied volumetric current density can be found in the “constants” window (Figure 4.24). The solver used was the one suggested by the software, the direct SPOOLES solver.

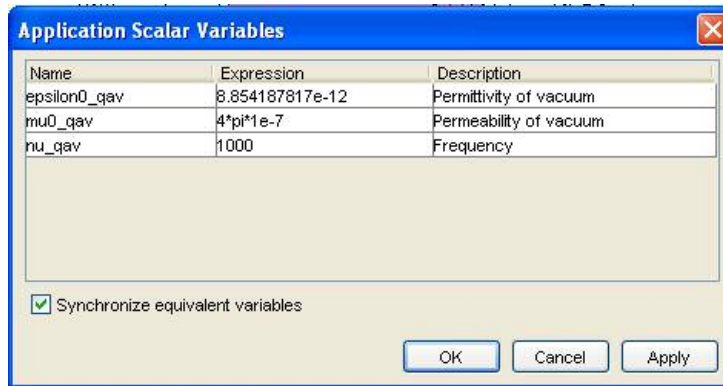


Figure 4.22: “Application scalar variables” window.

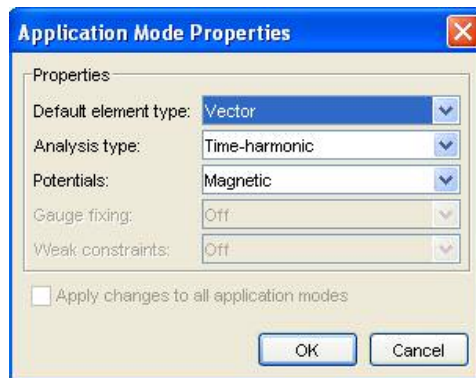


Figure 4.23: “application mode properties” window.

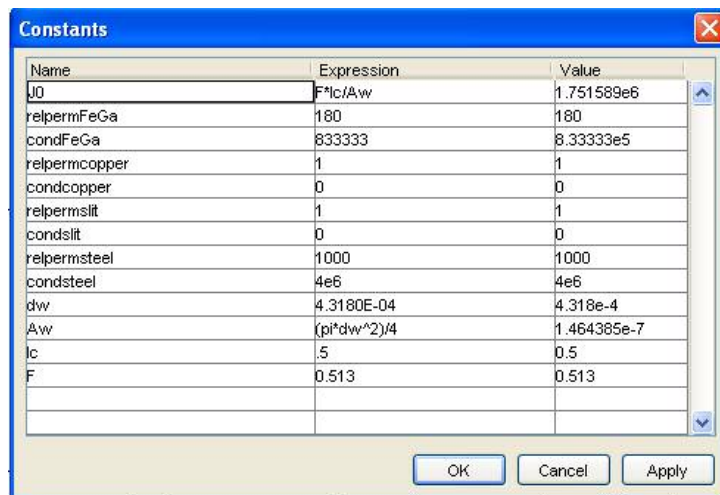


Figure 4.24: “constant” window.

4.3.2. Fully coupled electro-magneto-mechanical FEM of a magnetostrictive material

Unfortunately, a “3-D, dynamic, electromagnetic” application mode is not available on FEMLAB 3.1© electromagnetic module. This application mode is scheduled for the version 3.2 of the software which should be on the market by fall 2005. Attempts to write a program from the PDE mode, which allows implementing almost any type of PDEs systems, were not successful. The FEMLAB© technical support strongly suggested postponing this implementation until version 3.2 became available and therefore the implementation presented below is just a suggestion of implementation of a fully couple non-linear electro-magneto-mechanical model based on the current “3-D dynamic solid mechanics” application mode and the future “3-D dynamic electromagnetic” application mode.

Assuming that the application mode extensions are respectively “_solid3” and “_em”, suggested implementation “variables” are displayed in Table 4.2 (Table split on the next two pages). The suggested formulations of the time derivatives of those variables necessary to get a time dependent model are given below in Table 4.3. These should both be implemented for the magnetostrictive subdomain only. Note that the time derivative of variable has a “_t” after the variable name. This does not mean that the variable is time differentiated on its own. It is just the common notation for these types of time derivatives of variables. For example the velocity vector, \mathbf{v} , used to transform the second order derivative term in the equation of motion can be expressed as $\mathbf{v}=\{u_t,v_t,w_t\}^t$.

Name	Expression	Description
ex_solid3	ux	Strain "x" component
ey_solid3	vy	Strain "y" component
ez_solid3	wz	Strain "z" component
exy_solid3	0.5*(uy+vx)	Strain "xy" component
eyz_solid3	0.5*(vy+vz)	Strain "yz" component
exz_solid3	0.5*(uz+wx)	Strain "xz" component
Bx_em	Axy-Ayz	Magnetic induction "x" component
By_em	Axz-Azx	Magnetic induction "y" component
Bz_em	Ayz-Axy	Magnetic induction "z" component
Ex_em	Vx-Axt	Electric field "x" component
Ey_em	Vy-Ayt	Electric field "y" component
Ez_em	Vz-Azt	Electric field "z" component
sx_solid3	(c11*ex_solid3+c12*ey_solid3+c13*ez_solid3)+(h11*Ex_em+h12*By_em+h13*Bz_em)+Hx_em*Ex_em-0.5*mu0_em*(Hx_em+Hx_em+Hz_em*Hz_em)	Stress "x" component
sy_solid3	(c12*ex_solid3+c22*ey_solid3+c23*ez_solid3)-(h21*Bx_em+h22*By_em+h23*Bz_em)+Hy_em*By_em-0.5*mu0_em*(Hx_em+Hy_em+Hz_em*Hz_em)	Stress "y" component
sz_solid3	(c13*ex_solid3+c23*ey_solid3+c33*ez_solid3)-(h31*Bx_em+h32*By_em+h33*Bz_em)+Hz_em*Bz_em-0.5*mu0_em*(Hx_em+Hy_em+Hz_em*Hz_em)	Stress "z" component
sxy_solid3	(c11*ex_solid3+c12*ey_solid3+c13*ez_solid3)+(h41*Ex_em+h42*By_em+h43*Bz_em)	Stress "xy" component
syz_solid3	(c11*ex_solid3+c12*ey_solid3+c13*ez_solid3)+(h51*Ex_em+h52*By_em+h53*Bz_em)	Stress "yz" component
sxz_solid3	(c11*ex_solid3+c12*ey_solid3+c13*ez_solid3)+(h61*Ex_em+h62*By_em+h63*Bz_em)	Stress "xz" component
Hx_em	Bx_em/(mu0_em*musr1)+(h11*ex_solid3+h12*ey_solid3+h13*ez_solid3-h14*2*eyz_solid3+h15*2*exz_solid3+h16*2*exy_solid3)	Magnetic field "x" component
Hy_em	By_em/(mu0_em*musr2)+(h21*ex_solid3+h22*ey_solid3+h23*ez_solid3-h24*2*eyz_solid3+h25*2*exz_solid3+h26*2*exy_solid3)	Magnetic field "y" component
Hz_em	Bz_em/(mu0_em*musr3)+(h31*ex_solid3+h32*ey_solid3+h33*ez_solid3-h34*2*eyz_solid3+h35*2*exz_solid3+h36*2*exy_solid3)	Magnetic field "z" component
Dx_em	eps0_em*epsr11*Ex_em	Electric displacement "x" component
Dy_em	eps0_em*epsr22*Ey_em	Electric displacement "y" component
Dz_em	eps0_em*epsr33*Ez_em	Electric displacement "z" component

Table 4.2: Suggested implementation of the "Variables" for magnetosubdomain

in an electro-magneto-mechanical model.

Other Variables		
Mx_em	(muS11/mu_0-Ex_em)	Equation (2.35)
My_em	(muS22/mu_0-By_em)	"
Mz_em	(muS33/mu_0-Ez_em)	"
Px_em	(Dx_em-eps11*Ex_em)	Equation (2.36)
Py_em	(Dy_em-eps22*Ey_em)	"
Pz_em	(Dz_em-eps33*Ez_em)	"
Jex_em	0 for all but coil where Jex_em = -J0*z/sqrt(x^2+z^2) when coil symmetry axis is the "y" axis	
Jey_em	0 for all but coil where Jey_em = 0 when coil symmetry axis is the "y" axis	
Jez_em	0 for all but coil where Jez_em = J0*x/sqrt(x^2+z^2) when coil symmetry axis is the "y" axis	
Jx_em	Jex_em+cond11*Ex_em	Equation (2.28)
Jy_em	Jey_em+cond22*Ey_em	"
Jz_em	Jez_em+cond33*Ez_em	"
Vax_em	(Vx+Ax)	
Vay_em	(Vy+Ay)	
Vaz_em	(Vz+Az)	
Q_em	-(Jex_em*Vax_em+Jey_em*Vay_em+Jez_em*Vaz_em) +cond*(Vax_em*Vax_em+Vay_em*Vay_em+Vaz_em*Vaz_em)	Equation (2.47)
		Time-average Dissipated Energy (Used to quantify Eddy current losses)
		Magnetization "x" component
		Magnetization "y" component
		Magnetization "z" component
		Polarization "x" component
		Polarization "y" component
		Polarization "z" component
		Externally applied J "x" component
		Externally applied J "y" component
		Externally applied J "z" component
		Total J "x" component
		Total J "y" component
		Total J "z" component
		Computational Variable for Q
		Computational Variable for Q
		Computational Variable for Q

Table 4.2: Suggested implementation of the "Variables" for magnetostrictive subdomain in an electro-magneto-mechanical model (continued)

Name	Expression	Description
ex_t_solid3	uxt	Strain "x" component
ey_t_solid3	vyt	Strain "y" component
ez_t_solid3	wzt	Strain "z" component
exy_t_solid3	0.5*(uyt+vxt)	Strain "xy" component
eyz_t_solid3	0.5*(vyt+vzt)	Strain "yz" component
exz_t_solid3	0.5*(uzt+wzt)	Strain "xz" component
Bx_t_em	Azyt-Ayzt	Magnetic induction "x" component
By_t_em	Axzt-Azxt	Magnetic induction "y" component
Bz_t_em	Ayxt-Axyt	Magnetic induction "z" component
sx_t_solid3	(c11*ex_t_solid3+c12*ey_t_solid3+c13*ez_t_solid3)+(h11*Ex_t_em+h12*By_t_em+h13*Bz_t_em)+Hx_t_em*Em*mu0_em*(Hx_t_em+Hy_t_em+Hz_t_em*Hz_t_em)	Stress "x" component
sy_t_solid3	(c12*ex_t_solid3+c22*ey_t_solid3+c23*ez_t_solid3)-(h21*Bx_t_em+h22*By_t_em+h23*Bz_t_em)+Hy_t_em*By_t_em-0.5*mu0_em*(Hx_t_em+Hy_t_em+Hz_t_em*Hz_t_em)	Stress "y" component
sz_t_solid3	(c13*ex_t_solid3+c23*ey_t_solid3+c33*ez_t_solid3)-(h31*Bx_t_em+h32*By_t_em+h33*Bz_t_em)+Hz_t_em*Bz_t_em-0.5*mu0_em*(Hx_t_em+Hy_t_em+Hz_t_em*Hz_t_em)	Stress "z" component
sxy_t_solid3	(c11*ex_t_solid3+c12*ey_t_solid3+c13*ez_t_solid3)+(h41*Ex_t_em+h42*By_t_em+h43*Bz_t_em)	Stress "xy" component
syz_t_solid3	(c11*ex_t_solid3+c12*ey_t_solid3+c13*ez_t_solid3)+(h51*Ex_t_em+h52*By_t_em+h53*Bz_t_em)	Stress "yz" component
szx_t_solid3	(c11*ex_t_solid3+c12*ey_t_solid3+c13*ez_t_solid3)+(h61*Ex_t_em+h62*By_t_em+h63*Bz_t_em)	Stress "xz" component
Hx_t_em	Bx_t_em/(mu0_em*mustr11)+(h11*ex_t_solid3+h12*ey_t_solid3+h13*ez_t_solid3+h14*2*eyz_t_solid3+h15*2*ex_t_solid3+h16*2*exy_t_solid3)	Magnetic field "x" component
Hy_t_em	By_t_em/(mu0_em*mustr22)+(h21*ex_t_solid3+h22*ey_t_solid3+h23*ez_t_solid3+h24*2*eyz_t_solid3+h25*2*ex_t_solid3+h26*2*exy_t_solid3)	Magnetic field "y" component
Hz_t_em	Bz_t_em/(mu0_em*mustr33)+(h31*ex_t_solid3+h32*ey_t_solid3+h33*ez_t_solid3+h34*2*eyz_t_solid3+h35*2*ex_t_solid3+h36*2*exy_t_solid3)	Magnetic field "z" component

Table 4.3: Suggested implementation of the time derivatives "variables" for

magnetostrictive subdomain in an electro-magneto-mechanical model.

In Table 4.3, some terms like “Axt” or “uxt” are short notation recognized by the software for time derivative of variables like the “x” components of the magnetic vector potential, \mathbf{A} , or the derivative with respect to “x” of the displacement vector “ux”. Whereas for “uxt”, the “x” and the “t” both indicates the displacement vector “x” component, “u”, is differentiated with respect to “x” and “t”. Short notation can be confusing for this reason but are very practical when inputting all the equations in the software. An alternative is to use Matlab function as $\text{diff}(\mathbf{A},t)$ or $\text{diff}(\text{diff}(u,x),t)$ for respectively, “Axt” and “uxt”. One last example of this type of notation to perfectly understand the notation system is “Axyt” which could be written as $\text{diff}(\text{diff}(\mathbf{A},y),t)$.

Note that some terms have an extension “_time” which is the notation for the time derivative of variables which are not degrees of freedom of the model like the stress and magnetic induction tensor components in contrast with the displacement vector components or the magnetic vector potential components.

Table 4.4 and 4.5 summarize the expression to implement in the “weak” and “dweak” tab of the “Equation system/ Subdomain setting” window. They are based on the derivation originally introduced by Aparicio and Sosa [1] which was introduced in Chapter 2 and 3. The formulation was validated by Aparicio and Sosa [1] which suggests that a correct implementation of such a model on FEMLAB is achievable.

To conclude this section and this chapter I will remind the readers that a time-dependent electro-magneto-mechanical model is a non-linear problem that requires a time-dependent, non-linear solver. The elements type should at least be Lagrange quadratic to achieve reasonable accuracy. I also want to emphasize that this type of model was never successfully implemented due to the current absence of a dynamic

electro-magneto-mechanical application mode. The formulation was however validated by experimental results in Aparicio and Sosa [1] using a research FEM code (FEAP).

Corresponding Variable row	"weak" tab
u	$-(ex_solid3_test*sx_solid3+ey_solid3_test*sy_solid3+ez_solid3_test*sz_solid3+2*exy_solid3_test*sxy_solid3+2*eyz_solid3_test*syz_solid3+2*exz_solid3_test*sxz_solid3)$
v	0
w	0
u t	$u_t*u_t_test$
v t	$v_t*v_t_test$
w t	$w_t*w_t_test$
Ax	$-(test(Bx_em)*Hx_em+test(By_em)*Hy_em+test(Bz_em)*Hz_em)+(Ax_test*Jex_em+Ay_test*Jey_em+Az_test*Jez_em)-cond*(Ax_test*Vx+Ay_test*Vy+Az_test*Vz)$
Ay	0
Az	0
V	$-(Vx_test*Dx+Vy_test*Dy+Vz_test*Dz)$

Table 4.4: Suggested implementation of the time independent parts of the governing equations in the “weak” tab.

Corresponding Variable row	"dweak" tab
u	$\rho_{solid3}*(u_test*u_t_time+v_test*v_t_time+w_test*w_t_time)$
v	0
w	0
u t	$u_time*u_t_test$
v t	$v_time*v_t_test$
w t	$w_time*w_t_test$
Ax	$-cond*(Ax_test*Axt+Ay_test*Ayt+Az_test*Azx)$
Ay	0
Az	0
V	0

Table 4.5: Suggested implementation of the time dependent parts of the governing equations in the “dweak” tab.

Chapter 5: Validation of the FEM Implementations on FEMLAB 3.1©

In Chapter 4, details of the methods used for implementation of the BVPs introduced in this thesis were presented in conjunction with their use in appropriate examples. The examples were selected either to better understand the software capabilities or to help in the design of magnetostrictive-based applications currently being developed using Galfenol at the University of Maryland. In Chapter 5, the results obtained with these models are summarized. The purely structural model was presented only to introduce FEMLAB 3.1© to an unfamiliar reader. It is based on an unmodified application mode and does not provide relevant data on magnetostrictive-based applications. Results of this model will not be discussed further in this Chapter. The examples used to illustrate magnetostatic and quasi-static, time-harmonic, electromagnetic models are both based on existing application modes. In the first section of this Chapter, results are presented and discussed for two types of magnetic field sources, permanent magnets for the magnetostatic example and a coil for the quasi-static electromagnetic model. Both of these models require calibration with experimental data. The second section focuses on the results of the static coupled magneto-mechanical model. This section includes comparison with experimental data and an explanation of how to choose the magnetostrictive material properties (assumed constant) for such a model.

5.1. Examples of Uncoupled Finite Elements Models based on existing Application Modes

5.1.1. Example using the magnetostatic application mode

As introduced previously, the magnetostatic example is a model of a magnetic circuit used in an experimental set-up. The purpose of this apparatus was to obtain in-plane magnetostriction measurements while applying a magnetic field at different angles with respect to the easy axis of the magnetostrictive sample. The sample was mounted on a rotating support and the magnetic circuit fixed while the sample rotates through 360° .

The FEM model purpose was to provide the magnetic induction distribution inside the sample for different length gaps between the two permanent magnets. The method one would use to successively go from one separation distance to another was to go to the geometry entered in the drawing mode and move the cylinders on which the permanent magnets are attached to the desired length gap. Note that both the cylinders and the permanent magnets subdomains require being moved. The subdomain modeling air also needs to be modified since it consists of a rectangular brick-shaped subdomain from which all other subdomains lying within this volume are subtracted. Modifying geometry is always a tedious and time consuming task, especially for magnetic models, since it requires restarting the analysis at the first step of a FEM implementation, the drawing of the geometry. Moreover, one must make sure revised subdomains boundaries are well connected to adjacent subdomains surfaces. Generally, the air gap is modeled using a

cylindrical subdomain sharing boundaries with the flat pole faces of both permanent magnets that face the air gap. Any small gap between the permanent magnet subdomains and the new “air gap” subdomain will result in a meshing error. An efficient method for avoiding this type of meshing error is to make a slightly larger “air gap” subdomain and to subtract copies of the permanent magnets subdomains to ensure proper subdomain dimensions. Once this is performed, the air gap cylinder needs to have the volume of the Galfenol plate subtracted in order to get consistent subdomain boundaries.

For this research the two gap sizes investigated were 12.0mm and 43.2mm. The first corresponds to the minimum gap size needed to accommodate the longest dimension of the 8x8x1 mm³ Galfenol plate as it was rotated. The larger gap was selected for study because the experimental apparatus was also configured for operation at this gap. Having two air gap distances allowed verification of the accuracy of the calibration of the permanent magnets.

To calibrate the permanent magnets, one must first experimentally measure the peak magnetic field on the pole faces of the permanent magnets as well as the minimum magnetic field obtained half way between the permanent magnets on the axial symmetry axis (x-axis in Figure 4.15). The location of the minimum field generally corresponds to the midpoint of the Galfenol sample’s location. Then, in the FEM model, assign the permanent magnet subdomains a magnetization similar that of the pole faces and increase its value until a magnetic field distribution is observed in the air gap that is similar to the one observed experimentally. In Table 5.1, one can see that for both gap lengths the experimentally measured magnetic fields in the air gap are predicted quite well when a magnetization value of 950kA/m is assigned to the permanent magnets subdomains.

Gap (mm)	Magnetic Field (kA/m) Experimental measurement		Magnetic Field (kA/m) FEM results	
	between magnets	near Magnets	between magnets	near Magnets
43.2	291	477	290	479
12.0	685	704	683	706

Table 5.1: Calibration of the permanent magnets chart.

The material used for the magnetic circuit was 1018 magnetic steel. Since no B-H curve for 1018 steel was available, the B-H curves of 1010 magnetic steel were used. The main difference between the two steels is the level of carbon, which is lower for 1010 magnetic steel. The permeability of 1018 magnetic steel should be slightly smaller than the one of 1010 magnetic steel. The B-H curves of the 1010 magnetic steel shows a steep linear rise in magnetic induction from 0 to 1.35 Tesla for an increase in applied magnetic field from 0 to 150kA/m [6]. A relative permeability of 7161 can be obtained by dividing the increase magnetic induction by the product of the increase in magnetic field and the permeability of vacuum.

The general magnetic field flux path along with the normalized magnetic induction distribution inside the magnetic circuit with a 12.0-mm and a 43.2-mm gap length can be observed in, respectively, Figure 5.1 (a) and (b). On both, a thick line between the two permanent magnets represents the line along which the value of the magnetic field is plotted in Figures 5.2. The normalized magnetic induction is given by the formula

$$B_{norm} = \sqrt{B_x + B_y + B_z} \quad (5.1).$$

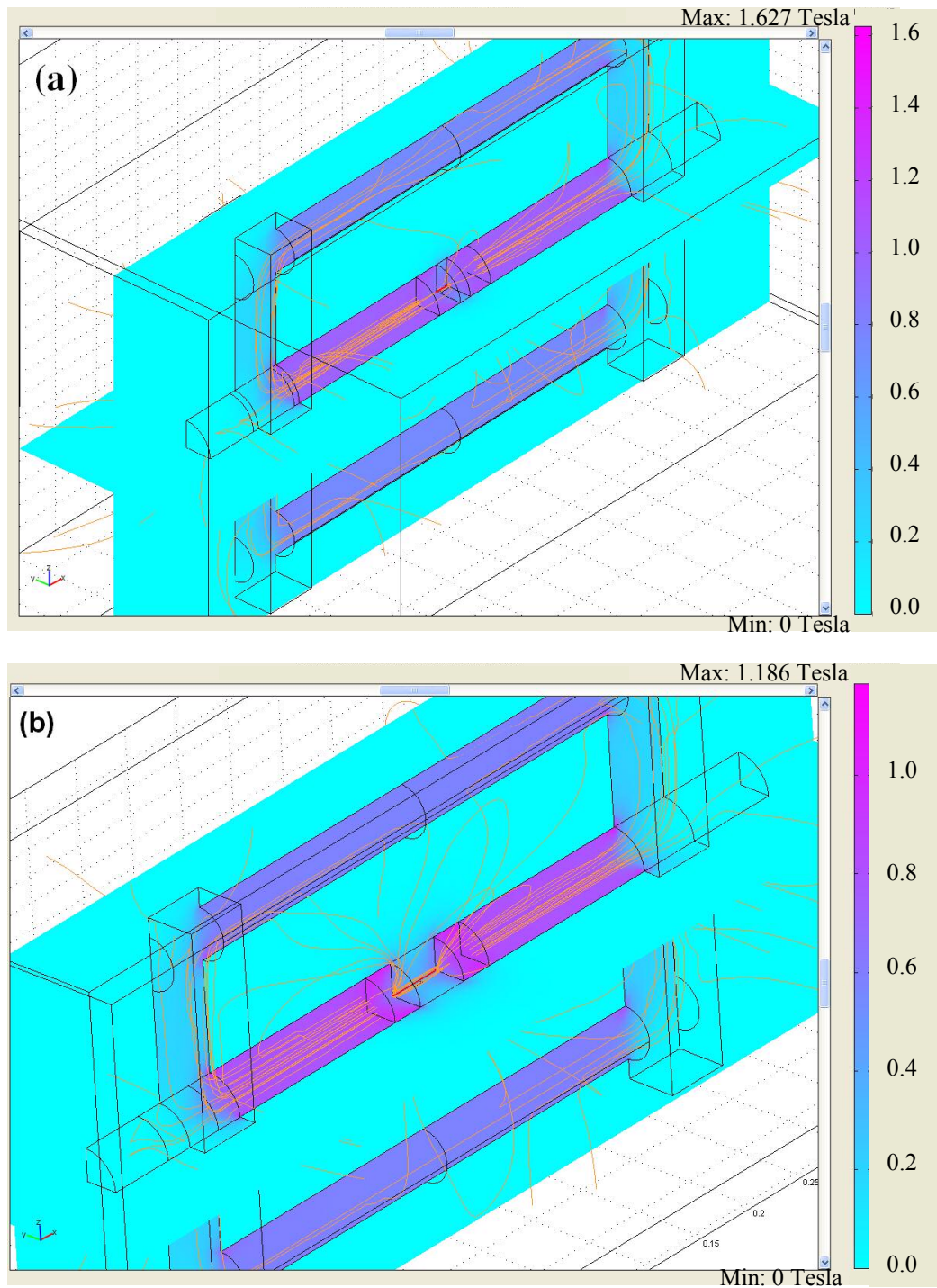


Figure 5.1: 3-D plot of the normalized magnetic induction (in Tesla) (slice plot) and the magnetic field's path (streamlines) inside, respectively, (a) the 12.0-mm and (b) the 43.2-mm air gap models with no Galfenol sample between the permanent magnets.

In Figure 5.1, the number of streamlines passing through the bottom and top magnetic steel cylinders can quantify how much of the field is actually going through the high permeability magnetic circuit. One may observe that more streamlines pass outside of the magnetic circuit for the 43.2-mm model than for 12.0-mm model. The slice plots are 2D distribution of the normalized magnetic induction along the two planes of symmetry, the x-y plane and the x-z plane. As, expected, the level of magnetic induction observed in the top and bottom cylinders of the magnetic circuit is about half the one observed in the cylinders holding the permanent magnets.

Figure 5.2a&b show the magnetic field level between the two permanent magnets along their axis of symmetry for, respectively, a 12.0-mm and a 43.2-mm air gap. The permeability of the Galfenol sample is set to the 1 for these calibration models since their goal is to reproduce the experimentally measured magnetic field in the air gap as discussed earlier. The relative permeability of 1018 steel used in the model for the results in Figures 5.2a & b was 6000. Figure 5.2c is the same Figure as 5.2b but with a magnetic steel relative permeability increased to 8000. All three figures have an “x” axis going from 0 to either 12.0mm (Figure 5.2a) or 43.2mm (Figure 5.2b&c) representing the distance from the left permanent magnet along the axial symmetry axis of the permanent magnets.

As expected, comparison of Figure 5.2a and 5.2b shows that the field strength inside the 12.0-mm gap length is significantly larger than for the 43.2-mm gap length. As one may observe, less than a 1% drop in magnetic field occurs in the air gap when decreasing the permeability of the magnetic steel from 8000 to 6000. This can be explained by the significantly larger permeability of magnetic steel with respect to the permeability of air.

For all three cases, the experimental values of the field measured in the air gap are very close to the FEM results. Therefore, one can conclude that to optimize the magnetic circuit the gap length should be reduced as much as the experimental set up allows.

Regarding the FEM post processing tool, one may observe on Figure 5.2a that the quality of the line plot is inferior to the one of Figure 5.2b&c. This can be explained by the density of the meshing in the region in which the line plot's values are extracted. In a line plot, the step size depends of the number of points used along the line chosen by the user. A large step size where the meshing is coarse will result in distinct small steps in the region of curve as can be observed on each ends of the curves in Figures 5.2b&c and in most of Figure 5.2a. The line plots use average values of a chosen quantity along a chosen line using the values computed at the two (or more) closest nodes. Every time two or more points are located in between the same two nodes along the x-axis, they all get the same value and therefore flat steps are visible in the curve. If the meshing is dense like near where the Galfenol sample would be (midpoint of the x-axis on the line plots), then the steps size decreases and the curve looks smooth. This is what occurs on the middle of the curve of Figure 5.2b&c. For Figure 5.2a, the meshing is not as dense because the magnetic field x-component is only plotted for along a 12.0-mm line. The density of the mesh in the 8-mm region where the sample should be is similar for all three models. Therefore, the number of elements used in Figure 5.2a is significantly smaller than the one used in Figure 5.2b&c. Consequently, less node values are used for the 12.0-mm gap models than for the 43.2-mm gap models. However, by reducing the number of points used in the line plot, one can obtain a smoother curve. Figure 5.1a used 70 points which does not decrease the size of the steps so that one may visualize the elements size.

In all three graphs, one also can observe that although the field strength minimum is at the midpoint and maximum at the pole faces, as expected, the curves do not increase monotonically as expected. Increasing the mesh size would reduce this numeric artifact.

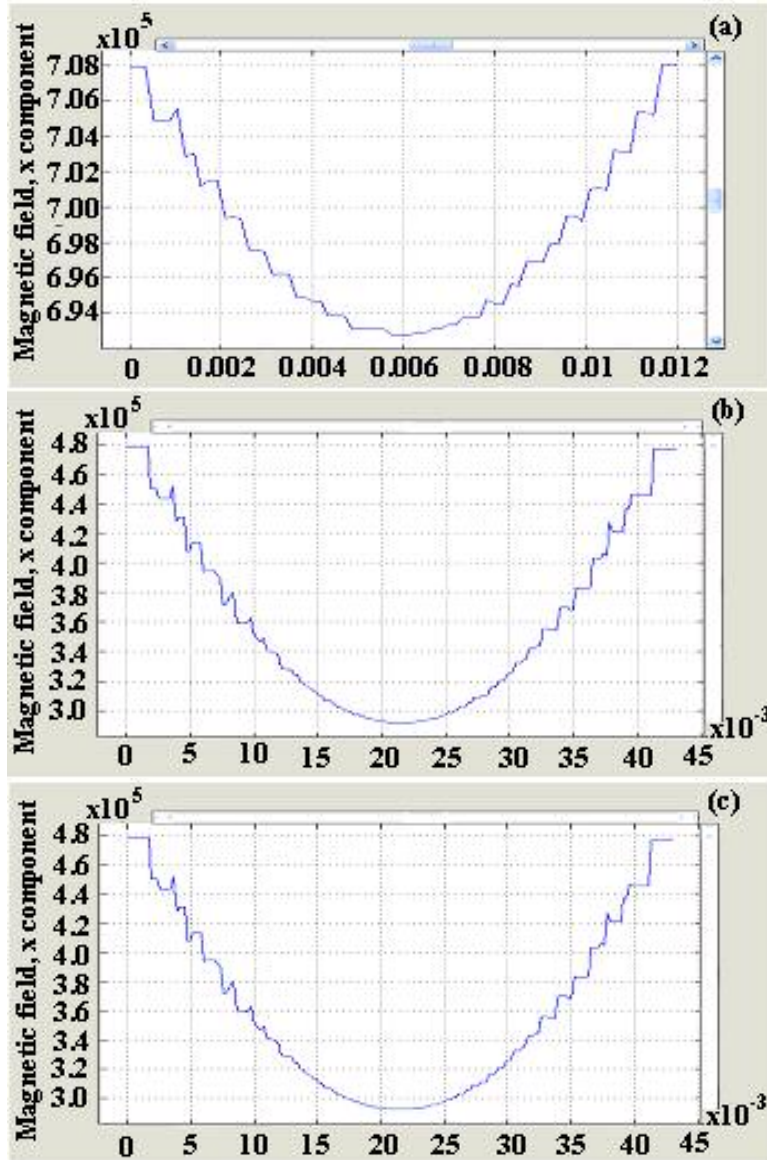


Figure 5.2: Line plot of the magnetic field (in A/m) along the x-axis between the two magnets (no sample) for respectively (a) a 12.0mm and (b&c) a 43.2 mm gap size, and using value of, respectively, (a&b) 6000 and (c) 8000 for the magnetic steel permeability.

The relative permeability of Galfenol can be read on the B-H curve with no applied pre-stress. Unfortunately, the quasi-static M-H curves provided in Kellogg's thesis [19] for a single crystal 19% Galfenol sample only included a B-H curves for a 14.4 MPa (or higher) pre-stress. The relative permeability for this pre-stress is of the order of 360. However, for a pre-stress of 87.1MPa, the relative permeability decreased 6-fold. On the other hand, for a 19% polycrystal Galfenol sample tested under quasi-static conditions with a 6.9MPa pre-stress, the relative permeability is of the order of 400 for a research grade (for fields below 2kA/m) and 220 for the production grade (for fields below 3.6kA/m). The B-H curves of, respectively, a production grade polycrystal 19% Galfenol sample and a research grade polycrystal 19% Galfenol sample are displayed in Figure 5.3a&b (provided by ETREMA products, Inc. [56]). For the models presented in this section, the relative permeability of Galfenol used is 220 (polycrystal production grade 19% sample) and 360 (single crystal 19% sample). Depending on the sample tested, the user of this model must choose the appropriate value since the permeability slightly affects the magnetic induction level in the sample ($\mathbf{B} = \mu_0 \mu_r \mathbf{H}$).

The results obtained are presented in Figures 5.4 and 5.5. Figure 5.4a to Figure 5.4d are line plots of the magnetic induction along the x-axis passing inside the Galfenol sample subdomain for, respectively, (a) a single crystal sample in the 12.0-mm gap model, (b) a single crystal sample in the 43.2-mm gap model, (c) a production grade polycrystal sample in the 12.0-mm gap model, and, (d) a production grade polycrystal sample in the 43.2-mm gap model. Figure 5.5 shows 2-D slice plot on the "x-y plane" of the magnetic induction in the same models as Figure 5.4a to 5.4d. The thick lines in Figure 5.5a to 5.5d represent the line along which Figure 5.4a to 5.4d were plotted.

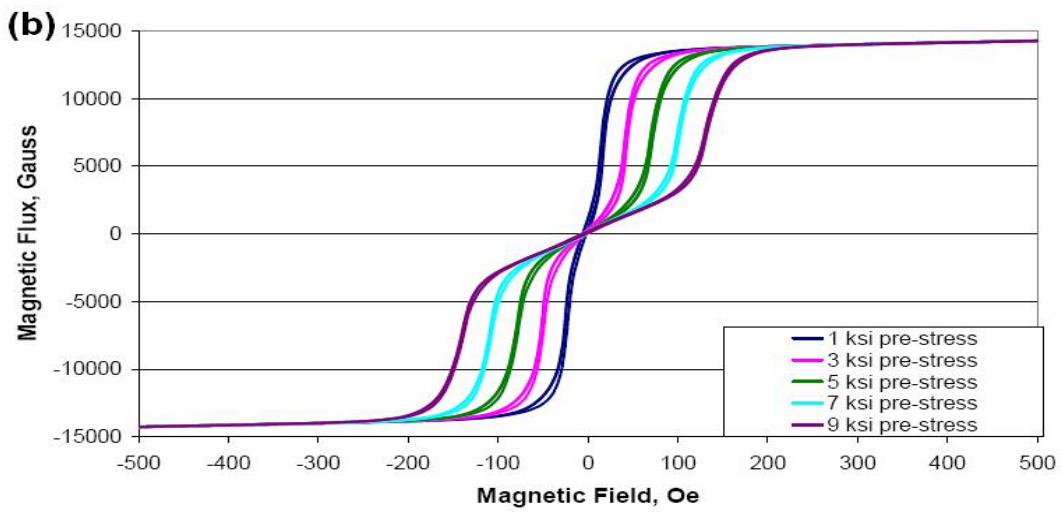
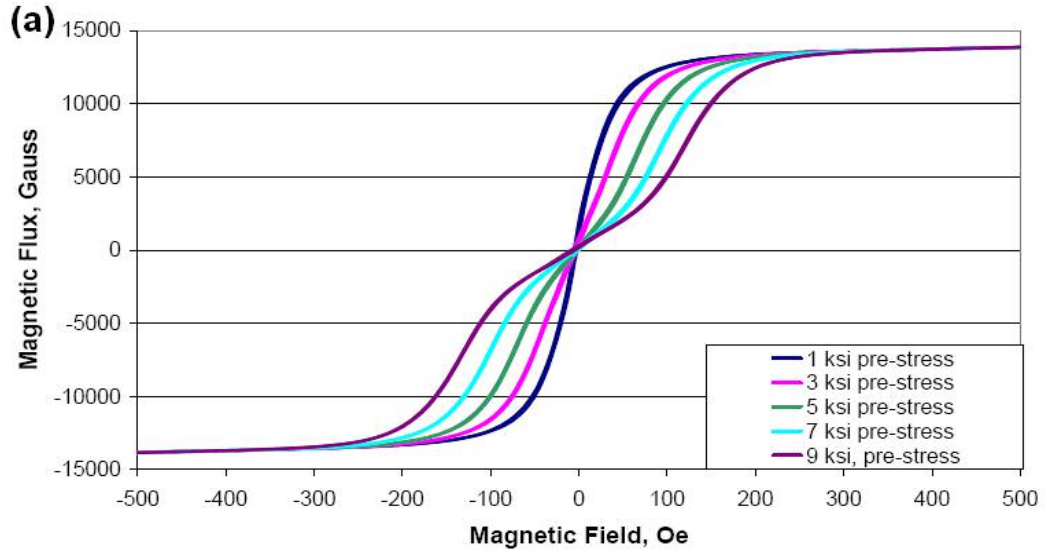


Figure 5.3: B-H curves of 19% Galfenol polycrystal (a) production grade sample and (b) research grade sample [56].

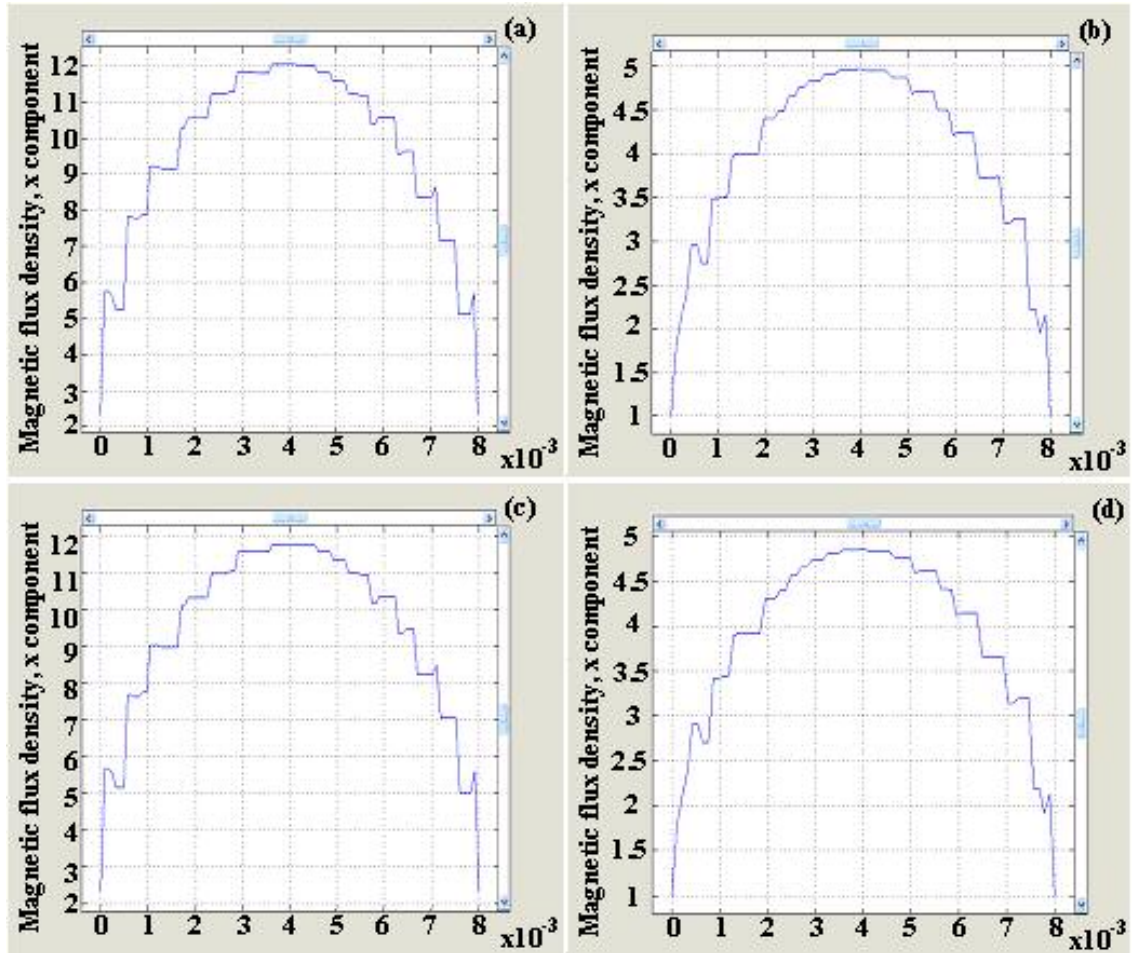


Figure 5.4: Line plots of the magnetic induction (in Tesla) along the x-axis of (a) a single crystal sample in the 12.0-mm gap model, (b) a single crystal sample in the 43.2-mm gap model, (c) a production grade polycrystal sample in the 12.0-mm gap model, and, (d) a production grade polycrystal sample in the 43.2-mm gap model.

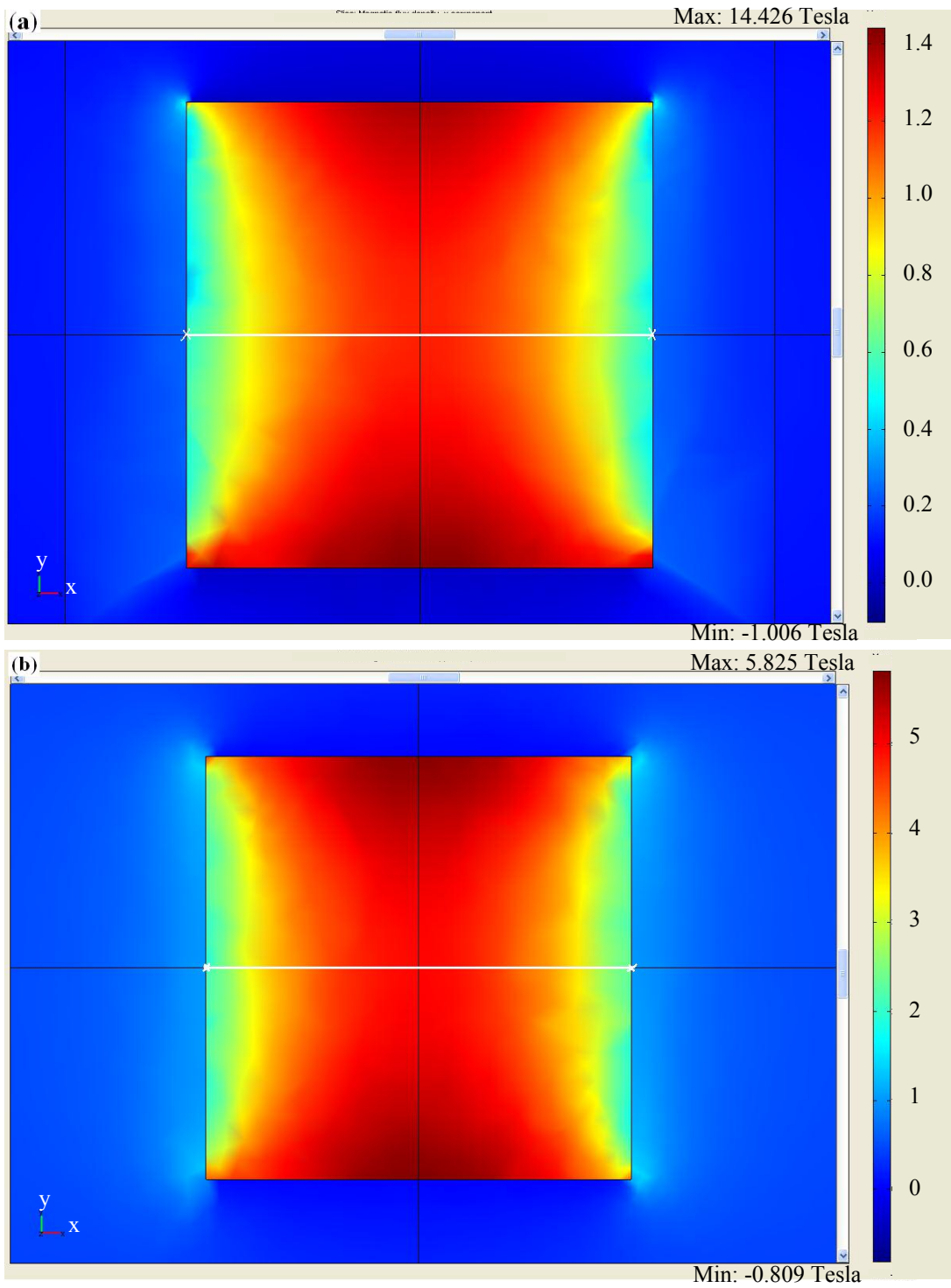


Figure 5.5: 2-D x-y plane slice plots of the magnetic induction (in Tesla) inside the sample for (a) a single crystal sample in the 12.0-mm gap model, and (b) a single crystal sample in the 43.2-mm gap model.

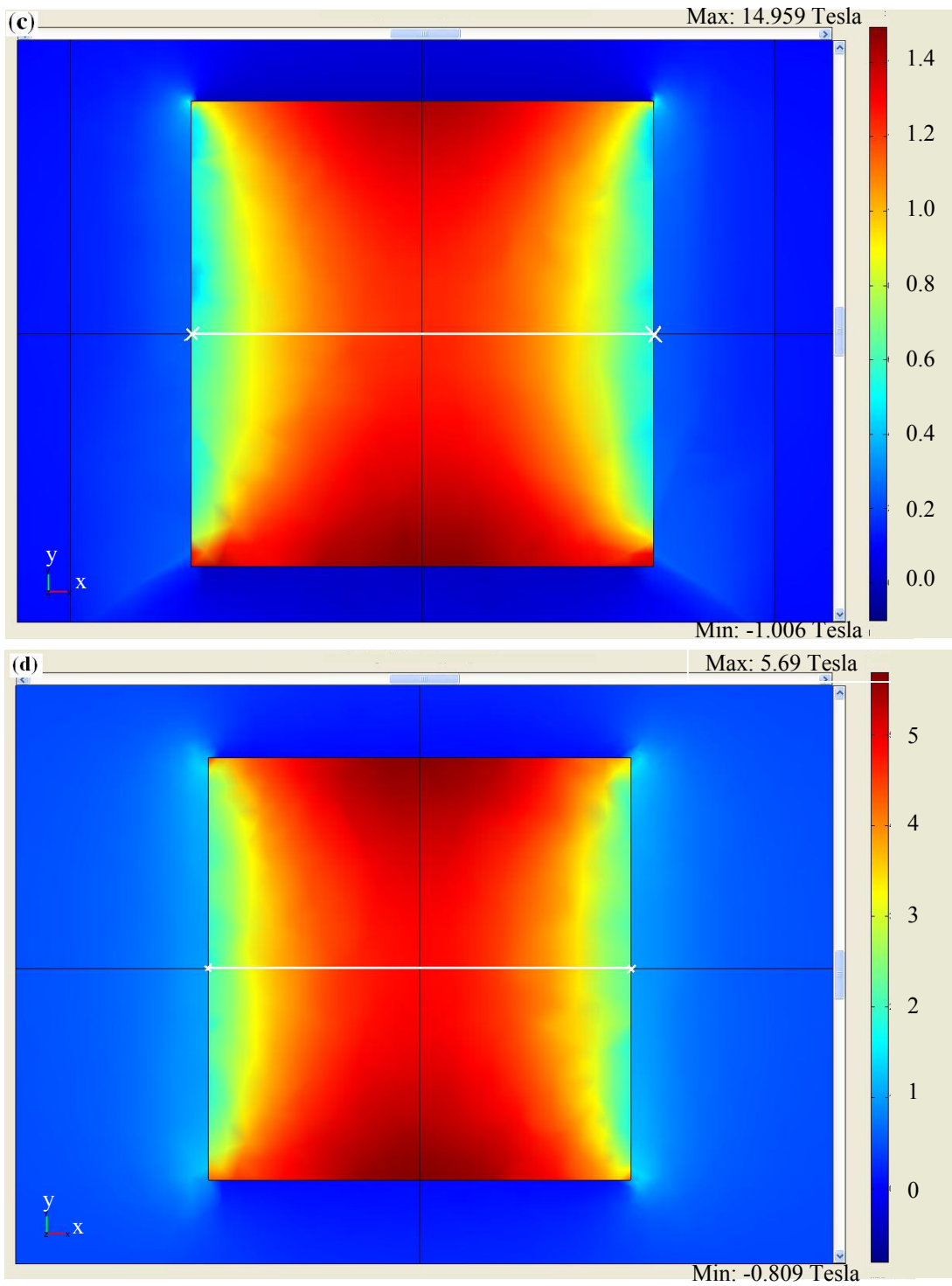


Figure 5.5 (cont.): 2-D x-y plane slice plots of the magnetic induction (in Tesla) inside the sample for (c) a production grade polycrystal sample in the 12.0-mm gap model, and, (d) a production grade polycrystal sample in the 43.2-mm gap model.

Comparing the peak magnetic induction in Figure 5.4a and 5.4c or Figure 5.4b and 5.4d, one may observe that the permeability of the Galfenol sample does not significantly affect this quantity. Similar conclusions can be drawn from comparison of the magnetic induction distribution in Figures 5.5a and c or Figures 5.5b and d. Comparing Figures 5.4a and 5.4b or Figures 5.4c and 5.4d, one can observe that for the 12.0-mm gap models (5.4a&c), the magnetic induction “x” components is always above the saturation magnetic induction which is of the order of 1.8 Tesla for single crystal 19% Galfenol and 1.3 Tesla for production grade polycrystal Galfenol. For the 43.2-mm model the minimum value of the magnetic induction is 1 Tesla. Therefore, the sample is not totally saturated. However, if one looks closely, the sample is saturated after 0.1 mm for the polycrystal sample and 0.2 mm for the single crystal sample. This is convenient since this represent less than respectively 2% and 4% of the sample if you account for this effect on both ends.

In Figures 5.5a to 5.5d, the shape of the magnetic induction distribution is quite similar for the cases where the same gap length is used. Comparing the shape of the distribution for the two different gap lengths, the demagnetization effects are more visible and larger when the gap length is larger, as one could expect. Finally, note that on both case the highest magnetic induction is seen half way along the two edges which do not face the permanent magnets.

Another major result to discuss is that the predicted magnetic induction levels shown in Figure 5.4 and 5.5 are above Galfenol saturation magnetic induction for all four cases. In reality, the magnetic induction should not exceed 1.8 Tesla for a 19% single crystal

sample and 1.3 Tesla for a production grade polycrystal sample. Since the permeability values entered in these models are constant and no saturation effect is taken into account, any points above the saturation magnetic induction should be considered to be equal to the saturation magnetic induction. For Figures 5.4a&c that would mean one would obtain a straight horizontal line at respectively 1.8 and 1.3 Tesla for single crystal and polycrystal. For Figure 5.4b and 5.4d, one would keep all point with magnetic induction levels below the saturation level as predicted, but a horizontal line should be drawn everywhere else as displayed in Figure 5.6.

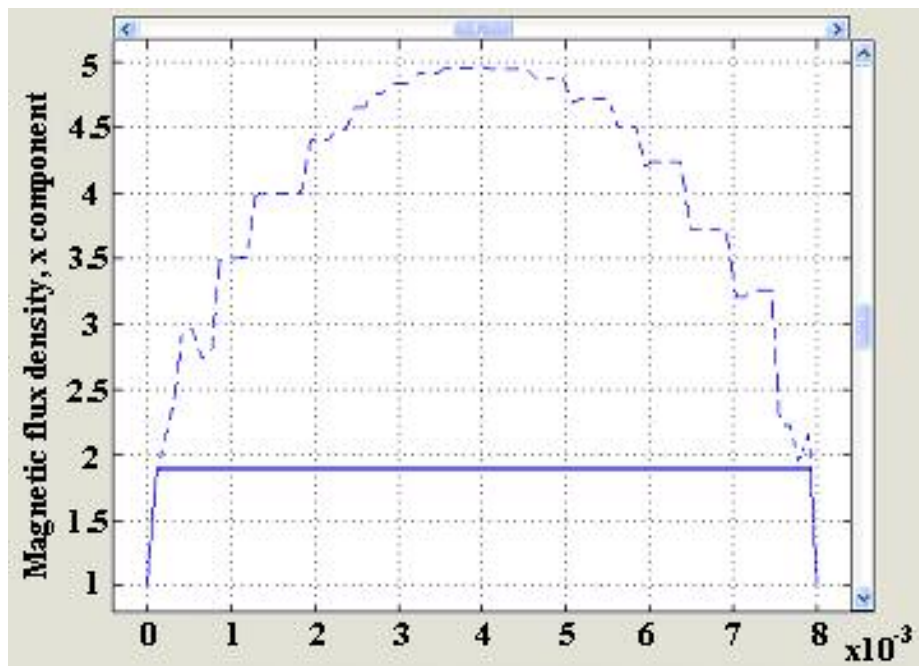


Figure 5.6: (Figure 5.4b modified) Line plots of the magnetic induction (in Tesla) in a single crystal sample accounting for the saturation effects

5.1.2. Example using the time-harmonic, electromagnetic application mode

The time-harmonic electromagnetic model was developed to study the effect of eddy currents in a magnetostrictive based pump. The geometry used was almost identical to the actual device in terms of magnetic circuit components, dimensions and material properties. The main difference is that the pre-stress mechanism and the bolt transferring the load to the pump chamber were modeled in the same subdomain as the end caps, as they had the same material properties. This way, instead of having many subdomains and interior boundaries, the model consists of a Galfenol rod, a coil, two end caps, a housing (a hollow cylinder) and four subdomains where the housing is slit. The four slit subdomains can be seen in Figure 5.7. The reason for having four slit subdomains was to make it easy to vary the length of the slit and study the effect of slit length on eddy current losses. By selecting the permeability of air and/or magnetic steel for these subdomains, a “full” slit, a “half” slit or no “slit” model can be obtained.

The material properties used in this model are the same as the one used in the magnetostatic model. The Galfenol relative permeability was the one of a single crystal 19% sample (~ 360). The magnetic steel used for the housing and the end caps is 1018 magnetic steel with a relative permeability of 6000. The coil is made of copper, a paramagnetic material with a relative permeability of one. In this model, the electric properties of all materials used are required. The eddy current power losses occur from an electromagnetic coupling in which the electrical conductivity and the permeability of the materials used has considerable impact on the performance of the apparatus when

operating at a high frequency. Since no values for the electrical conductivity (or resistivity) of Galfenol were made available, the author tested electrical resistivity on single crystal samples of various stoichiometries and for various crystallographic orientations. Appendix 1 includes results obtained from this series of testing. The Galfenol electrical resistivity used for this model is 8.33×10^5 S/m (Seimens/meter) which correspond to an electrical resistivity of $120 \mu\Omega\text{-cm}$. The electrical conductivity of the magnetic steel was set to 40×10^5 S/m, an average value for steel alloys.

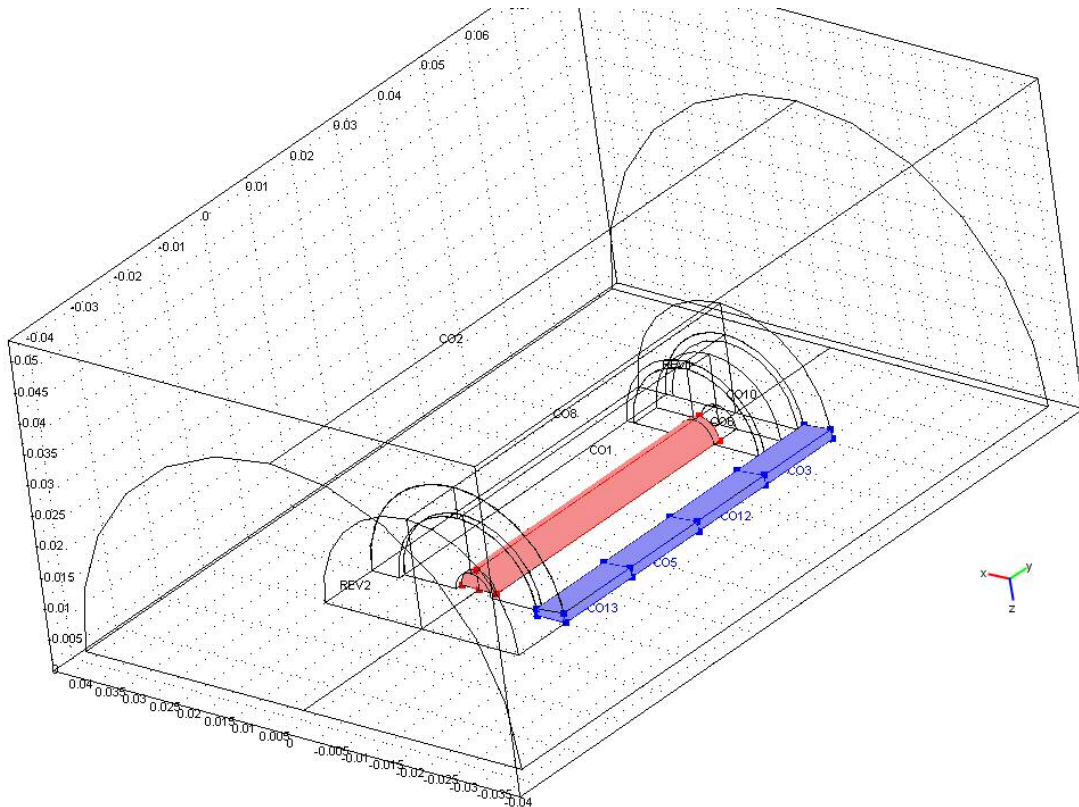


Figure 5.7: Geometry of the magnetostrictive pump with the four slit subdomains shaded.

To calibrate the coil, the coil was removed from the experimental apparatus and the magnetic field strength was measured inside the coil for selected frequency. The effects of eddy currents induced in the copper coil are therefore taken into account in the experimental measurements. Therefore, no additional eddy current should be generated in this subdomain in order to calibrate the coil properly, so the electrical conductivity of the coil subdomain is set to zero. Then by varying the value of J_0 in the “constant” tab (see section 4.3.1), one can get an equivalent magnetic field distribution inside the coil in air in a similar manner than the permanent magnets magnetization value was set. A 3-D view of the magnetic field generated by the coil in air for 1Hz frequency is shown in Figure 5.8. In this Figure, the permeability and conductivity of all components are set to, respectfully, 1 and 0. The streamline and the slice plot show the magnetic field path and normalized magnitude.

Figure 5.9a to 5.9c are 2-D slice plot of the magnetic induction distribution in the Galfenol rod and in the rest of the magnetic circuit for, respectively, a housing with no slit, a half slit housing and a full slit housing. On these plots one can observe the effect of the slit on high operating frequency. More details on the effect of a slit in the housing are given in Figure 5.10 and 5.11.

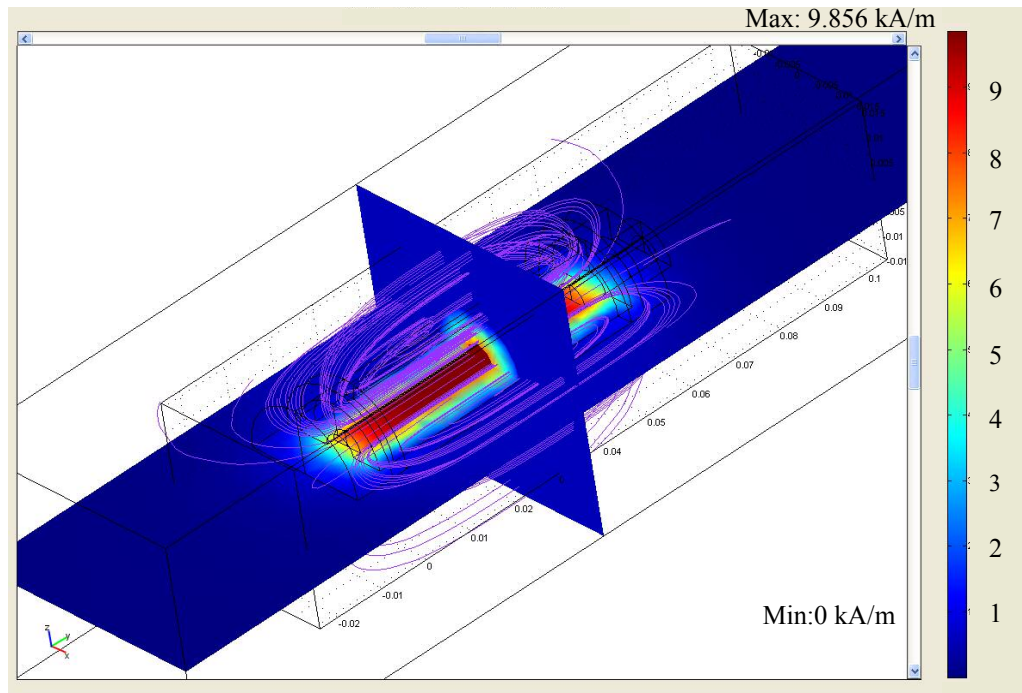


Figure 5.8: Magnetic field distribution and flux path for a coil modeled in air.

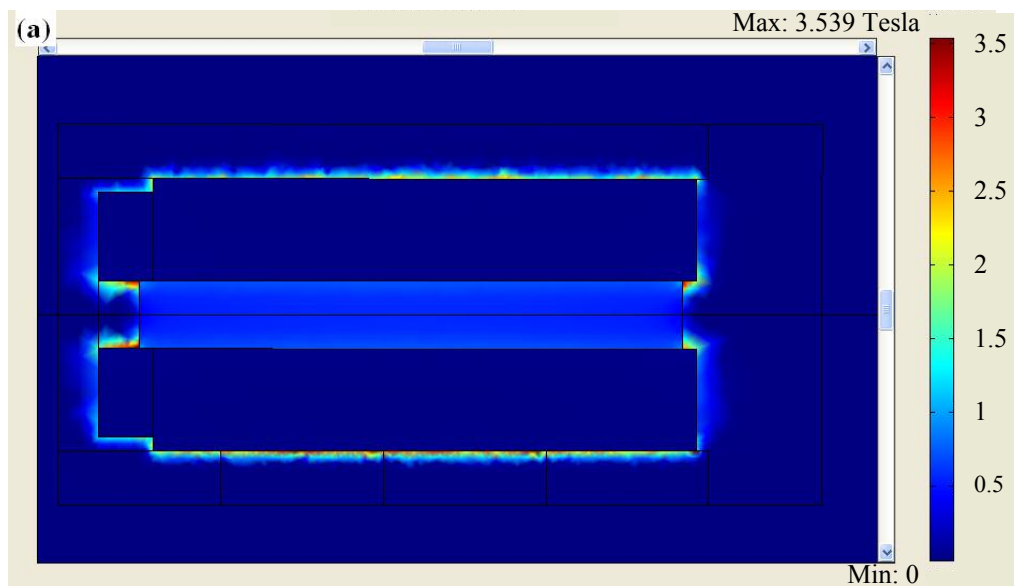


Figure 5.9: Sample 2-D slice plot of the normalized magnetic induction for an operating frequency of 2KHz with a no slit in the housing.

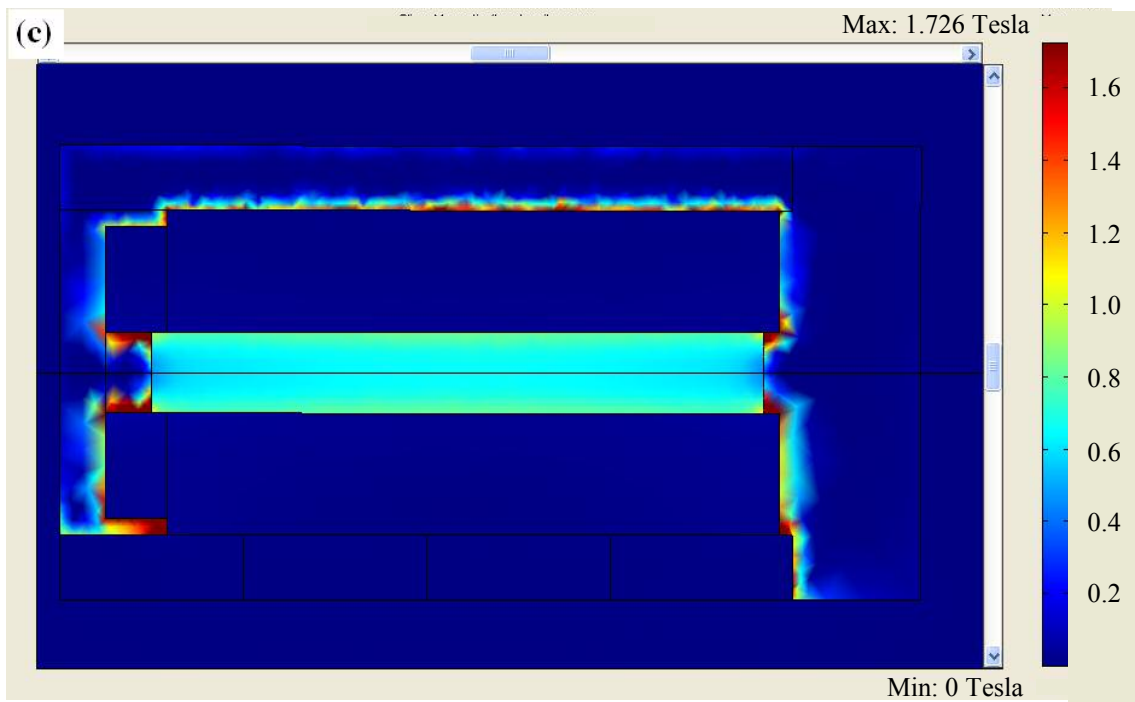
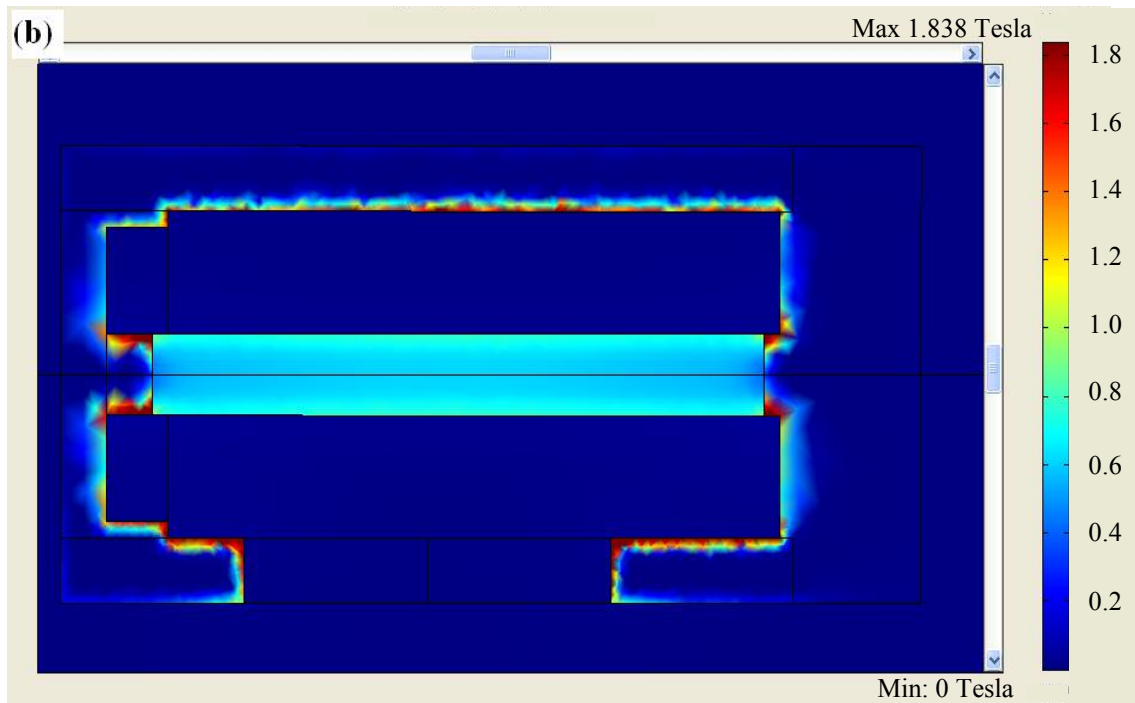


Figure 5.9: Sample 2-D slice plot of the normalized magnetic induction for an operating frequency of 2KHz with (b) a half slit housing and (c) a full slit housing.

The goal of this model was to provide the magnetic induction distribution inside the 2 inch long, ¼ inch in diameter, magnetostrictive rod. The different frequencies tested are 1Hz, 1kHz, 1.5kHz, 1.8kHz and 2 kHz. In order to better visualize the results, the line plots of the magnetic induction along the symmetry axis of the rod for various frequencies and various slit lengths were extracted to an excel file in order to plot all result on the same graph. For 2-D FEM, extracting results is easy: the x and y coordinate of each point have an associated value of the chosen quantity. For 3-D FEM, having three coordinates, the text file is usually hard to read so a small program called “datathief” was used on the 2-D line plots to extract the results to an excel sheet. The magnetic induction distributions along the 2” Galfenol rod are shown in Figure 5.10. Similarly, the various magnetic induction distributions along the rod diameter at the midpoint of the rod length, i.e. at 1” from each end are shown in Figure 5.11.

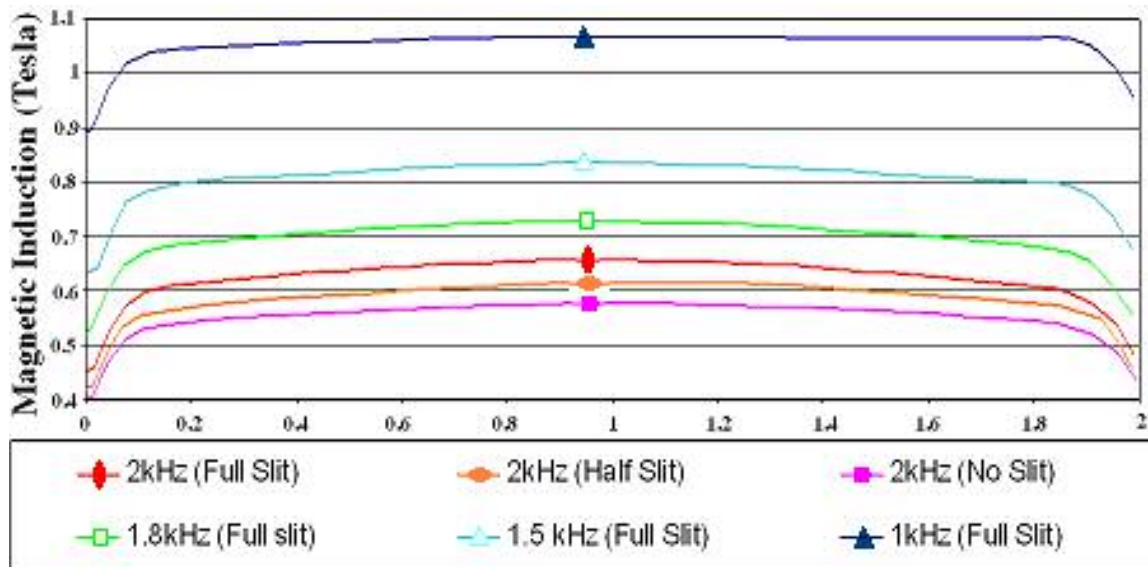


Figure 5.10: Magnetic Induction along the 2 inch magnetostrictive rod under various actuation frequencies.

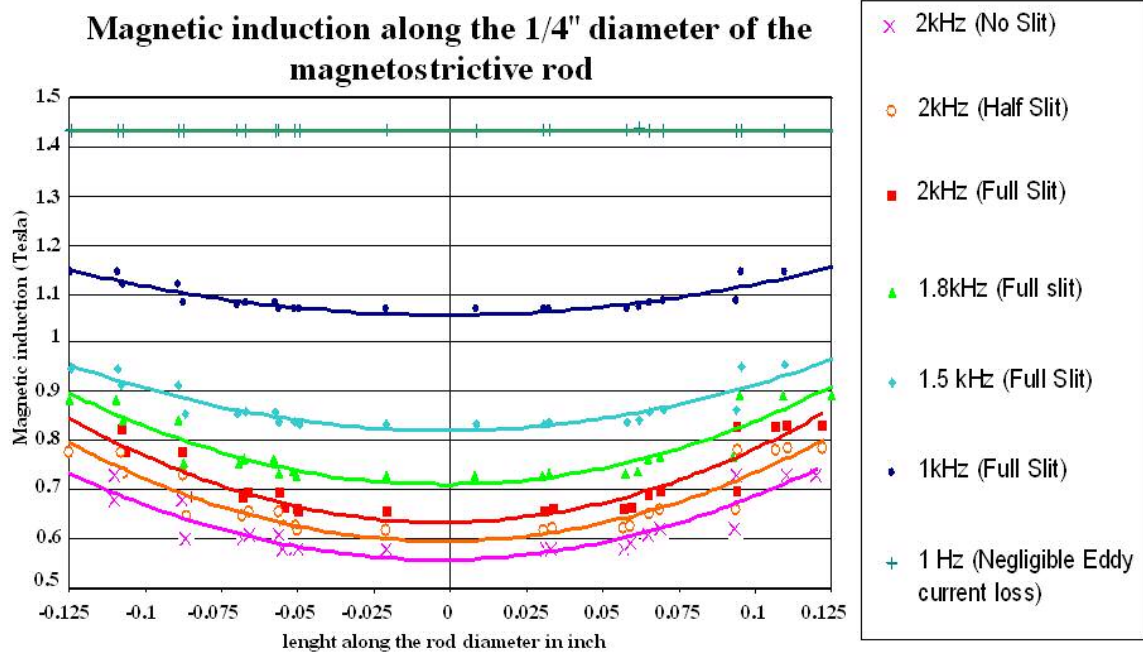


Figure 5.11: Magnetic Induction along the ¼ inch diameter of the magnetostrictive rod at the midpoint of the rod length.

Results plotted in Figures 5.10 and 5.11 leads to four main discussion points: the effect of the frequency on the level of eddy current power losses, the effects of eddy currents on the each end of the rod, the eddy current effect on the level of penetration of the field inside the rod, and the effect of a slit in the housing to solve this problem. Looking at both Figures 5.10 and 5.11, one can see that in a magnetic circuit with a full slit in the housing, the magnetic induction level is frequency-dependent. If one takes the magnetic induction in the center of the rod (1” from each end of the rod on symmetry axis), then looking at Figure 5.11, one can see that the magnetic induction level for operating frequencies of 1 Hz, 1 kHz, and 2 kHz, are respectively, 1.43 Tesla, 1.08 Tesla and 0.64 Tesla. The decrease in magnetic induction between 1 Hz and 1 kHz is 0.35 Tesla. And from 1 kHz to 1.5 kHz, the magnetic induction drops off 0.44 Tesla. As

expected, the predicted trend shows that with increasing operating frequency, higher eddy currents losses occur and therefore, a larger drop in magnetic induction is observed.

The second point to discuss is visible on Figure 5.10 only. At each end of the rod, the magnetic induction drops over the first and last 0.1” of the rod. This phenomenon can be explained by looking at the 2-D slice plot introduced earlier. Each of them displays a high level of magnetic induction in the magnetic steel pieces in contact with the Galfenol rod. In these pieces, the high level of magnetic induction generally induce a high level of eddy current which have a tendency to lower the magnetic induction inside the Galfenol rod ends. The third point to discuss is the decrease in magnetic induction in the core of the Galfenol rod. The eddy currents generated inside the sample itself shield the core of the sample from the magnetic field. This phenomenon is well known of the magnetostrictive dynamic transducer designer and is generally the considered to be the primary illustration of the effect of eddy current.

To solve these two problems (lack of penetration of the core and effects of eddy current in the end caps), one could laminate the rod, slit the housing and potentially slit the end caps where the most eddy current are generated and affect the end of the Galfenol rod. These pieces are usually structurally-involved in the mechanical design of the transducers, and therefore it is important to balance structural integrity and magnetic circuit efficiency. In these models, the slit in the housing was the solution of interest to solve these eddy currents related drops in magnetic induction in the Galfenol rod. Looking at the 2 kHz results in Figure 5.9, 5.10 and 5.11, one can see that slitting the housing decreases the eddy current power losses. The increase in magnetic induction obtained from a full slit with respect to the same magnetic circuit without a slit is of the

order of 0.07 Tesla which represents a 10.8% increase. A half slit creates an increase of 6.1% in magnetic induction in the Galfenol rod. These results illustrate some of the utility of FEM models for optimization of a full structural design to aid in building an efficient transducer.

5.2. Example of Coupled Finite Element Model of a Magnetostrictive-based Application

The geometry modeled is based on an experimental set-up used at the University of Maryland for measurement of the static response of Galfenol when used as a sensor. The set-up consists of a $317.5 \times 24.85 \times 1.6 \text{ mm}^3$ Aluminum beam with two $25.1 \times 8.35 \times 1.57 \text{ mm}^3$, 18.4% production grade Galfenol plates (provided by ETREMA products, Inc.) attached symmetrically on the top and the bottom of the beam at 25 mm from the clamped end (Figure 5.12). A coil is used to provide a DC bias field. The data presented is for different static loadings applied downwards at the free tip of the beam. The experiment was performed for a 26.66 kAm^{-1} magnetic bias by S. Datta [36].

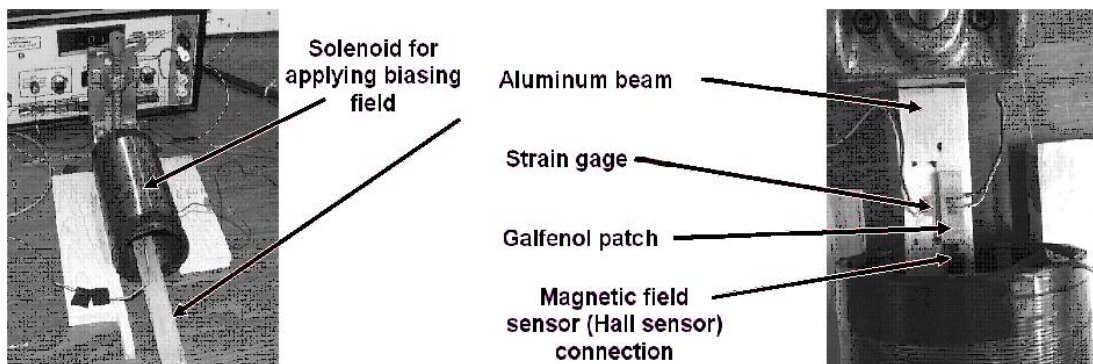


Figure 5.12: Experimental set up (Figure provided by S. Datta [36]).

The goal of the model was to predict the magnetic response of the upper Galfenol patch to different applied static loads and magnetic biasing fields. In the experiment, there is a strain gage attached on the top of the top Galfenol sensor plate (visible on the top of the Galfenol patch in the right picture of Figure 5.12) and another strain gage on the top of the aluminum beam next to the top Galfenol patch. The strain gages helped establish that bending induced strains were transferred from the beam to the Galfenol patch and were used in verifying the structural loads in the FEM model. A Hall sensor is also attached in front of the Galfenol patch to measure the passive change in magnetic field as the beam was deformed. The locations of all the measurement devices are important for the validation of the FEM model. In fact, in order to validate the results obtained by the FEM model, the strain at each strain gage location and the magnetic field induction at the location of the Hall probe need to be compared with the experimentally obtained measurements.

5.2.1. Magnetostrictive material properties selection

There are two main differences between the FEM model and the experimental set up. First the magnetic bias applied by the coil is reproduced using a permanent magnet instead of a coil. This is because, for the static case, modeling permanent magnets requires less memory than modeling a coil. In dynamic models this simplification will not apply and the implementation given in section 4.2.3 should be used. Second, the properties of the polycrystalline, production grade, 18.4 % Galfenol used, are based on preliminary data provided by the manufacturer of the material (ETREMA products, Inc. [56]) and on characterization curves of a single crystal 18.4% or 19% Galfenol,

depending of the property [19]. No complete set of characterization curves existed for this specific stoichiometry of Galfenol when this model was done (Quasi-static characterization of the polycrystal sample is currently being done at the University of Maryland). Recall in Figure 5.3b, the B-H curve for a production grade polycrystal 18.4 % Galfenol sample is provided in section 5.1.1. The associated λ -H curves are given in Figure 5.13. The coupling factor “33”-component d_{33}^T can be extracted from the magnetostriction versus magnetic field plot for different applied mechanical pre-stress (slope of the curve). Similarly the permeability can be extracted from the magnetic induction versus magnetic field plot. Note that the λ -H and B-H curves were done early in the development of the first polycrystal Galfenol samples. Enhanced properties should be expected for the current polycrystal material. The stiffness matrix can be extracted from a regular stress versus strain plot at constant magnetic field.

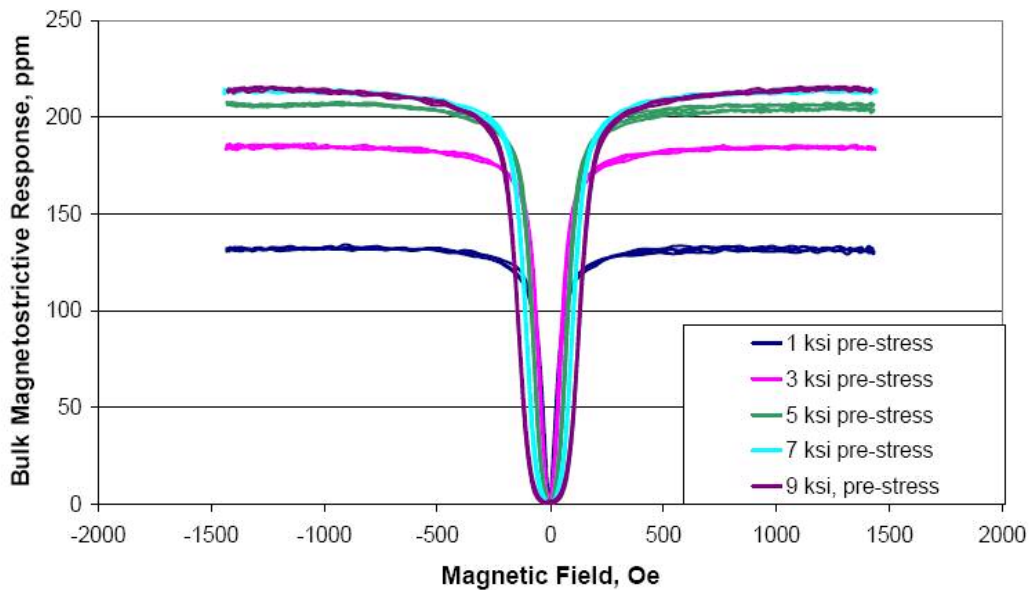


Figure 5.13: Magnetostriction vs Magnetic field curves of 18.4% production grade polycrystal Galfenol for various stress level [56].

Since this implementation does not take in account the nonlinearity of these characterization curves, it is necessary to run preliminary static models. First, by running a magnetic model of the permanent magnet in air (i.e. fixing the relative permeability of all the other material to 1), one can check that the applied bias magnetic field is equal to the one measured experimentally (see Figure 5.3a). Second, by running a new magnetic model but including the Galfenol as a permeable ferromagnetic material with no magnetostrictive effect, one can get an approximated biasing magnetic field. Here, the biasing field obtained varies between 3 kA/m and 6 kA/m. The peak magnetic induction inside the sample is of the order of 0.5 Tesla. Figure 5.14 shows (a) a 3-D plot of the “x” component of the magnetic flux density and (b) the line plot of the magnetic field “x” component on the top surface of the upper sensor plate. The “x” axis starting point of the line plot corresponds to the top sensor plate edge closest to the clamped end. The last ending point corresponds to the opposite edge.

Third, by running a static mechanical model of the aluminum beam and Galfenol patches under a given applied load, one can get a fair approximation of the stress state of the Galfenol sensors (usually different especially in bending). The obtained peak stress level in the Galfenol samples are, respectively, for top and bottom sensor plate, 3.75 MPa and -3.75 MPa. Figures 5.15a&b show, respectively (a) the 2-D plot of the “x” component of the stress tensor and (b) the line plot of the same quantity along the z-axis on the plane 37 mm from the attached end which is the plane half way through the sensor plates (see thick line on Figure 5.15a).

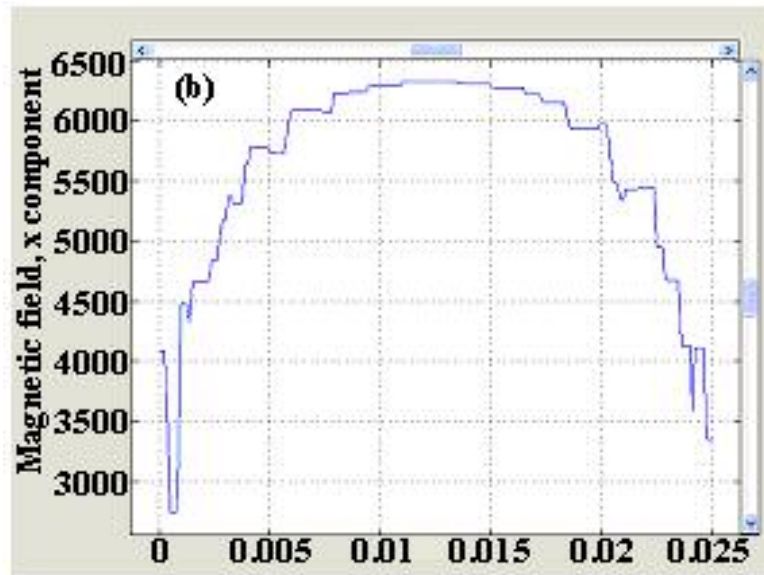
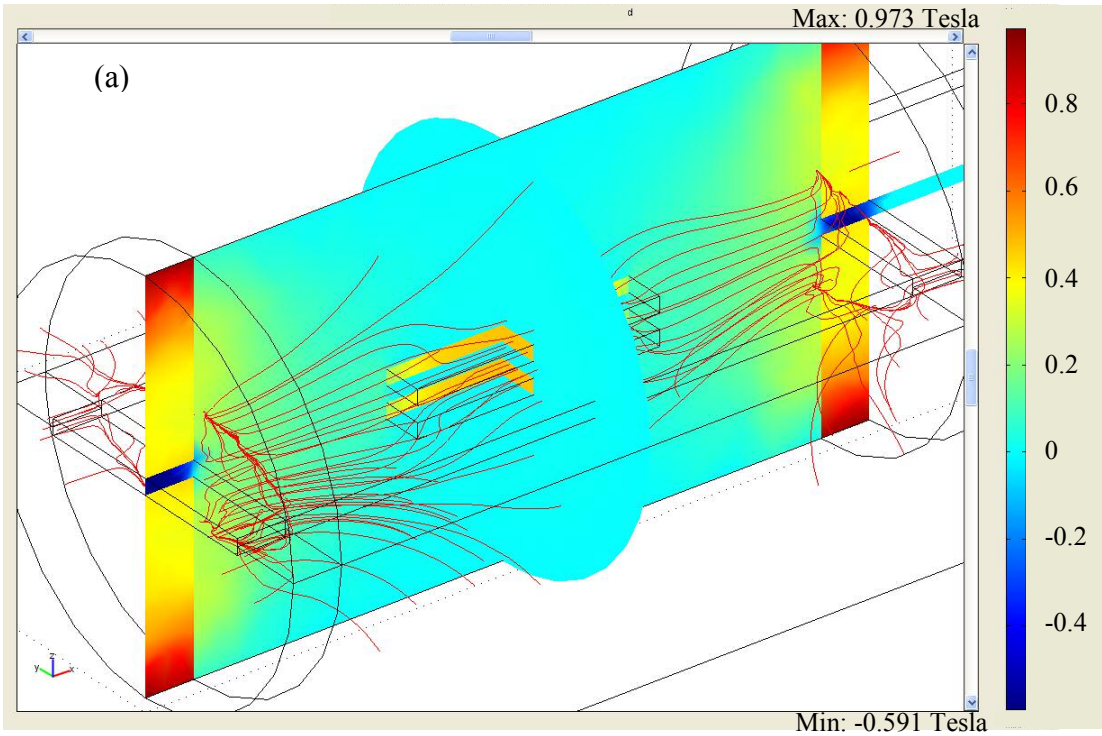


Figure 5.14: (a) a 3-D plot of the "x" component of the magnetic flux density and (b) the line plot of the magnetic field "x" component on the top surface of the upper sensor plate.

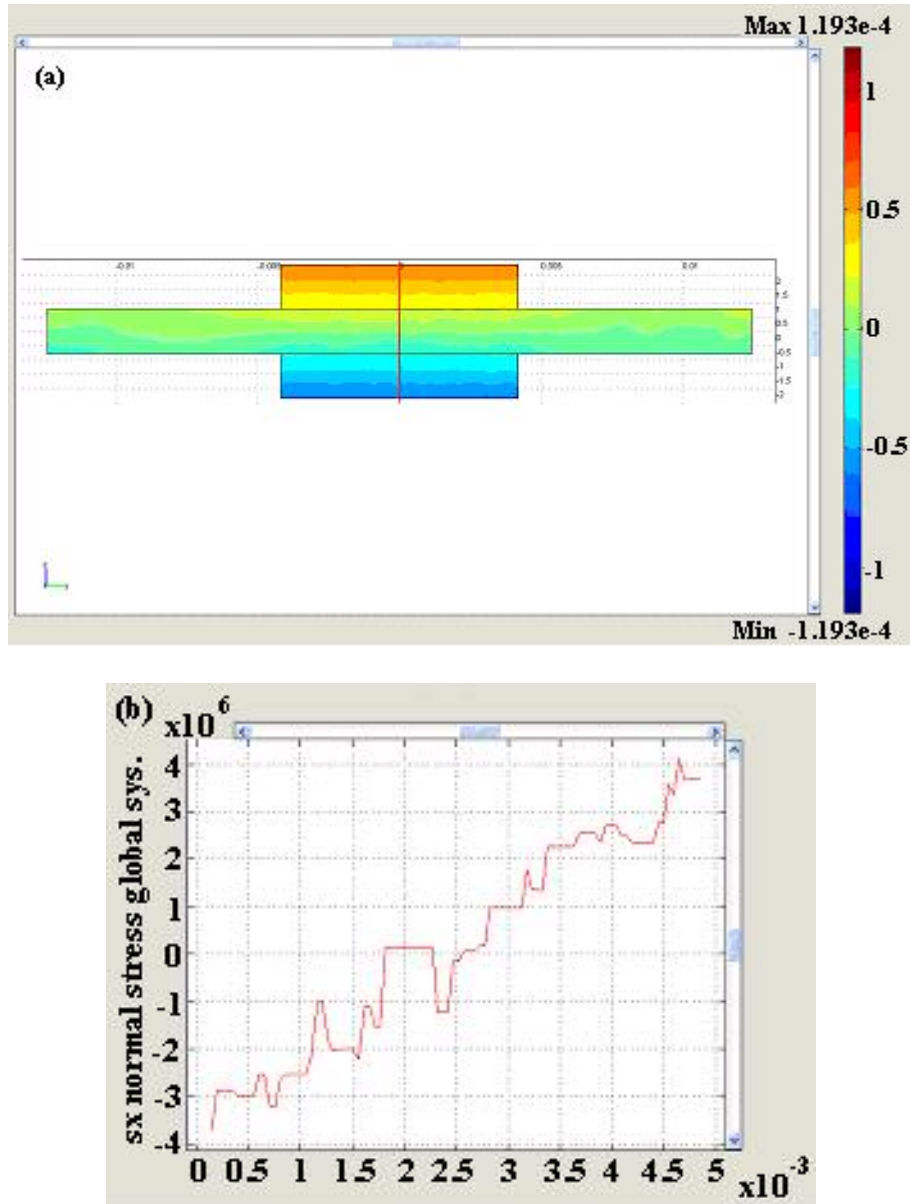


Figure 5.15: (a) 2-D plots of the “x” component of the stress tensor and (b) the line plot of the same quantity along the z-axis on the plane 37 mm from the attached end.

Now using those predicted applied field and applied stress, one can go to the characterization curves and measure the slope of the various curves to get the stiffness matrix, the coupling factor, and the permeability in the application range of the sensor.

Note that for the Galfenol plate under tension, properties from data measured at the lowest available pre-stress were chosen from λ -H and B-H curves. Often zero pre-stress was the closest value to the ± 3.75 MPa encountered in this model. Extensive work on the behavior under tension of an annealed polycrystal Galfenol is currently being performed by Restorff [32].

The next step is to run a magneto-mechanical model of the set up accounting for all the coupled effects. Ideally, to get a better convergence, this last step can be repeated a couple times (2 or 3 are usually good enough) with readjusting the Galfenol properties based on the new stress state and magnetic state of the Galfenol patches. Using this method to choose the material properties, it's a fair assumption to use the piezomagnetic constitutive equations in the derivation of the boundary value problem as presented in Chapter 2 and 3 (static magneto-mechanical fully coupled model). However the lack of characterization curves for this region of applied stress makes it difficult to pursue this task adequately in this model. The model was run for five different tip loading cases used in experiments applied on the free end of the aluminum beam: 0N, 0.0833N, 0.255N, 0.338N and 0.552N.

5.2.2. Results and comparison to experimental data

Once a model is solved, any dependant or independent variable can be plotted in many ways (slice plot, boundary plot, streamline, etc.). In Figures 5.16a and b, a slice plot of the magnetic induction “x”-component and a streamline plot of the magnetic field are presented for two different loading cases. An additional case it can be compared to is the one plotted in Figure 5.14a&b. The first plot (5.16a) shows a purely static magnetic

model of the permanent magnet in air and the second, (5.16b) shows a coupled magneto-mechanical model of the set up with Galfenol patches under 0.552N tip loading. These plots do not provide information about the magnetic field magnitude but are very helpful for comparing the path of the magnetic field. Figure 5.17 is a 2-D surface plot of the magnetic induction on the top surface of the top sensor plate. It allows for visualization of the magnetic induction in the Galfenol sensor. Note that the white cross indicates where the change in magnetic field is measured by the Hall sensor. Figure 5.18 is a 3-D surface plot of the strain “x”-component for 0.552N loading using the coupled magneto-mechanical model. It allows for visualization of the strain distribution on the beam and the sensor plate. The white cross in Figure 5.18 indicates the location of the strain gage on the experimental set up.

Note that on both Figure 5.17 and 5.18, the strain and magnetic induction near the edge of the Galfenol plate are substantially lower than in the center of the plate where the distribution is more evenly distributed. The magnetic induction near the edge is lower because of the demagnetization effect. One may observe that this phenomenon is diminished near the corners of the Galfenol plates. In order to properly read the values of the computed data it is easier to use line plot along a line passing through the point of interest. For example, the change in magnetic field was measured 3 mm from the Galfenol top sample. To estimate the change in magnetic induction, we plotted the dependent variable along a line parallel to the “x”-axis passing through the Galfenol sensor plate and ending 3mm after the Galfenol plate in both cases : with no applied load (Figure 5.19a) and with the desired applied load (Figure 5.19b, for an applied load of 0.552N). The white line in Figure 5.17 is the one used for these line plots. The

intersection point between the dashed lines on Figure 5.19 is where the change in magnetic induction was recorded. Figure 5.19 shows that a quasi identical figure would be obtained if one was to plot Figure 5.17 for the case where no load would be applied.

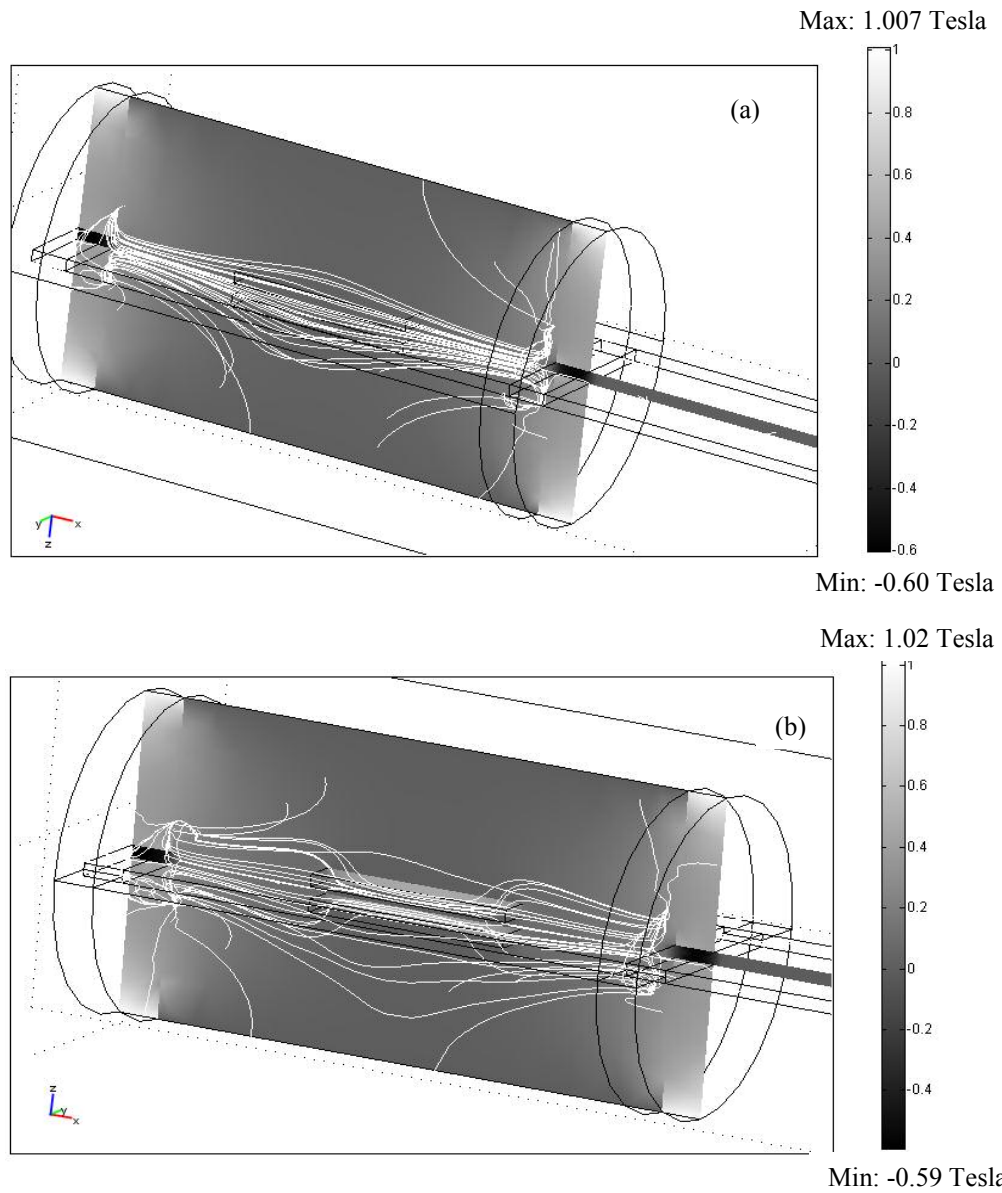


Figure 5.16: (a) 3-D plots of the magnetic induction and field for the calibration of the permanent magnets in air obtained by a purely magnetostatic model (top), and (b) for a 0.552N loading on the beam using the coupled magneto-mechanical model (bottom).

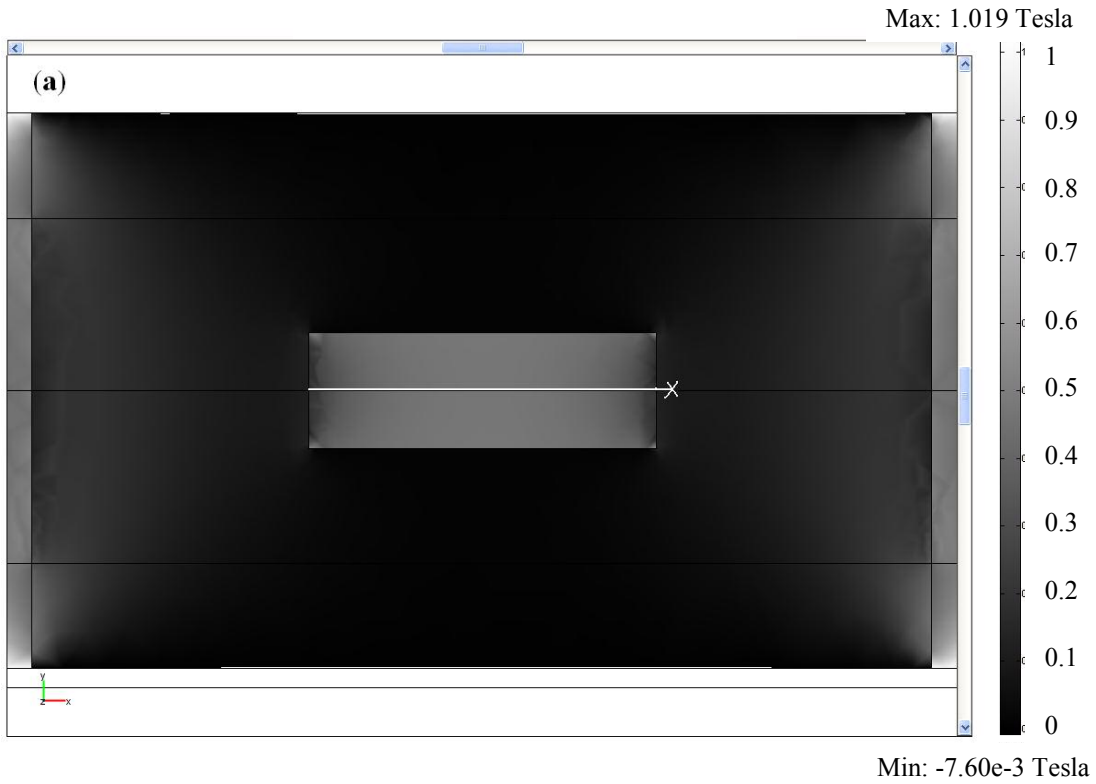


Figure 5.17: Magnetic Flux density (Tesla) on the top of the Galfenol plate.

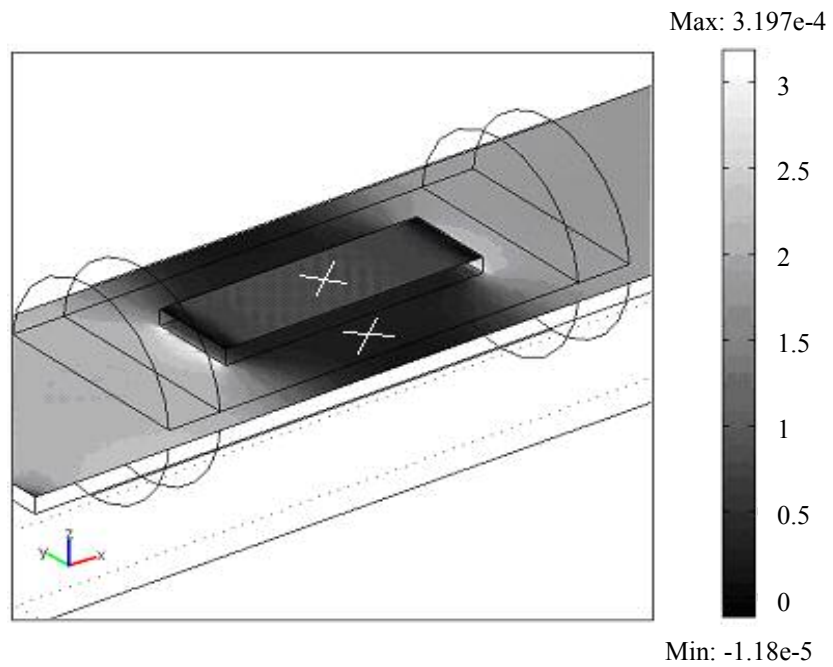


Figure 5.18: Strain x-component on the top of the beam (lower surface plot) and on the top of the Galfenol sensor plate (higher surface plot).

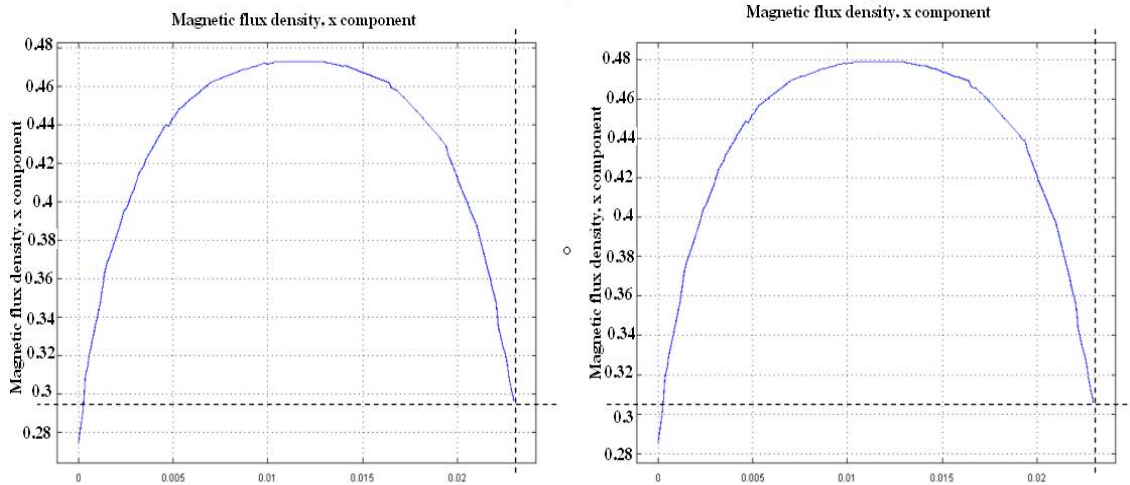


Figure 5.19: Line plot of the magnetic induction along the white line plotted in Figure 5.17 for a) no loading and b) 0.552N loading.

Similarly, a line plot passing respectively, on the surface of the beam 2.5 mm from the edge of the Galfenol plate, and on the surface of the top Galfenol sensor, are used to estimate the strain measured by the beam and sensor strain gauges. In Figure 5.20 one can see the experimental results obtained by Datta [36] in which four masses were placed on the free end of the aluminum beam at ~4-6 seconds and removed at ~12 seconds. The masses produced loads of 0.083 N, 0.225 N, 0.338 N and 0.552 N as shown in Figure 5.20a-d, respectively. The strain in the beam and the upper Galfenol patch, and the change in field measured by the Hall probe are plotted as the mass loads are applied and removed. All three traces exhibit either drift or hysteresis, as they do not return to their initial values of zero upon removal of the mass loads.

The FEM results given by each of the four mass loads are superimposed on Datta's time trace results in Figure 5.20a to 5.20d as constant value lines. FEM model results are extrapolated from line plots as the one presented in Figure 5.19. In Figure 5.20, one

can observe the small difference obtained between the experimental measurements and the FEM Model. Note however that for a 0.255N and 0.338N loading, the experimental results shows very little difference in the strain measured on the top of the sensor and on the top of the beam next to the sensor. This is unexpected since the top surface of the sensor is higher with respect to the neutral axis and therefore should have higher strain since the beam is in bending. For these two cases the difference in the shape of the results is different than for the one obtain in the FEM. Otherwise one can observe the FEM results are always slightly above the experimental results. As pointed out earlier source of difference in the experimental and modeled results can be attributed to the properties used to model the active material. Another explanation is that the model does not account for the bonding layer between the sensor plates and the beam which in the model transmits all the stress but in reality transmit only a portion of the beam stress. Results presented in Figure 5.20, show that the implementation on FEMLAB of this model seems to be valid.

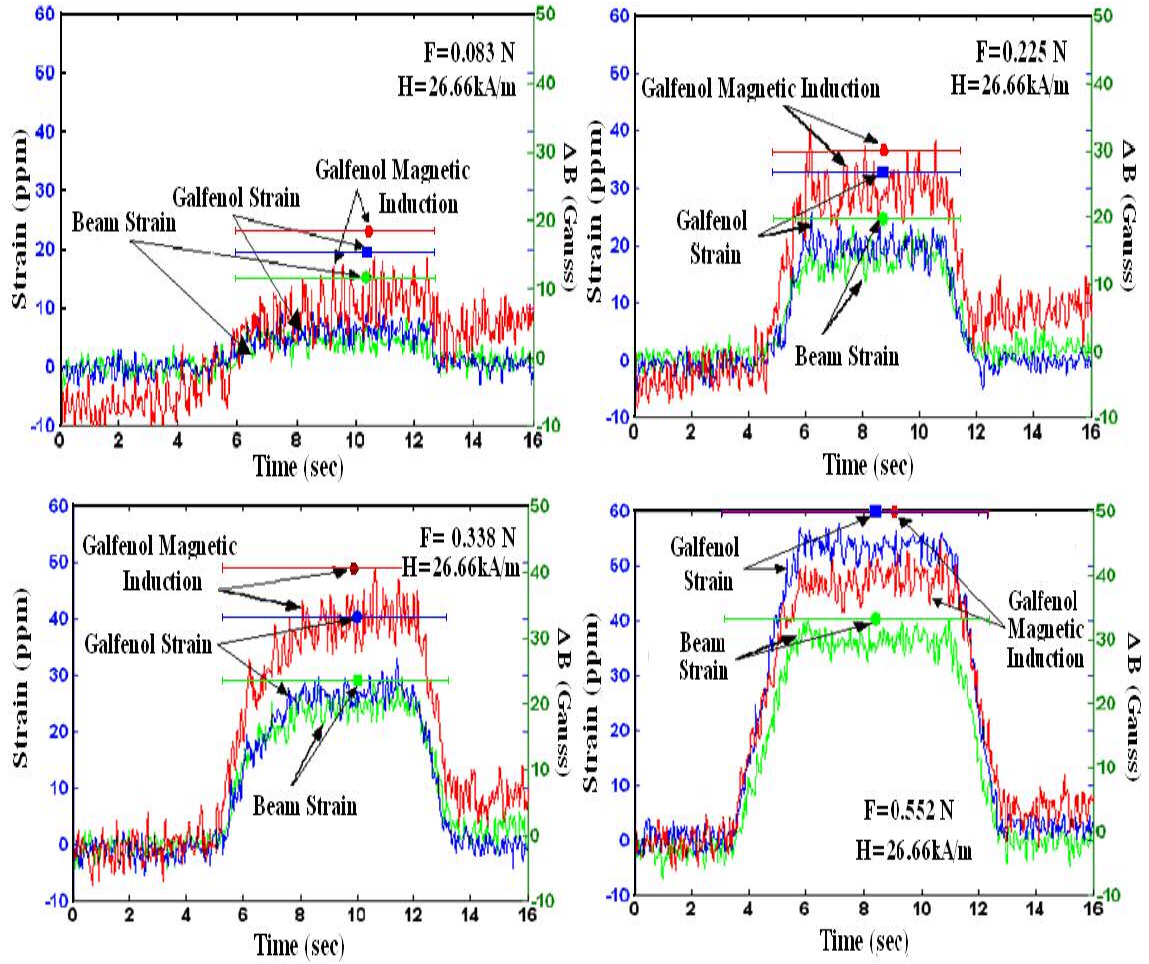


Figure 5.20: Experimental results provided by S. Datta [36] and modeled results computed from the FEM model. Change in magnetic induction, strain on the sensor surface and strain on the beam surface next to the sensor for (a) 0.0833N (top left), (b) 0.255N (top right), (c) 0.338N (bottom left) and (d) 0.552N (bottom right).

Chapter 6: Conclusion

6.1. Summary

After providing appropriate background information on magnetostrictive materials, a set of boundary value problems was introduced to model magnetostrictive-based applications under various operating conditions. These included: (1) static and dynamic structural mechanics BVPs for purely elastic materials designed to model the behavior of structurally involved part of a magnetostrictive-based devices, (2) a magnetostatic BVP designed to predict the magnetic field in static magnetic circuit with permanent magnets (does not apply to applications using coils), (3) a quasi-static, time-harmonic, electromagnetic BVP designed to study electro-magnetic coupling effects in the magnetic circuits and in particular to model eddy current power losses, (4) a static, fully coupled, magneto-mechanical BVP and (5) a dynamic, fully coupled, electro-magneto-mechanical BVP, both designed to predict the behavior of magnetostrictive material based sensor and actuators.

The structural mechanics BVPs are based on the equations of motion and the stress-displacement relationships associated with standard, modified (for material under pre-stress), or coupled (for magnetostrictive materials), constitutive equations. Similarly, the electromagnetic BVPs are based on Maxwell's equations associated with electric and magnetic potential formulations and coupled or uncoupled constitutive equations. The various BVPs were introduced in the "differential" form in Chapter 2. For each BVP type, different formulations based on different assumptions depending on the

operating condition or the material type used were presented. In Chapter 3, the continuum mechanics BVP, as well as the magnetostrictive static and dynamic coupled BVPs, were derived in the “weak” form using weighted-residual principles.

Implementation methods for all the BVPs presented were proposed in chapter 4. Using a format similar to that of a tutorial manual, this chapter focused on magnetostrictive-based applications and provided implementation tips. A set back encountered was the absence of a dynamic electromagnetic application mode necessary to implement the dynamic coupled electro- magneto-mechanical BVP for magnetostrictive materials. Memory requirements for 3-D models also caused concern, especially when using Lagrangian quadratic elements. Meshing techniques to prevent the use of unnecessary memory while solving were employed for large 3-D geometries with small details as well as for narrow geometries. Solvers and post-processing techniques are also detailed in this chapter. In Chapter 5, validation of the static magneto-mechanical models and results from the magnetostrictive-based applications presented in Chapter 4 are discussed.

6.2. Suggestions for future work

A number of tasks can be suggested to enhance the work presented in this thesis. The dynamic electro-magneto-mechanical FEM implementation was not validated by a FEMLAB model. Using another FEM code, Aparicio and Sosa were able to validate the formulation with a basic 1-element model. Therefore, it can be assumed that this formulation is valid [1]. Using the new dynamic electromagnetic application mode scheduled for released in fall 2005 in the electromagnetic module of the FEMLAB

3.2© software, one could attempt to verify the implementation proposed in chapter 4 to validate this formulation.

Additionally, linear constitutive equations were used to model the magnetostriction effect. Saturation magnetostriction and the quadratic shape of the λ -H curves suggests an alternate formulation in which incremental FEM schemes would better capture this essential behavior. Similarly, stiffness matrix components, permeability matrix components and coupling coefficients are all dependent on magnetic field and mechanical load levels. FEMLAB allows implementing dependent formulas for material constant, especially for sequentially-solved coupled models. Since most material properties exhibit non-linear relationships, one would need to develop a model where non-linear material properties are modeled using results a preliminary uncoupled solution.

Appendix 1: Electrical Resistivity Measurements

Electrical resistivity measurements were conducted to aid in design of magnetostrictive-based applications operating under dynamic conditions. The electrical resistivity values were experimentally determined for various stoichiometries of both single crystal and polycrystal Galfenol samples. A conventional four-probe method as described in ASTM B193-02 was performed on all specimens. Figure A1 summarized the measurement obtained.

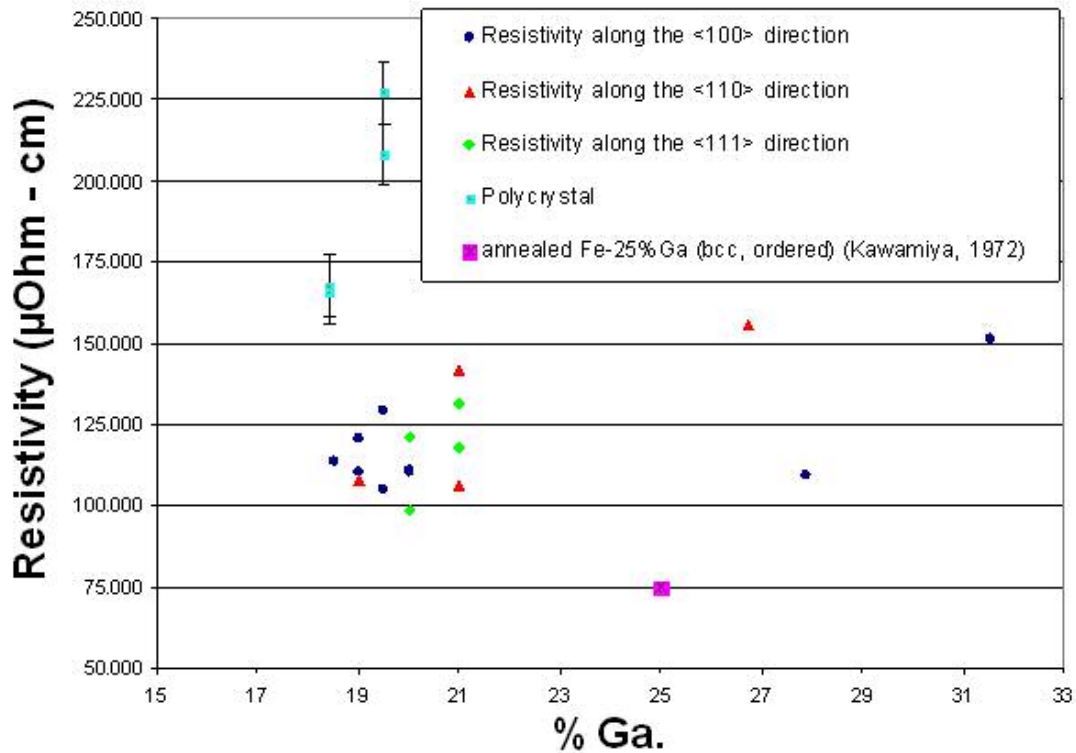


Figure A1: Resistivity measurements for various stoichiometries and various crystallographic orientations.

Single crystal and polycrystalline samples of 19.5 at.% Gallium content exhibit resistivity values of $110 \pm 10 \mu\Omega\text{-cm}$ and $96 \pm 10 \mu\Omega\text{-cm}$ respectively. For the single crystal samples, measurements taken along the [100], [110] and [111] crystallographic orientations did not show significant variation. Between 18 and 22 % Gallium content, the stoichiometry or crystallographic direction does not affect the resistivity significantly. Results from very few specimens at greater than 22% Gallium suggest a slight increase (~15%) in resistivity values at 27-30% Gallium content. Availability of specimen was too limited to assess if crystallographic orientation is a factor. Muto and Takagi [57] showed by comparing resistivity of an ordered and disordered Au-Cu alloy, that ordered samples may have significantly lower resistivity depending on stoichiometry. This explains the lower value obtained by Kawamiya [58] for an ordered Fe₃Ga compared to the values presented here.

Temperature vs. Resistivity measurements were performed on Fe₃Ga by Kawamiya [58] and the residual resistivity obtained was half the one obtained for 18.5% in the case shown in Figure A2. This difference can be explained by comparing the stoichiometry and the crystallographic structure (ordered vs. disordered) of the samples. Single crystal samples exhibited stronger temperature dependence than polycrystalline samples.

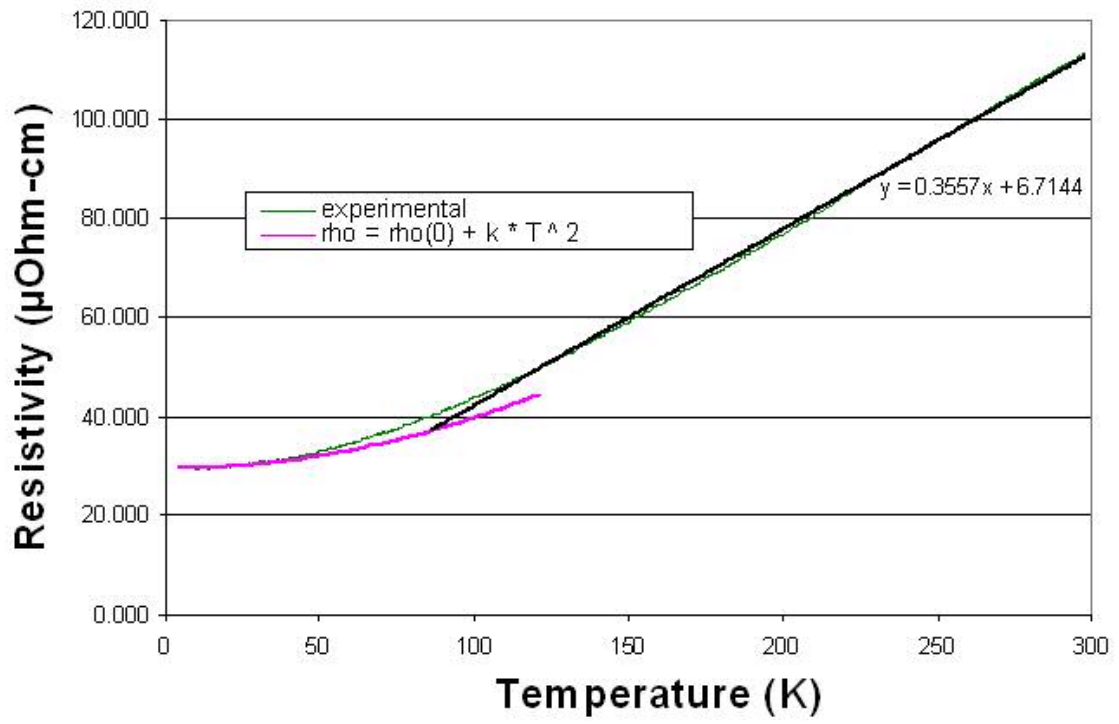


Figure A.2: Resistivity vs Temperature plots with quadratic and linear analytical model.

References

- [1] Pérez-Aparicio, J. L., and Sosa, H., “A continuum three dimensional, fully coupled, dynamic, non-linear finite element formulation for magnetostrictive materials”, *Smart Materials and Structures*, **13**, p 493-502, 2004.
- [2] Lee, S., “ENAE 652 class note on Computational Structural Mechanics”, University of Maryland, Department of Aerospace Engineering, Spring 2004.
- [3] Dasgupta, A., “ENAE 673 class note on Energy and Variational Methods in Applied Mechanics”, University of Maryland, Department of Aerospace Engineering, Fall 2005.
- [4] *FEMLAB 3 manuals*, Comsol© (including the manuals of the structural mechanics and electromagnetic modules), 2004.
- [5] Boresi, A. P., Chong, K. P., “Elasticity in Engineering Mechanics”, [J. Wiley & Sons](#), New York, 1999 (2nd Ed.).
- [6] Jiles, D., “Introduction to Magnetism and Magnetic Materials”, Chapman and Hall, 1991.
- [7] Mayergoyz I., “Mathematical Models of Hysteresis”, Springer, 1991.
- [8] Venkataraman, R., Tan, X., and Krishnaprasad, P., “Control of hysteresis: Theory and experimental results”, *Smart Structures and Materials 2001: Modeling, Signal Processing, and Control in Smart Structures* (V. Rao, ed.), vol. **4326**, Mar. 2001.
- [9] Gorbet, R., Wang, D., and Morris, K., “Preisach model identification of a two-wire SMA actuator”, *Proceedings of IEEE International Conference on Robotics and Automation*, pp. 2161–2167, 1998.
- [10] W. Galinaitis and R. C. Rogers, “Control of a hysteretic actuator using inverse hysteresis compensation”, *Mathematics and Control in Smart Structures*, Smart Structures and Materials 1998 (V. V. Varadhan, ed.), vol. **3323**, pp. 267–277, Mar. 1998.
- [11] Chopra, I., “Review of State-of-Art of Smart Structures and Integrated Systems,” *AIAA Journal*, Vol. **40**. No. 11, November 2002, pp. 2145-2187.
- [12] Chopra I., “ENAE 651 class note on Smart Structures”, University of Maryland, Department of Aerospace Engineering, Fall 2004.
- [13] Hubbard, J.E., “ENAE 757 class note on Advance Structural Dynamic”, University of Maryland, Department of Aerospace Engineering, Spring 2005.

- [14] G., Engdahl, “*Handbook of Giant Magnetostrictive Materials*”, Academic press, 2000.
- [15] Banks, H.T., Smith, R.C., Wang, Y., “*Smart Materials and Structures. Modeling, estimation and control*”, John Wiley & Sons, Canada, 1996.
- [16] Srinivasan, A.V., “*Smart Structures: Analysis and Design*”, Cambridge University press, 2000.
- [17] Clark, A.E., Restorff, J.B., and Wun-Fogle, M., “Magnetization, Magnetic Anisotropy and Magnetostriction of Galfenol alloys”, *Galfenol Workshop*, University of Maryland, 01/2005.
- [18] Wu, R., “First Principles Theory of Anisotropy and Magnetostriction”, *Galfenol Workshop*, University of Maryland, 01/2005.
- [19] Kellogg, R.A., “Development and Modeling of Iron-Gallium alloys”, PhD Thesis, Engineering Mechanics, Iowa State University, Ames, Iowa, 2003.
- [20] Datta, S., conversation on unpublished data, University of Maryland, Department of Aerospace Engineering.
- [21] Matweb.com.
- [22] Atulasimha, J., Flatau, A.B., Chopra, I., Kellogg, R., “Effect of Stoichiometry on Sensing Behavior of Iron-Gallium”, *Proc. Of SPIE : Smart structure and Materials*, **Vol. 5385**, 2004.
- [23] Clark, A.E., Teter, J.P., “Magnetostriction ‘jumps’ in twinned Tb 0:3 Dy 0:7 Fe 1:9”, *J. Appl. Phys.*, 63(8), pp 3910-12, 1988.
- [24] Clark, A.E., and Belson, H.S., “Magnetostriction of Tb-Fe and Tb-Co compounds”, *Magnetism and Magnetic Materials*, C.D Graham and J.J. Rhyne, editors, **5**, *AIP Conference Proceedings*, p.1489, American Institute of Physics , 1972.
- [25] Clark, A.E., and Belson, H.S., “Magneto-crystalline anisotropy in cubic rare earth compounds”, *Magnetism and Magnetic Materials*, C.D Graham and J.J. Rhyne, editors, **10**, Part 1, *AIP Conference Proceedings*, p.749-753, American Institute of Physics , 1973.
- [26] Clark, A.E., H.S., “Magnetic and Magneto-elastic properties of highly magnetostrictive rare earth laves phases compounds”, *Magnetism and Magnetic Materials*, C.D Graham and J.J. Rhyne, editors, **18**, Part2, *AIP Conference Proceedings*, p.1015-1029, American Institute of Physics , 1973.

- [27] Clark, A.E., Cullen, J.R. and Sato, K., "Magnetostriction of single crystal and polycrystal rare-earth Fe₂ compound", *Magnetism and Magnetic Materials*, C.D Graham and J.J. Rhyne, editors, **24**, *AIP Conference Proceedings*, p.670-671, American Institute of Physics , 1975.
- [28] Clark, A.E., "Magnetostrictive Rare Earth Fe₂ ", *Ferromagnetic Material*, **Vol. 1**, Chap 7, p.531-589, Ed. E.P. Wohfarth, North-Hollande Publishing Co. 1980.
- [29] Clark, A.E., Wun-Fogle, M., Restorff, J.B., Lograsso, T.A., and Schlagel, D.L., "Magnetostrictive properties of b.c.c. Fe-Ga and Fe-Ga-Al Alloys", *IEEE Transaction on Magnetics*, **36**, p. 3238-3240, 2000.
- [30] Cullen, J.R., Clark, A.E., Wun-Fogle, M., Restorff, J.B., and Lograsso, T.A., "Magnetoelasticity of Fe-Ga and Fe-Al alloys", *Journal of Magnetism and Magnetic Materials*, 226, p. 948-949, 2001.
- [31] Clark, A.E., Restorff, J.B., Wun-Fogle, M., and Lograsso, T.A., "Magnetostrictive properties of Galfenol alloys under compressive stress", *Materials Transactions (Japan)*, 43, p. 881-886, 2002.
- [32] Restorff, J.B., "Stress Annealing of Fe-Ga Alloys", *Galfenol Workshop*, University of Maryland, 01/2005.
- [33] Summers, E., "Investigation into Texture Development in Fe-Ga alloys", *Galfenol Workshop*, University of Maryland, 01/2005.
- [34] Lograsso, T., "High Resolution Powder X-Ray Diffraction for DO3 Detection and Quantification", *Galfenol Workshop*, University of Maryland, 01/2005.
- [35] Na, S.M., Flatau, A. B., "Magnetostriction and surface-energy-induced selective grain growth in rolled Galfenol doped with sulfur", *Proc. Of SPIE: Smart structure and Materials*, yet to be published Volume, 2005.
- [36] Datta, S., Flatau, A. B., "Application of Iron Gallium alloy as Magnetostrictive Sensors", *Proc. Of SPIE: Smart structure and Materials*, yet to be published Volume, 2005.
- [37] Engdahl, G., and Svensson, L., "Simulation of the magnetostrictive performance of terfenol-d in mechanical devices", *Journal of Applied Physics*, 63(8):3924-3926, 1988.
- [38] Kvarnsjo, L., and Engdahl, G., "Nonlinear 2-d transient modeling of Terfenol-D rods", *IEEE Transactions on Magnetics*, 27(6),5349-5351,1991.
- [39] Claeysen, F. , Bossut, R., and Boucher, D., "Modeling and characterization of the magnetostrictive coupling", B. F. Hamonic, O. B. Wilson, and J.-N. Decarpigny,

editors, *Power Transducers for Sonics and Ultrasonics*, pages 132 {151. *Proceedings of the International Workshop*, Toulon, France, Springer-Verlag, June 12-13, 1990.}

[40] Carman, G. P. , and Mitrovic, M., “Nonlinear constitutive relations for magnetostrictive materials with applications to 1-d problems”, *Journal of Intelligent Material Systems and Structures*, 6(5):673-683, 1995.

[41] Hom, C., and Shankar, N., “A Finite element method for electrostrictive ceramic devices”, *International Journal for Solids and Structures*, 33(12), 1757-1779, 1995.

[42] Duenas, T. A., Hsu, L., and Carman, G. P., “Magnetostrictive composite material systems analytical/experimental”, *Symposium on Advances in Smart Materials - Fundamentals Applications*, Boston MA, 1996.

[43] Dapino, M. J., Smith, R., Faidley, L. E., and Flatau, A. B., “A coupled structural magnetic strain and stress model for magnetostrictive transducers”, *Journal of Intelligent Material Systems and Structures*, 11(2):135 {152, February 2000.

[44] *ATILA -3-D CAD software for piezoelectric and magnetostrictive structures*, ISEN, Lille, Distr. CEDRAT, Meylan & MAGSOFT.

[45] Stillesjö, F., Engdahl, G., Wei, Z., and Cedell, T., “Dynamic simulation and performance of magnetostrictive transducers for ultrasonic applications”, *Proc. Of SPIE : Smart structure and Materials*, Vol. 3992, pp 594-602, 2000.

[46] Kannan, K. S., “*Galerkin Finite Element Scheme for Magnetostrictive Structures and Composites*”, PhD thesis, Department of Mechanical Engineering, University of Maryland, 1997.

[47] Anjanappa, M., and Bi, J., “A theoretical and experimental study of magnetostrictive mini-actuators”. *Smart Structures and Materials*, 3,83-91, 1994.

[48] Anjanappa, M., and Wu, Y., “Magnetostrictive particulate actuators configurations, modeling and characterization. *Smart Structures and Materials*”, 6,393-402, 1997.

[49] Wu, Y., and Anjanappa, M., “Modeling of embedded magnetostrictive particulate actuators”, *Proceedings of the 1996 SPIE Conference on Smart Structures and Materials*, San Diego, CA, February 1996.

[50] Krishnamurty, A. V., Anjanappa, M., and Wu, Y., “Use of magnetostrictive particle actuators for vibration attenuation of flexible beams”, *Journal of Sound and Vibration*, 206(2):133 {149, 1997.

- [51] Flatau, A. B., Dapino, M. J., and Calkins, F. T., “*Comprehensive Composite Materials Handbook*”, volume 5, chapter Magnetostrictive Composites, pages 563-574. Elsevier Science, 2000.
- [52] Pradhan, S. C., Ng, Y. T., Lam, K. Y., and Reddy, J. N. “Control of laminated composite plates using magnetostrictive layers” *Smart Materials and Structures*, 10(4),657-667, 2001.
- [53] Hughes, T. J. R, *The finite element method. Linear static and dynamic analysis*, Englewood cliffs, NJ, 1987.
- [54] Cheng, D.K., *Field and Wave Electromagnetics*, Addison-Wesley, 1989.
- [55] Raamachandran, J., “*Boundary and Finite Elements Theory and Problems*”, [CRC Press.](#), Boca Raton, FL, 2000.
- [56] Summers, E., “State of the art Galfenol processing”, *Galfenol Workshop*, University of Maryland, 01/2004.
- [57] T. Muto and Y. Takagi, “*Solid State Physics*”, edited by F. Seitz and D. Turnbull (Academic Press, New York), Vol. 1, 1955.
- [58] Kawamiya, N., Adachi, K., Nakamura, Y., “Magnetic properties and Mossbauer investigations of Fe-Ga alloys”, *Journal of the Physical Society of Japan*, vol.33, no.5, pp. 1318-1327, Nov. 1972.